Multireference configuration interaction theory using density matrix renormalization group reference function

Masaaki Saitow

Department of Functional Molecular Science
School of Physical Science
The Graduate University for Advanced Studies

Contents

Publication List

M. Saitow, Y. Kurashige, and T. Yanai, "Multireference configuration interaction theory using cumulant reconstruction with internal contraction of density matrix renormalization group wave function", *The Journal of Chemical Physics*, **139**, 044118 (2013).

Y. Kurashige, M. Saitow, J. Chalupský, and T. Yanai, "Radical O-O coupling reaction in diferrate-mediated water oxidation studied with multireference wave function theory", *Physical Chemistry Chemical Physics*, (under review).

M. Saitow, Y. Kurashige, and T. Yanai, "Multireference theoretical stydy of the Iron-oxo porphyrin electromers on top of the ab initio density-matrix renormalization group reference function", *The Journal of Chemical Physics*, (in preparation).

Other Publications

M. Saitow, T. Ida, and M. Mizuno, "Spin-adaptation of open-shell electron propagator theory", *Chemical Physics Letters*, **486**, 171 (2010).

M. Saitow, and Y. Mochizuki, "Excited state calculation for free-base and metallo-porphyrins with the partially renormalized polarization propagator approach", *Chemical Physics Letters*, **525**, 144 (2012).

M. Saitow, T. Ida, and Y. Mochizuki, "Improved description of the orbital relaxation effect by practical use of the self-energy", *International Journal of Quantum Chemistry*, (in press).

Acronyms

ACPF	Averaged Coupled-Pair Functional
ADC(n)	n-th order Algebraic-Diagrammatic Construction
AQCC	Averaged Quadratic Coupled-Cluster
CAS	Complete Active Space
CC	Coupled-Cluster Theory
CIS	Configuration Interaction Singles
CIS(D)	Configuration Interaction Singles with Doubles correction
CSF	Configuration State Function
CT	Canonical Transformation Theory
cu(4)	Neglect of 4-particle rank cumulant
CW	Celani-Werner internal contraction
DFT	Density-Functional Theory
DMRG	Density-Matrix Renormalization Group
FCI	Full Configuration Interaction
EPV	Exclusion Principle Violating
ERI	Electron-Repulsion Integral
FIC	Full-Internal Contraction (or Full-Internally Contracted-)
IC	Internal Contraction (or Internally Contracted-)
MO	Molecular Orbital
MPI	Message Passing Interface
MR	Multireference
MRCI	Multireference Configuration Interaction
RAS	Restricted Active Space
n-RDM	n-particle rank Reduced-Density Matrix
SCF	Self-Consistent Field
SOPPA	Second-Order Polarization Propagator Approach
SR	Single Reference
WR	Werner and Reinsch internal contraction
WK	Werner and Knowles internal contraction

Acknowledgements

First of all, I would like appreciate my parents, and each and single member of my whole family supporting my graduate study. Without their help, it would be evident that I could not accomplish all these things. My grandfather, who has passed away on 2010 at the age of 85, was once dreaming of my graduating from the PhD course. He was given born in Nagano as a youngest son in his family member. I suppose that, in those days, he would not have so much choices on what he wanted to be. He had been working since he was a junior-high school student and has survived the war. I would like to dedicate this dissertation to him.

The present research has been conducted under the supervision of Professor Takeshi Yanai and Professor Yuki Kurashige at Institute for Molecular Science (IMS). The author would like to wholeheartedly express gratitude for Professor Yanai's patience and kind guidance. Throughout this quantum chemical research carried out in Professor Yanai's group, the author has notably realized the flexibility of the multireference framework that enables to capture almost any kinds of the electronic state. From a more technical point of view, the author has learned the use of the spin-free construction method of the (multireference) wave function and the massively-parallel implementation of the quantum chemical method. Moreover, at IMS, the author feels blessed to being given a beautiful opportunity to develop the automation program that derives the complicated quantum chemical formulas and translates them into an efficient computer code. The author believes that such a computer-aided approach becomes indispensable technique in near future since the recent advances in the electronic structure theory have pushed the complexity of the quantum chemical models.

The author would like to appreciate all the members of Professor Yanai's group for not only scientific but also non-scientific discussions (sometimes over a glass of beers). The studies on the *ab inio* polarization propagator described in Chapters 5 and 6 have been carried out in collaboration with Professor Tomonori Ida and Professor Motohiro Mizuno at Kanazawa University and Professor Yuji Mochizuki at Rikkyo University. The

author gratefully acknowledges their guidance and fruitful discussions. Being a developer of `Psi4`, an open-source quantum chemistry program package, has been an enjoyable and exciting experience for the author. Hence, the author would like to express his own appreciation to Professor C. David Sherrill at Georgia Institute of Technology since he gave the author such a wonderful experience.

Chapter 1

General Introduction

The Hartree-Fock (HF) approximation to the molecular electronic Schödinger equation can recover more than 95 % of the molecular electronic energy within a single-particle picture. In the single-particle or mean-field picture, the correlated motion of the electrons is not taken into account. Many-electron nature that goes beyond the single-particle picture is called as *electron correlation*, which does give rise to the rest of the electronic energy. The magnitude of the electron correlation effect in energy is of the same order of the chemical energetics such as the reaction and the dissociation energies[1]. Therefore, in modern quantum chemistry, inclusion of the electron correlation is an indispensable key for quantitative computational prediction of molecular properties. When the HF description is qualitatively correct as a reference and the electron correlation can be accounted for as its relative perturbation, the single-reference correlation theories such as Møller-Plesset perturbation (MP), configuration interaction (CI) and the coupled-cluster (CC) can improve upon the HF wave function and associated energy.

When the HF wave function may not give even a qualitatively correct description, one has to use the multireference electronic structure theory. In the multireference framework, the reference function is not confined to be a single Slater determinant, but is described using multiple reference determinants or configurations on an equal footing. Consequently, the multireference wave function is suitable for encoding a portion of the electron correlation, the so-called *static correlation*, which is physically characterized as a superposition state of the configurations rather than a scattering of the electrons. The remaining portion of the correlation is referred to as the *dynamic correlation* and stems mainly from the short-range interaction amongst the electrons.

The concept of the Complete-Active Space (CAS) of Roos *et al.*[2, 3], or equivalently the fully-optimized reaction space (FORS) of Ruedenberg *et al.*[4] has provided an innovative way to capture the static correlation, leading to a multireference analogue of the HF self-consistent field theory; the Complete-Active Space Self-Consistent Field (CASSCF) theory. In the CAS model, molecular orbitals (MOs) are classified into three types; doubly occupied *core*, fractionally occupied *active* and unoccupied *virtual* orbitals as depicted in Fig. 1.1. In the CASSCF procedure, the wave function is constructed as a linear combination of the determinants that are generated by (1) occupying all the core MOs with a pair of electrons, and (2) distributing 0, 1, or 2 electrons in the active MOs in all the possible way. The expansion coefficients for determinants as well as MOs are optimized variationally to yield minimal electronic energy. Consequently, the static correlation in the active space is described in the CASSCF wave function and the optimized MOs. On top of the CASSCF reference function, the dynamic correlation is taken into account by considering electronic interactions among core, active and virtual MOs. The introduction of dynamic correlation is carried out by means of the multireference MP, CI and CC approaches as addressed hereinafter.

To the best of our knowledge, the eldest multireference theory is the multireference configuration interaction (MRCI) in which, typically, singly- and doubly-excited configurations with respect to the (multiple) reference configurations are taken into account[5, 6]. When the reference function or CAS space is formed properly, the MRCI wave function is known to give extremely accurate description even in case that bond formation or breaking takes place, involving substantially strong quasi-degeneracy. A primal draw-

back of the MRCI is a lack of the size-consistency in the energy i.e. the total energy of the super-system composed of subsystems A and B is not equal to a sum of the energies of the subsystems. The quadruple excitations contributions referred to as the *exclusion principle violating* (EPV) terms are responsible for retaining this property[7, 8].

Starting from the multireference coupled-cluster (MRCC) ansatz[9, 10, 11, 12, 13, 14, 15], which is a potentially size-consistent parameterization, several formulae to approximate the effect of the EPV terms have been proposed; Multireference Averaged Coupled-Pair Functional (MR-ACPF) by Gdanitz and Ahlrichs[16, 17, 18], Multireference Averaged Quadratic Coupled-Cluster (MR-AQCC) by Szalay and Bartlett[19, 20, 21], Multireference Full Coupled-Pair Functional (MR-FCPF) by Malrieu *et al.*[22, 23, 24, 24], and Multiconfigurational Coupled Electron-Pair Approximation (MCCEPA) by Staemmler *et al.*[25]. All of these methods are formulated on the basis of the approximate energy functional by which the energy and the reduced density matrices (RDMs) are determined variationally. It is notable that the MRCI energy obeys the upper-bound nature; the MRCI energy is always much higher than the exact energy. Nevertheless, the approximately size-consistent variants do not fulfill this property because their energy functionals are constructed by means of the *a priori* parameters. Amongst the above mentioned size-consistency correction schemes, only MR-FCPF and MCCEPA give the exactly size-consistent energy although their implementations into the MRCI programs require much greater development efforts than those of the rests. The other means to approximate the effect of the EPV terms is the so-called Davidson-type correction[26, 27, 28, 29, 30], by which the MRCI energy is scaled by using the reference amplitude (or CI coefficients).

With inclusion of the approximate EPV terms into the MRCI formulae, the lack of the size-consistency in the MRCI approach is no longer a practical impedance for the accurate application to the systems such as the chemical reactions.

The multireference second-order perturbation theory (CASPT2) was developed as a (potentially) size-consistent and computationally affordable alternative to the MRCI approaches by Roos *et al.*[31, 32]. The CASPT2 is a multireference extension of the second-order MP (MP2) method and indeed produce the MP2 correlation energy when the reference function is set to the HF wave function. Despite the resemblance to the MP2, in multireference case, there is an ambiguity on the definition of the zeroth order Hamiltonian. For this reason, several forms of the zeroth order Hamiltonian have been developed so as to better produce experimental results[33, 34]. Since the CASPT2 is developed on the basis of the single state perturbation theory, if there exists a closely degenerated state to the reference state as seen in case of the conical intersections, or the crossing avoidance amongst the several state, the CASPT2 is known to be ill-behaved. With the intention of dealing with such a case, the Multiconfigurational Quasi-Degenerate Perturbation Theory (MC-QDPT)[35], or the Multi-State CASPT2 (MS-CASPT2)[36] is developed in the framework of the multi-state perturbation theory.

Under the existence of the so-called *intruder states*, which is typically characterized as an excitations from the active MOs into the low-lying occupied or virtual MOs, the CASPT2 indicial equation often shows the singular behavior where the zeroth Hamiltonian minus the zeroth energy $(H_0 - E_0)$ may become small or negative[37]. This can be circumvented by varying the type of the zeroth Hamiltonian, or by using the

level-shift[34]. However, the choice of the zeroth Hamiltonian and the magnitude of the level-shift may affect the quality of the energy and the wave functions. Another way to avoid the intruder state problem is to combine the MRCI and CASPT2 frameworks; the excitations from the active MOs ((active, active) → (active, virtual) and (active, active) → (virtual, virtual)) are treated in the MRCI framework while the rests, which involve at least one core MOs, are handled within the CASPT2 framework[37]. The joint approach is referred to as CIPT2. The CIPT2 is known as being liberated from the intruder state problem since the excitations solely from the active MOs are responsible for this phenomenon and are treated in the CI framework.

The MRCC has been extensively developed by Mukherjee *et al.*[9, 11], Jeziorski and Monkhorst[10], Simons *et al.*[14], Bartlett *et al.*[15], Hanrath[13], Hanauer and Köhn[38, 39], Gauss *et al.*[40, 41, 42, 43, 44, 45], Yanai and Chan *et al.*[46, 47, 48, 49, 50, 51], and many others[12, 52, 53]. For the HF reference function, the CC theories are conceived as the most successful electron correlation theory because it is size-consistent and unitary-invariant. Moreover, the CCs are more robust than the MP perturbation expansions, which often become ill-behaved under the existence of the quasi-degenerated configurations. Despite the prosperity of the single-reference CC, as far as we know, the MRCC approaches are still under development and so far the *gold standard* MRCC has never been established yet.

Computational complexity of the conventional multireference electron correlation theory within the CAS framework directly depends on the dimension of the Hilbert space. This means that the computational demands increase exponentially with respect to the

molecular size. Therefore, the applicability of the CAS-based multireference approach is limited to utmost an active space with 16 electron in the 16 MOs. A way to avoid this complexity is to use the concept of the Restricted Active Space (RAS)[54, 55, 56], or the Generalized Active Space (GAS)[57, 58] instead of the CAS model. The RAS (or GAS) can be conceived as a generalization of the CAS, and the correlation in the active space is solved by means of the truncated CI at several excitation levels. It has been shown that the RAS based multireference perturbation theory (RASPT2) can indeed handle a large-size active space, such as active space with 29 electrons distributed in 28 active MOs[56, 59], which is far from tractable for the conventional CASPT2 method. However, a specific care has to be taken into account in order to achieve the chemical accuracy because, unlike the CAS case, the RAS framework can cover only a selected portion of the active-space correlations within the Hilbert space. In addition, the adequacy of the RAS setting may strongly depend on specific expertise of the users.

The recent progress in *ab initio* Density-Matrix Renormalization Group (DMRG) has opened a new way to eliminate the exponentially growing complexity from the multireference electron correlation theory[60, 61, 62, 63, 64, 65, 66, 67, 68, 69, 70, 71, 72, 73, 74, 75]. The DMRG algorithm is an efficient alternative to the full CI method. The compact parameterization of the DMRG wave function achieves the drastic reduction in the computational cost for overcoming the exponential complexity in the CI treatment required for the multireference theory. Accurate DMRG calculations of the active-space energy and the energy differences for the systems with the approximately 30 – 40 active MOs have been reported in Refs.[63, 68, 76, 70, 77]. The breathtaking performance of the *ab initio*

DMRG has greatly extended the applicability of the multireference quantum chemistry.

The CASSCF that uses the DMRG algorithm for the full CI treatment in the active space is referred to as the DMRG-CASSCF (or DMRG-SCF at the earlier stage) and is originally proposed independently by Zgid and Nooijen[78], and by Chan *et al.*[79]. In the DMRG-CASSCF procedure, one- and two-body RDMs in the active space are generated by the DMRG for construction of the energy gradient with respect to the orbital rotation and then, the subsequent orbital optimization is carried out like the conventional CASSCF method. The only difference between the DMRG- and conventional CASSCF methods lies in the algorithm to perform the active space CI; the *ab initio* DMRG for the former and the usual full CI for the latter. Recently, the DMRG-CASSCF study by Kurashige *et al.*[80] reported high-level electronic structure calculations on the Mn_4CaO_5 cluster, a catalytic metalloenzyme in photosystem II. In this study, a fairly large basis set and the CAS with 44 electrons distributed in the 35 MOs are used and such a large active space is apparently far beyond the reach of the conventional CAS methods.

The CASPT2 with the DMRG reference function is developed by Kurashige and Yanai[81] and applied to the potential energy calculation of the Cr_2 molecule. The calculation involved the active space with the 12 electrons in the 28 MOs and promising agreement with the experimental results was confirmed. The equilibrium inter-nuclear distance and spectroscopic parameters for Cr_2 were also calculated by using the DMRG-CASPT2 and conventional MR-AQCC, the latter of which used the active space with 12 electrons in 12 MOs. The obtained values were reasonably well in comparison to the experimental values. However, by the nature of the CASPT2, the choice of the

zeroth Hamiltonian certainly affected the accuracy of the results. The connectivity of the CASPT2 framework is borne by the *internally contracted* (IC) representation of the wave function ansatz, which was originally proposed by Meyer[82].

The IC basis is an alternative constitutional unit of the many-body wave function to the Slater determinant. When the CAS-based multireference wave function is constructed as a linear combination of the determinants, the expansion length would increase exponentially with respect to the molecular size. The Hamiltonian matrix elements appear to be represented as a product of the one- or two-body molecular integral and a coupling coefficients of the determinants, which are efficiently calculated by means of the group theoretical algorithms[83, 84, 85, 86]. On the other hand, when the wave function is represented as a linear combination of the IC basis, increase in the expansion length stays polynomial order with respect to the molecular size. In this case, the matrix elements can be represented as a product of the molecular integrals and the active space RDMs instead of the coupling coefficients. In a combination of the multireference wave function and the DMRG reference, the RDMs produced by the DMRG algorithm are used for construction of the Hamiltonian.

In Chapter 2, the development of the MRCI that can use the DMRG reference function, referred to as DMRG-MRCI, is presented and the performance to the linear polyene molecules ranging from C_6H_8 to $C_{24}H_{26}$ is given. In this calculation, it has been shown that the computational scaling of the DMRG-MRCI is polynomial order while that of the most sophisticated implementations of the conventional MRCI[87, 88, 89, 90] scale exponentially. The adiabatic singlet and triplet gap for the free-base porphyrin was also

calculated by using the DMRG-MRCI where all the π electrons and MOs were taken into account in the active space. As a consequence, extremely promising agreement with the experimental and the diffusion Monte Carlo (DMC) results has been confirmed. Originally, the IC-MRCI was developed by Werner *et al.* in 1982[91]. However, their ansatz necessitates the five-body RDM (5-RDM) in construction of the semi-internal excitation blocks, leading to the computational scaling at least of $O(N^{11})$ where N is a magnitude of the molecular size. The quite high computational effort of the earliest IC-MRCI has hindered its practical application to the medium-size molecules. To eliminate this drawback, we express the semi-internal Hamiltonian elements by using the multiple-commutators and then, the lengthy 5-RDM has proven to vanish exactly[92, 93]. Moreover, we employ the cumulant-approximation[94, 95, 96, 97] to decompose the 4-RDMs, which is still large for the systems with approximately 20 – 30 active MOs. As a consequence, in our IC-MRCI formalism, the construction of the Hamiltonian requires only 1 – 3 RDMs and its computational scaling is estimated to be of $O(N^9)$. Due to the introduction of the IC basis, the tensor-contracted form of the MRCI equation becomes so complicated that the manual implementation into the computer code, which is an error-prone procedure, seems impossible. To this end, we develop the tensor generator[98] to expand the many-body ansatz according to the Wick's theorem and to translate into the efficiently-vectorized computer code using the Message-Passing Interface (MPI) parallelism. On the basis of the DMRG-MRCI program, we have implemented the MR-ACPF, MR-AQCC and MR-CEPA0 that can also use the DMRG reference function.

In Chapter 3, we report the practical applications of the DMRG-MRCI to the iron-

oxo porphyrins. The iron-oxo porphyrin derivatives are known to play a crucial role in the cytochrome P450 catalytic cycle[99, 100]. In such a *in vivo* enzymatic reaction, the active intermediate is supposedly conceived as iron(IV)-oxo porphyron radical cation, which is often referred to as *Compound I* (Cpd I). The spectroscopic consensus supports this speculation[101, 102, 103, 104, 105, 106]. Nonetheless, the recent advances in the laser-flash photolysis (LFP) spectroscopic technique has suggested the existence of the relatively stable iron(V)-oxo porphyrin[107, 108] and coincides with the data from the UV/vis spectroscopy. The existence and, if it exists, the stability of the low-lying iron(V)-oxo porphyrin electronic isomer (electromer) have been studied by means of density functional theory (DFT) and RASPT2 by Pierloot *et al.*[59]. In the RASPT2 calculations, they used the 16 π MOs of the porphyrin, all of the $3d$ orbitals of iron and 3 double-shell d orbitals in the active space, leading to the RAS with 29 electrons in the 28 MOs. Contrary to the experimental consensus, their extremely large calculations have suggested that the iron(V)-oxo porphyrin may be much more stable than the iron(IV) electromer *in vacuo*, which is, however, considered to be the ground state. The key to address this collision of the calculations against the experiments is speculated as the existence of the solvent: Under a presence of the polarizable continuum surrounding, iron(IV)-oxo porphyrin is stabilized relative to the iron(V)-oxo electromer within their DFT calculations. Against this background, we perform the highly-accurate DMRG-MRCI calculations on these electromers with a much larger active space; 29 electrons in the 30 MOs.

For carrying out the extremely-large scale MRCI calculation, we have rewritten a symbolic manipulation and optimization module in our tensor generator by using Haskell, a

purely-functional programming language[109]. By expanding the cumulant-approximated form of the 4-RDM in the MRCI formulae explicitly, and by factorizing them into a stream of the binary contraction, the formal scaling of the DMRG-MRCI has been reduced to $O(N^8)$ from the previous order of $O(N^9)$. For evaluation of the tensor contractions, use of the matrix-matrix multiplication routine (like `DGEMM`) as a kernel may require the sorting of each tensor in the binary contraction as a preprocess. For the larger molecules, or much more active MOs, the inefficient sorting algorithm often causes a substantial amount of cache-miss. Hence, for the large systems such as an iron-oxo porphyrin with 30 active MOs, optimization of the loop structure for the sorting step is an indispensable key. To this end, we have added a functionality to optimize the loop structure in the code generator. Due to these modifications, the current version of the DMRG-MRCI program is more than 20 times faster than the earlier one. In Chapter 4, the plausibility of the oxygen-oxygen bond formation process from water, that is catalyzed by a differate intermediate ($[H_4Fe_2O_7]^{2+}$), is evaluated by using the DMRG-based methods (CASSCF, CASPT2 and MRCI) and DFTs. For the multireference calculation, an extremely large active space with 36 electrons distributed in the 32 active MOs is used. The optimization in the algorithms is a key to such an extraordinarily large scale MRCI calculation. Finally, the general conclusion is drawn in Chapter 7.

Apart from the multireference electron correlations, Appendices A and B are devoted to the developments of the second order polarization propagator in the algebraic-diagrammatic construction framework, which is referred to as ADC(2)[110, 111, 112, 113]. The ADC(2) propagator can be conceived as a linear-response to the ground state MP2

wave function. Therefore, the excitation energy and the expectation values with respect to the excited state, which are calculated by seeking the pole structure of the ADC(2), are consistent with the MP2 treatment of such ground state properties. The numerical problem to calculate the excitation energy and the transition amplitude from the ADC propagator is given as a symmetric eigenvalue equation with respect to the response matrix. In case of the ADC(2), the response matrix is expanded in the singly and doubly excitation manifolds and similarly to the configuration interaction singles with doubles correction (CIS(D))[114, 115], the triply excited configurations come into play in the singly excited block as a second order contribution. Hence, all the contributions are *connected* so that the ADC(2) is a size-consistent and unitary-invariant theory by the nature. The ADC(2) can also be seen as a second order extension to the configuration interaction singles and the relationship to the quasi-degenerated perturbative variant of the CIS(D) is addressed in Refs. [116, 117, 118].

The other second order approach to the excited state would be the usual second order polarization propagator (SOPPA) originally proposed by Oddershede and Jørgensen[119, 120]. The response matrix of SOPPA is expanded in both excitation and de-excitation manifolds and is a second order extension to the random-phase approximation (RPA)[121, 122]. The SOPPA excitation energy does not exactly corresponds to the MP2 ground state energy since the presence of the de-excitation block in the response matrix causes higher than the second order contributions. From the computational point of view, the SOPPA has been recognized as a more demanding alternative to the ADC(2) because the second order treatment of the excitation/de-excitation coupling block necessitates the rel-

atively large four-virtual ($\langle vv|vv\rangle$) electron repulsion integrals. Refs.[120, 123] detail the implementation of the SOPPA. Recently, the second order polarization propagator with the coupled-cluster singles and doubles (CCSD) reference function has been vigorously developed by several groups[124, 125, 126, 127, 128, 129, 130].

In Appendix A, the partial renormalization technique proposed by Dykstra and Davidson[131] is applied to the ADC(2) framework. The partially-renormalized ADC(2), which we call PR-ADC(2), has shown to possess a strong resistance to the quasi-degeneracy when applied to a series of the porphyrin derivatives. As a consequence, the PR-ADC(2) produced the accurate excitation energies for these molecules in comparison to the experimental values. In Appendix B, the self-energy shifting proposed by Surján *et al.*[132, 133] is applied to the ADC(2). When the optimal damping parameter is also introduced, as in case of Ref. [134], the excitation energies of the CCSD quality is shown to be available. This modification requires the floating-point operations of utmost $O(N^4)$ while the formal scaling of the ADC(2) itself is $O(N^5)$. Therefore, the additional computational effort is negligibly small and when compared to the CCSD whose cost is of $O(N^6)$, this approach possesses quite promising scaling.

Bibliography

[1] S. Wilson, *Electron Correlation In Molecules*, Dover Publications, New York, 1984.

[2] B. O. Roos, P. R. Taylor, and P. E. Siegbahn, Chem. Phys. **48**, 157 (1980).

[3] B. O. Roos, Adv. Chem. Phys. **69**, 399 (1987).

[4] K. Ruedenberg, L. M. Cheung, and S. T. Elbert, Int. J. Quantum Chem. **16**, 1069 (1979).

[5] R. J. Buenker and S. D. Peyerimhoff, Theor. Chim. Acta. **35**, 33 (1974).

[6] R. J. Buenker and S. D. Peyerimhoff, Theor. Chim. Acta. **39**, 217 (1975).

[7] P. G. Szalay, T. Müller, G. Gidofalvi, H. Lischka, and R. Shepherd, Chem. Rev. **112**, 108 (2012).

[8] J. Paldus, Mol. Phys. **108**, 2941 (2010).

[9] D. Mukherjee, R. Moitra, and A. Mukhopadhyay, Mol. Phys. **33**, 955 (1977).

[10] B. Jeziorski and H. J. Monkhorst, Phys. Rev. A **24**, 1668 (1981).

[11] U. S. Mahapatra, B. Datta, and D. Mukherjee, Mol. Phys. **94**, 157 (1998).

[12] J. Mášik and I. Hubač, Adv. Quantum Chem. **31**, 75 (1999).

[13] M. Hanrath, J. Chem. Phys. **123**, 084102 (2005).

[14] A. Banerjee and J. Simons, Intern. J. Quantum Chem. **19**, 207 (1981).

[15] W. D. Laidig, P. Saxe, and R. J. Bartlett, J. Chem. Phys **86**, 887 (1987).

[16] R. Gdanitz and R. Ahlrichs, Chem. Phys. Lett. **143**, 413 (1988).

[17] R. Gdanitz, Intern. J. Quantum Chem. **85**, 281 (2001).

[18] W. Cardoen and R. Gdanitz, Chem. Phys. Lett. **364**, 39 (2002).

[19] P. G. Szalay and R. J. Bartlett, Chem. Phys. Lett. **214**, 481 (1993).

[20] L. Füsti-Molnár and P. G. Szalay, J. Chem. Phys. **100**, 6288 (1996).

[21] P. G. Szalay, Chem. Phys. **349**, 121 (2008).

[22] J. L. Heully and J. P. Malrieu, Chem. Phys. Lett. **199**, 545 (1992).

[23] J. P. Daudey, J. L. Heully, and J. P. Malrieu, J. Chem. Phys. **99**, 1240 (1993).

[24] J. P. Malrieu, J. P. Daudey, and R. Caballol, J. Chem. Phys. **101**, 8908 (1994).

[25] R. Fink and V. Staemmler, Theor. Chim. Acta. **87**, 129 (1993).

[26] S. R. Langnoff and E. R. Davidson, Intern. J. Quantum Chem. **8**, 61 (1974).

[27] E. R. Davidson and D. W. Silver, Chem. Phys. Lett. **52**, 403 (1977).

[28] K. A. Brueckner, Phys. Rev. **100**, 36 (1955).

[29] J. A. Pople and R. Krishnan, Intern. J. Quantum Chem. **S11**, 149 (1977).

[30] L. Meissner, Chem. Phys. Lett. **146**, 204 (1988).

[31] K. Andersson, P.-Å. Malmqvist, B. O. Roos, A. J. Sadlej, and K. Wolinski, J. Phys. Chem. **94**, 5483 (1990).

[32] K. Andersson, P.-Å. Malmqvist, and B. O. Roos, J. Chem. Phys. **96**, 1218 (1992).

[33] K. Andersson, Theor. Chim. Acta. **91**, 31 (1995).

[34] G. Ghigo, B. O. Roos, and P.-Å. Malmqvist, Chem. Phys. Lett. **396**, 142 (2004).

[35] H. Nakano, J. Chem. Phys. **99**, 7983 (1993).

[36] J. Finley, P.-r. Malmqvist, B. Roos, and S. Luis, Chem. Phys. Lett. **288**, 299 (1998).

[37] P. Celani, H. Stoll, H. Werner, and P. Knowles, Mol. Phys. **102**, 2369 (2004).

[38] M. Hanauer and A. Köhn, J. Chem. Phys. **137**, 131103 (2012).

[39] M. Hanauer and A. Köhn, J. Chem. Phys. **136**, 204107 (2012).

[40] T.-C. Jagau, E. Prochnow, F. Evangelista, and J. Gauss, J. Chem. Phys. **132**, 144110 (2010).

[41] F. Evangelista and J. Gauss, J. Chem. Phys. **134**, 114102 (2011).

[42] F. Evangelista, M. Hanauer, A. Köhn, and J. Gauss, J. Chem. Phys. **136**, 204108 (2012).

[43] T.-C. Jagau and J. Gauss, Chem. Phys. , 73 (2012).

[44] T.-C. Jagau and J. Gauss, J. Chem. Phys. **137**, 044115 (2012).

[45] T.-C. Jagau and J. Gauss, J. Chem. Phys. **137**, 044116 (2012).

[46] T. Yanai and G. K.-L. Chan, J. Chem. Phys. **124**, 194106 (2006).

[47] T. Yanai and G. K.-L. Chan, J. Chem. Phys. **127**, 104107 (2007).

[48] E. Neuscamman, T. Yanai, and G. K.-L. Chan, J. Chem. Phys. **130**, 124102 (2009).

[49] T. Yanai, Y. Kurashige, E. Neuscamman, and G. K.-L. Chan, J. Chem. Phys. **132**, 024105 (2010).

[50] E. Neuscamman, T. Yanai, and G. K.-L. Chan, J. Chem. Phys. **132**, 024106 (2010).

[51] Y. Yanai, Y. Kurashige, E. Neuscamman, and G. K.-L. Chan, Phys. Chem. Chem. Phys. **14**, 7809 (2012).

[52] V. V. Ivanov and L. Adamowicz, J. Chem. Phys. **112**, 9258 (2000).

[53] D. Datta, L. Kong, and M. Nooijen, J. Chem. Phys. **134**, 214116 (2011).

[54] J. Olsen, B. O. Roos, P. Jørgensen, and H. J. A. Jensen, J. Chem. Phys **89**, 2185 (1988).

[55] P.-Å. Malmqvist, A. Rendell, and B. O. Roos, J. Phys. Chem. **94**, 5477 (1990).

[56] P.-Å. Malmqvist et al., J. Chem. Phys. **128**, 204109 (2008).

[57] D. Ma, G. Li Manni, and L. Gagliardi, J. Chem. Phys **135**, 044128 (2011).

[58] G. L. Manni, D. Ma, F. Aquilante, J. Olsen, and L. Gagliardi, J. Chem. Theory Comput. **9**, 3375 (2013).

[59] M. Radoń, E. Broclawik, and K. Pierloot, J. Chem. Theory Comput. **7**, 898 (2011).

[60] S. R. White, Phys. Rev. Lett. **69**, 2863 (1992).

[61] S. R. White, Phys. Rev. B **48**, 10345 (1993).

[62] S. R. White and R. L. Martin, J. Chem. Phys. **110**, 4127 (1999).

[63] A. O. Mitrushenkov, G. Fano, F. Ortolani, R. Linguerri, and P. Palmieri, J. Chem. Phys. **115**, 6815 (2001).

[64] G.-L. Chan and M. Head-Gordon, J. Chem. Phys. **116**, 4462 (2002).

[65] G. K.-L. Chan and M. Head-Gordon, J. Chem. Phys. **118**, 8551 (2003).

[66] J. Hachmann, W. Cardoen, , and G. K.-L. Chan, J. Chem. Phys. **125**, 144101 (2006).

[67] J. Hachmann, J. J. Dorando, M. Avilés, and G. K.-L. Chan, J. Chem. Phys. **127**, 134309 (2007).

[68] K. H. Marti, I. M. Ondík, G. Moritz, and M. Reiher, J. Chem. Phys. **128**, 014104 (2008).

[69] D. Zgid and M. Nooijen, J. Chem. Phys. **128**, 014107 (2008).

[70] Y. Kurashige and T. Yanai, J. Chem. Phys. **130**, 234114 (2009).

[71] G.-L. Chan and D. Zgid, Ann. Rep. Comput. Chem. **5**, 149 (2009).

[72] W. Mizukami, Y. Kurashige, and T. Yanai, J. Chem. Phys. **133**, 091101 (2010).

[73] G. K.-L. Chan and S. Sharma, Ann. Rev. Phys. Chem. **62**, 465 (2011).

[74] S. Sharma and G. K.-L. Chan, J. Chem. Phys. **136**, 124121 (2012).

[75] W. Mizukami, Y. Kurashige, and T. Yanai, J. Chem. Theory Comput. **9**, 401 (2013).

[76] D. Zgid and M. Nooijen, J. Chem. Phys. **128**, 144116 (2008).

[77] S. Sharma and G. K.-L. Chan, J. Chem. Phys. **136**, 124121 (2012).

[78] D. Zgid and M. Nooijen, J. Chem. Phys. **128**, 144115 (2008).

[79] D. Ghosh, J. Hachmann, T. Yanai, and G. K.-L. Chan, J. Chem. Phys. **128**, 144117 (2008).

[80] Y. Kurashige, G. Chan, and T. Yanai, Nat. Chem. **5**, 660 (2013).

[81] Y. Kurashige and T. Yanai, J. Chem. Phys. **135**, 094104 (2011).

[82] W. Meyer, *Modern Theoretical Chemistry*, Plenum, New York, 1977.

[83] J. Paldus, J. Chem. Phys. **61**, 5321 (1974).

[84] I. Shavitt, Int. J. Quantum Chem. **S11**, 131 (1977).

[85] I. Shavitt, Int. J. Quantum Chem. **S12**, 5 (1978).

[86] W. Duch and J. Karwowski, Int. J. Quantum Chem. **22**, 783 (1982).

[87] H.-J. Werner, P. J. Knowles, G. Knizia, F. R. Manby, and M. Schütz, WIREs. Comput. Mol. Sci. **2**, 242 (2012).

[88] H.-J. Werner and P. J. Knowles, J. Chem. Phys. **89**, 5803 (1988).

[89] P. J. Knowles and H.-J. Werner, Chem. Phys. Lett. **145**, 514 (1988).

[90] K. R. Shamasundar, G. Knizia, and H.-J. Werner, J. Chem. Phys. **135**, 054101 (2011).

[91] H.-J. Werner and E. A. Reinsch, J. Chem. Phys. **76**, 3144 (1982).

[92] Personal communication with Prof. Dr. T. Shiozaki and Prof. Dr. K. R. Shamasundar.

[93] L. Kong and E. F. Valeev, J. Chem. Phys. **131**, 214105 (2011).

[94] D. A. Mazziotti, Phys. Rev. A **57**, 4219 (1998).

[95] K. R. Shamasundar, J. Chem. Phys. **131**, 174109 (2009).

[96] W. Kutzelnigg, K. R. Shamasundar, and D. Mukherjee, Mol. Phys. **108**, 433 (2010).

[97] M. Hanauer and A. Köhn, Chem. Phys. **401**, 50 (2012).

[98] FEMTO :: An Integrated Toolset For The Automated Tensor Generation, Version 0.1.0, M. Saitow (https://github.com/msaitow).

[99] S. Shaik, D. Kumar, S. de Visser, A. Altun, and W. Thiel, Chem. Rev. **105**, 2279 (2005).

[100] S. Shaik et al., Chem. Rev. **110**, 949 (2010).

[101] A. Gold and R. Weiss, J. Porph. Phthal. **4**, 344 (2000).

[102] R. Weiss, V. Bulach, A. Gold, and J. Terner, J. Biol. Inorg. Chem. **6**, 831 (2001).

[103] J. T.Groves, J. Inorg. Biochem. **100**, 434 (2006).

[104] S. H. Kim, R. Perera, L. P. Hager, J. H. Dawson, and B. M. Hoffman, J. Am. Chem. Soc. **128**, 5598 (2006).

[105] W. Nam, Acc. Chem. Res. **40**, 522 (2007).

[106] J. Rittle and M. T. Green, Science **330**, 933 (2010).

[107] K. Yamaguchi, Y. Watanabe, and I. Morishita, J. Chem. Soc., Chem. Commun. , 1721 (1992).

[108] T. Murakami, K. Yamaguchi, Y. Watanabe, and I. Morishita, Bull. Chem. Soc. Jpn **71**, 1343 (1998).

[109] The Haskell Programming Language, http://www.haskell.org/.

[110] J. Schirmer, Phys. Rev. A **26**, 2395 (1982).

[111] A. B. Trofimov, G. Stelter, and J. Schirmer, J. Chem. Phys. **111**, 9982 (1999).

[112] A. B. Trofimov, G. Stelter, and J. Schirmer, J. Chem. Phys. **117**, 6402 (2002).

[113] J. Schirmer and A. B. Trofimov, J. Chem. Phys. **120**, 11449 (2004).

[114] M. Head-Gordon, R. J. Rico, M. Oumi, and T. J. Lee, Chem. Phys. Lett. **219**, 21 (1994).

[115] Y. M. Rhee and M. Head-Gordon, J. Phys. Chem. A **111**, 5314 (2007).

[116] M. Head-Gordon, M. Oumi, and D. Maurice, Mol. Phys. **96**, 593 (1999).

[117] D. Casanova, Y. M. Rhee, and M. Head-Gordon, J. Chem. Phys. **128**, 164106 (2008).

[118] C. Hättig, NIC Series **31**, 245 (2006).

[119] J. Oddershede and P. Jørgensen, J. Chem. Phys. **66**, 1541 (1977).

[120] J. Oddershede, P. Jørgensen, and D. L. Yeager, Comput. Phys. Rep. **2**, 33 (1984).

[121] T. H. Dunning and V. M. McKoy, J. Chem. Phys. **47**, 1735 (1967).

[122] P. Jørgensen and J. Linderberg, Int. J. Quantum Chem. **4**, 587 (1970).

[123] M. J. Packer, E. K. Dalskov, T. Enevoldsen, H. J. A. Jensen, and J. Oddershede, J. Chem. Phys. **105**, 14 (1996).

[124] T. Korona, M. Przybytek, and B. Jeziorski, Mol. Phys. **104**, 2303 (2006).

[125] T. Korona, Mol. Phys. **108**, 343 (2010).

[126] T. Korona, Phys. Chem. Chem. Phys. **12**, 14977 (2010).

[127] T. Kjærgaard et al., J. Chem. Phys. **135**, 024112 (2011).

[128] S. Coriani, T. Fransson, O. Christiansen, and P. Norman, J. Chem. Theory Comput. **8**, 1616 (2012).

[129] J. Cukras, S. Coriani, P. Decleva, O. Christiansen, and P. Norman, J. Chem. Phys. **139**, 094103 (2013).

[130] J. Kauczor, P. Norman, O. Christiansen, and S. Coriani, J. Chem. Phys. **139**, 211102 (2013).

[131] C. E. Dykstra and E. R. Davidson, Int. J. Quantum Chem. **78**, 226 (2000).

[132] P. Surján and Á. Szabados, Int. J. Quant. Chem. **69**, 713 (1997).

[133] P. Surján, Á. Szabados, and Z. Szekeres, Int. J. Quant. Chem. **90**, 1309 (2002).

[134] Y. M. Rhee and M. H. Gordon, J. Phys. Chem. A **111**, 5314 (2007).

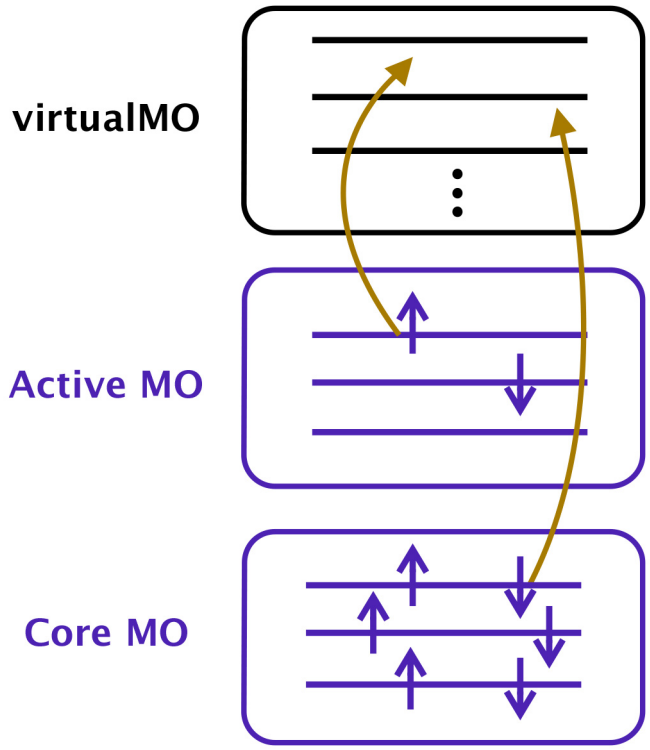

Figure 1.1: The MO classification in the CAS framework. The core and virtual MOs are doubly occupied and unoccupied, respectively while the occupation number of the active MOs can be a decimal fraction ranging from 0 to 2.

Chapter 2

Derivation and Development of the DMRG-MRCI Theory

M. Saitow, Y. Kurashige, and T. Yanai, "Multireference configuration interaction theory using cumulant reconstruction with internal contraction of density matrix renormalization group wave function", *The Journal of Chemical Physics*, **139**, 044118 (2013).

2.1 Introduction

Electron correlation in molecules is defined as the difference between the exact solution of the electronic Schrödinger equation and an approximate solution based on mean-field theory; such correlation is known to play a crucial role in the reliability of quantum chemistry calculations. The magnitude of the electron correlation effect in the chemical binding energy is of same order as that of such energetics itself.[1, 2] Thus, for quantitative energetics, which determine the consequences of various chemical processes, sophisticated electron correlation methods would be indispensable. For efficient computation of electron correlation, it is profitable to divide the correlation into two types: static and dynamic. Dynamic correlation is ascribed to short-range inter-electronic interactions, which can be interpreted from the scattering caused by Coulomb interactions. When the dynamic correlation is a major part of the total correlation, the single reference (SR) coupled-cluster[3, 4, 5, 6] (CC) theory serves as an effective model. In contrast, the static correlation is associated with the quasi-degeneracy of electronic configuration states. Although it also stems from the Coulomb interactions, they are characterized by the superposition of the electronic configurations rather than by a picture of the scattering of electrons. The complete active space (CAS) method provides a robust modeling of static correlation through the exact quantum mechanical treatment of a user-specified subset of electrons and orbitals, namely, the active space, which is responsible for the description of quasi-degenerate or multireference chemical interactions.

The multireference configuration interaction (MRCI) method has been widely used

as a powerful means for achieving highly accurate solutions to the electronic Schrödinger equation for multireference systems.[7, 8, 9, 10, 11, 12, 13, 14, 15, 16, 17, 18, 19, 20, 21] It was originally derived and implemented by Bünker and Peyerimhoff[7, 8] using determinants or configuration state functions (CSFs) as the CI basis. Despite its accuracy, its high computational cost has limited applicability of early variants of MRCI to small molecules composed of only a few atoms. This limitation arises because the length of the configuration expansion quite rapidly increases with the number of the active orbitals. Later, the highly efficient MRCI framework was developed with the introduction of the so-called *internally contracted* (IC) basis,[14, 15, 16, 17] which was originally proposed by Meyer.[22] The resulting method termed IC-MRCI was implemented into sophisticated computer code by Werner et al.[15, 16] in the MOLPRO program package.[23] To distinguish the CSF basis from the IC basis, the determinant or CSF basis employed in the early MRCI method is referred to as *uncontracted* basis. In IC-MRCI, dynamic correlation is calculated by correcting the active-space description by including single and double excitations from the reference. The latest version of the IC-MRCI program developed by Werner et al.[17] is readily applicable to molecules that are intractable in uncontracted MRCI implementations. Nevertheless, the applicability of conventional MRCI methods remains limited because the computational demands have strong exponential dependence on the size of the active space. This dependence essentially arises from the underlying full configuration expansion of the active-space wave function.

Recently, the *ab initio* density-matrix renormalization group (DMRG) method has been vigorously studied as an efficient substitute for the full CI method.[24, 25, 26, 27,

28, 29, 30, 31, 32, 33, 34, 35, 36, 37, 38, 39] By virtue of the compact parameterization of the DMRG wave function, the DMRG algorithm[24, 25, 26] has promising capabilities for overcoming the exponential complexity in the CI treatment of the CAS reference. Accurate DMRG predictions of active-space energies and energy differences can now be obtained for active-space sizes in the range of 30-40 active orbitals in compact molecules, including transition metal complexes[27, 32, 40, 34, 41] and to more than 100 active orbitals in the optimal case of long chains.[30, 31, 36, 39] This revolutionary performance greatly expands the domain of applications for multireference quantum chemistry calculations.

In this study, we present a new IC-MRCI method that can use the active-space DMRG wave function as the reference with much larger size CAS than is possible with conventional MRCI methods. The IC representation is the key to a smooth connection between the DMRG and MRCI methods. In the IC approach, information on the reference wave function entering into the equations and energy expressions are all managed by replacements with many-particle reduced density matrices (RDMs). Hereafter, we simply refer to the particle rank of RDMs and many-body operators as 'rank' unless otherwise stated. The IC approach allows for rather simplified treatments of the intrinsic high-dimensional entanglement of the active-space wave function. As a result, the IC approach is highly scalable to larger active space, while bypassing the exponential dependence of the underlying complexity. In recent technological advances in the DMRG method, an efficient algorithm to obtain the two-rank RDM of the DMRG wave function was developed by Zgid and Nooijen[42] and by Chan et al.[43] We have recently extended

this procedure to evaluate three- and four-rank RDMs.[44, 45] These RDMs were used in our previous studies to combine the DMRG wave function with types of multireference theory, including the orbital optimization method based on the CAS self-consistent field (CASSCF) model,[46, 47, 40, 43, 48] as well as dynamic correlation methods based on the canonical transformation (CT)[49, 50, 51, 52, 53, 54] and CAS second-order perturbation (CASPT2) models.[55, 56, 44, 45] We applied these methods to the copper-oxo dimer isomerization problem with CAS(28e,32o) [DMRG-CT][57] and to the dissociation curve of the chromium dimer in a double-shell active space [DMRG-CASPT2].[44] These previous developments are schematically similar to the present study in which we integrate the DMRG and IC-MRCI methods (DMRG-MRCI for short) by exploiting RDMs from the DMRG wave function to expand the available size of the active space. Nevertheless, there are several technical hurdles to be cleared.

In the present DMRG-MRCI approach, all single and double excitations relative to the reference function are treated in the IC representation. We term this strategy the full IC (FIC) scheme. The MRCI ansatz, in conjunction with the FIC representation, was initially studied by Werner and Reinsch;[14] they found that the error caused by the IC is negligible for energies and other properties. However, there are two major technical difficulties in the FIC-MRCI method, as was also pointed out by Siegbahn et al.:[58] (i) Hamiltonian matrix elements in the semi-internal double excitation basis involve the five-rank RDM, which is computationally formidable. (ii) The working equations need to be built from an extremely large number of tensor contraction terms; the number of terms is too large to implement into computer code by hand. To avoid these com-

plications, the work of Werner and Reinsch[14] as well as Werner and Knowles[15, 16] reintroduced determinants basis, uncontracting the internal and semi-internal parts of doubly excited functions. Although this scheme introduces an exponential bottleneck in part, a balanced admixture of IC and uncontracted basis actually gives the best performance for a typical size of conventional CAS, such as CAS(12e,12o).[14, 15, 16] Later, Werner's group incorporated their partial IC approach into the CASPT2[59, 60, 61, 62], CASPT3[63] and explicitly-correlated multireference[64, 18, 19] methods. In the development of DMRG-MRCI, we attempt to challenge the above two difficulties [(i) and (ii)] without using uncontracted basis, which is not available in DMRG calculations. A commutator-based reduction technique will be introduced to eliminate the five-rank RDM arising in semi-internal Hamiltonian elements; they are then expressed, without any approximation, using the four-rank RDM.[65, 66] Furthermore, we attempt to eliminate the four-rank RDM using its cumulant reconstruction, which does introduce approximation errors. The cumulant reduction for 4-RDM has been employed by several earlier studies[67, 68, 69, 70, 71, 72, 72, 73] in the multireference methods and also has been investigated by our group for the development of the cumulant-approximated DMRG-CASPT2 method, which will be published somewhere.[45] To deal with the huge complexity of computer implementation, an automated technique is employed to derive and factorize tensorial expressions and to generate efficient parallelized computer code, as has been done in previous studies on other developments.[74, 75, 76, 77, 78, 79, 80, 81, 82, 83, 84, 85, 86] In addressing these challenges, we will show that the DMRG-MRCI is free from the exponential bottleneck and its scalability is polynomial order versus the number of orbitals

including active orbitals.

This paper proceeds as follows. In Section 2.2, the formalisms of the conventional and present MRCI methods are given and extensions to size-consistency-corrected variants, including the averaged coupled-pair functional[87, 88, 89] (ACPF) and averaged quadratic CC[90, 91, 92] (AQCC), are given. In Section 2.3, the features of the automated equation and code generation techniques are briefly discussed. In Section 2.4, to reveal the scalability of the DMRG-MRCI, the computational times for a series of polyene molecules (C_6H_8 – $C_{24}H_{26}$) are measured using the references extended to CAS(24e,24o). The singlet and triplet gap for the free-base porphyrin molecule is calculated by means of the DMRG-MRCI with the *a posteriori* and *a priori* size-consistency corrections.[93, 94, 95, 96, 97] In addition, the errors caused by the FIC representation and the use of the cumulant approximation to the four-rank RDM are assessed employing a nitrogen molecule for benchmark. Finally, conclusions are drawn in Section 2.5.

2.2 Theory

2.2.1 Notation and conventions

Before proceeding to address our theoretical framework, we summarize the notation and abbreviations employed throughout this article. The notation for orbital indices and frequently used abbreviations are compiled in Table 2.1. Unless otherwise noted, the Einstein summation convention is imposed for tensor contraction expressions. In the multireference approach, the reference function is given as a linear combination of a set

of determinants that span the reference space as follows,

$$|\Psi_0\rangle := A^{I_\mu}|\Phi_{I_\mu}\rangle\,. \tag{2.1}$$

We proceed to the formulations in spin-free form using the unitary group generators given by

$$E_p^r = \sum_\sigma a_{r\sigma}^\dagger a_{p\sigma} \tag{2.2}$$

or

$$E_{pq}^{rs} = \sum_{\sigma,\tau} a_{r\sigma}^\dagger a_{s\tau}^\dagger a_{q\tau} a_{p\sigma} \tag{2.3}$$

for one- and two-rank operators, respectively, where σ and τ run over the spin states (α and β), and a ($a^\dagger$) denotes the annihilation (creation) operator. The previous work of Kutzelnigg and Mukherjee provided a multireference generalization of normal ordering, which facilitates the derivation of spin-free tensor contraction equations.[98, 99, 100, 67] The definitions of one- and two-rank generators [Eqs. (2.2) and (2.3)] are easily generalized to generators of higher rank, which are denoted by $E_{pq\cdots}^{rs\cdots}$. Using these generators, the electronic Hamiltonian can be defined by,

$$H = h_p^q E_q^p + \frac{1}{2} V_{pq}^{rs} E_{rs}^{pq} \tag{2.4}$$

where h_p^q and V_{pq}^{rs} are one- and two-body molecular integrals in the spatial MO basis. In the active space model, an entire set of orbitals in the reference is classified into three groups: core (doubly-occupied), active (with fractional occupancy ranging from 0 to 2), and external (unoccupied). In the MRCI method with CAS reference, dynamic

correlation arises from interactions between the active and remaining inactive (core and external) orbitals. Note that the intra-active interaction can also capture a part of dynamic correlation.

2.2.2 The MRCI theory

The ansatz of the MRCI wave function is classified into two types: uncontracted and internally contracted (IC). In the uncontracted MRCI type, which is the earliest scheme, the wave function is parameterized as a linear combination of all the singly and doubly excited determinants or CSFs from the reference configurations,[7]

$$|\Psi\rangle := C^{I_\mu}|\Phi_{I_\mu}\rangle + C_A^{S_\mu}|\Phi_{S_\mu}^A\rangle + C_{AB}^{D_\mu}|\Phi_{D_\mu}^{AB}\rangle \tag{2.5}$$

where the capital indices A and B denote the unoccupied orbitals of each reference determinant. The determinant amplitude, $\mathbf{C}$, is optimized variationally to yield the upper-bound for the eigenvalue of the electronic Schödinger equation. Then, the MRCI equation is written as a standard eigenequation,

$$\mathbf{HC} = \mathbf{CE}\,, \tag{2.6}$$

which determines the amplitude $\mathbf{C}$ and the electronic energy $\mathbf{E}$. The Hamiltonian matrix ($\mathbf{H}$) elements are constructed as a sum of products of molecular integrals and coupling coefficients; the latter can be calculated very efficiently using group theoretical approaches.[101, 102, 103, 104, 16] The uncontracted MRCI is algorithmically a straightforward approach to solving the Schödinger equation on the basis of the variation theorem , and it can provide a very accurate wave function when a good subset of N-electron

Hilbert space is used for the reference. However, the length of the configuration expansion of ansatz [Eq. (2.5)] increases exponentially with dimension of the active orbital space, so the practical applicability of the uncontracted MRCI is quite limited.

The first ansatz of the IC-MRCI wave function was proposed by Werner and Reinsch (WR)[14] as follows,

$$|\Psi\rangle := \left(C^0 + C^{rs}_{pq} E^{pq}_{rs}\right) |\Psi_0\rangle \tag{2.7}$$

where $\mathbf{C}$ refers to the CI amplitude of the IC basis. In this expression, the spin-free generators, which are independent of reference configurations, act on the reference wave function $|\Psi_0\rangle$. It is succinctly indicated that the WR ansatz of Eq. (2.7) can readily remove the exponential complexity of the dimension of the variational space. The consequence of this reduction is that we must evaluate the Hamiltonian matrix elements using high-rank RDMs up to rank five! Nontrivial RDMs arise in active space and are given as

$$D^k_i = \langle \Psi_0 | E^k_i | \Psi_0 \rangle \,, \tag{2.8}$$

$$D^{kl}_{ij} = \langle \Psi_0 | E^{kl}_{ij} | \Psi_0 \rangle \,, \tag{2.9}$$

$$\cdots$$

$$D^{kl\cdots}_{ij\cdots} = \langle \Psi_0 | E^{kl\cdots}_{ij\cdots} | \Psi_0 \rangle \,, \tag{2.10}$$

for the one-, two-, and general-order RDMs, respectively. These RDMs can be obtained from the full CI treatment in the active space; however, its computational cost increases exponentially as the number of active orbitals increases.

Werner and Knowles (WK) developed a more efficient contraction scheme from a hybrid approach mixing the uncontracted and IC frameworks by introducing the following

ansatz[15, 16]

$$
\begin{aligned}
|\Psi\rangle := C^{I_\mu}|\Phi_{I_\mu}\rangle + C_A^{S_\mu}|\Phi_{S_\mu}^A\rangle + C_{\{AB\}'}^{D_\mu}|\Phi_{D_\mu}^{\{AB\}'}\rangle \\
+ \left(C_{ab}^{ik}E_{ik}^{ab} + \frac{1}{2}C_{ab}^{wi}E_{wi}^{ab} \right. \\
\left. + C_{ab}^{ik}E_{ik}^{ab} + \frac{1}{2}C_{ab}^{iw}E_{iw}^{ab} \right) |\Psi_0\rangle
\end{aligned} \tag{2.11}
$$

where $\{AB\}'$ runs over pairs of active orbitals, as well as over pairs of active and external orbitals. Because of the compact representation of external excitations, the WK-MRCI method allows the use of much larger references with larger basis sets than earlier generations of the MRCI method. An improved variant of the WK ansatz [Eq. (2.11)] was later developed by the same group[17] using a contraction scheme of the Celani-Werner (CW) type,[59, 60] which introduced additional IC bases associated with excitations from core orbitals. The CW scheme significantly reduces the dimension of the CI space for systems having a number of core orbitals, but it gives rise to an enormous number of tensor contraction terms in the computational formulae. This complexity was resolved by means of an automated technique, in which a computer helps derive and implement the CW-MRCI method into efficient computer code. The CW-MRCI achieves better performance when many core orbitals exist and is liberated from the limitation of the WK-MRCI on the available number of core orbitals in calculations. The resulting CW-MRCI implementation generally performs much better than WK-MRCI, and the relative efficiency is increasingly enhanced as the number of core orbitals increases. Mathematical expressions for the variants of the MRCI ansatz appear somewhat complex at a glance; so for convenience, we summarize the contraction schemes of MRCI in Table 2.2.

2.2.3 The IC-MRCI framework

The spin-free generators that produce all single and double excitations from the reference function are classified into eight independent groups,

$$E^{ik}_{wy}, E^{km}_{wi} \tag{2.12}$$

for internal excitations,

$$E^{ia}_{wy}, \{E^{ka}_{wi}, E^{ka}_{iw}\}, E^{ma}_{ik} \tag{2.13}$$

for semi-internal excitations and

$$E^{ac}_{wy}, E^{ac}_{wi}, E^{ac}_{ik} \tag{2.14}$$

for external excitations. In constructing the Hamiltonian matrix, the reference function and all IC bases produced by these generators couple with each other through the Hamiltonian, which has up to two-body interactions. A beauty of the IC framework is that the dimension of the variational space is completely independent of that of the reference space. All singly and doubly excited determinants are contracted to form a basis

$$E^{pq}_{rs}|\Psi_0\rangle = A^{I_\mu} E^{pq}_{rs}|\Phi_{I_\mu}\rangle = A^{I_\mu}|\Phi^{pq}_{rs,I_\mu}\rangle. \tag{2.15}$$

By comparing Eq. (2.7) and Eq. (2.5), it is evident that there is a much greater degree of variational freedom in the uncontracted type. In the IC-MRCI, the parameters of the reference function [**A** in Eq. (2.15)] are kept fixed, and the IC amplitudes [**C** in Eq. (2.7)] are variationally optimized. Hence, the dimension of the IC-MRCI Hamiltonian matrix increases at merely a polynomial rate as the system size grows; thus, it is scalable

to exceedingly large CAS. Nevertheless, the Hamiltonian matrix elements are given by quite a complex expansion into numerous products of the molecular integrals and RDMs of ranks one through five.

2.2.4 Commutator-based reduction scheme of higher rank RDMs

Let us consider the diagonal blocks of the Hamiltonian matrix elements for the semi-internal IC basis E^{ma}_{ik} (*ooov*) and internal E^{km}_{wi} (*cooo*), which are given by

$$\langle \Psi_0 | E^{ik}_{ma} H E^{nb}_{jl} | \Psi_0 \rangle \,, \quad [ooov\text{-}ooov] \tag{2.16}$$

and

$$\langle \Psi_0 | E^{wi}_{km} H E^{ln}_{yj} | \Psi_0 \rangle \,. \quad [cooo\text{-}cooo] \tag{2.17}$$

In these elements, the excitation operators on the left and right sides provide a total of six active indices. Given that the Hamiltonian H is decomposed into the active space Hamiltonian $H_{\rm act}$ and the rest as

$$H = H_{\rm act} + H_{\Delta} \,, \tag{2.18}$$

with

$$H_{\rm act} = h^j_i E^i_j + \frac{1}{2} V^{kl}_{ij} E^{ij}_{kl} \,, \tag{2.19}$$

four active indices are provided by $H_{\rm act}$. These thus indicate that the tensor contraction expressions give rise to the RDM with ten (six plus four) active indices, namely 5-RDM, in the above Hamiltonian matrix elements [Eqs. (2.16) and (2.17)]. As mentioned earlier,

such a large number of indices in 5-RDM, as well as the high-order scaling of its size ($O(o^{10})$), is thought to prevent efficient use of the FIC scheme. Note that the 5-RDM arises in the semi-internal Hamiltonian matrix elements only.

In this study, we introduce an exact mathematical transformation that eliminates the dependence on 5-RDM. Our approach exploits a property of the reference function $|\Psi_0\rangle$, which is determined by the CASSCF method, achieving the following equation,

$$H_{\rm act}|\Psi_0\rangle = E_0|\Psi_0\rangle\,. \tag{2.20}$$

where E_0 is the reference energy, namely the CASSCF energy. The action of the Hamiltonian H on the reference function is written as

$$H|\Psi_0\rangle = E_0|\Psi_0\rangle + |\Psi_{\rm res}\rangle \tag{2.21}$$

and

$$|\Psi_{\rm res}\rangle = H_\Delta|\Psi_0\rangle \tag{2.22}$$

where $\Psi_{\rm res}$ refers to the residual interaction component. In addition, we consider the following equations for the double commutators of H and the generators of the *ooov* and *cooo* types,

$$\begin{aligned}\langle\Psi_0|[E^{ik}_{ma},[H,E^{nb}_{jl}]]|\Psi_0\rangle &= \langle\Psi_0|E^{ik}_{ma}HE^{nb}_{jl}|\Psi_0\rangle \\ &\quad - \langle\Psi_0|E^{ik}_{ma}E^{nb}_{jl}H|\Psi_0\rangle\,,\end{aligned} \tag{2.23}$$

and

$$\begin{aligned}\langle\Psi_0|[E^{wi}_{km},[H,E^{ln}_{yj}]]|\Psi_0\rangle &= \langle\Psi_0|E^{wi}_{km}HE^{ln}_{yj}|\Psi_0\rangle \\ &\quad - \langle\Psi_0|E^{wi}_{km}E^{ln}_{yj}H|\Psi_0\rangle\,,\end{aligned} \tag{2.24}$$

respectively. Note that the double commutators $\langle[...,[H,...]]\rangle$ do not contain RDM with rank larger than 4 because of the nature of the commutator; the five rank interaction is exactly cancelled out. Insertion of Eq. (2.21) into Eqs. (2.23) and (2.24) finally leads to the following formulae to evaluate the semi-internal Hamiltonian matrix elements:

$$\langle\Psi_0|E^{ik}_{ma}HE^{nb}_{jl}|\Psi_0\rangle = \langle\Psi_0|[E^{ik}_{ma},[H,E^{nb}_{jl}]]|\Psi_0\rangle + E_0\langle\Psi_0|E^{ik}_{ma}E^{nb}_{jl}|\Psi_0\rangle\,, \tag{2.25}$$

and

$$\langle\Psi_0|E^{wi}_{km}HE^{ln}_{yj}|\Psi_0\rangle = \langle\Psi_0|[E^{wi}_{km},[H,E^{ln}_{yj}]]|\Psi_0\rangle + E_0\langle\Psi_0|E^{wi}_{km}E^{ln}_{yj}|\Psi_0\rangle\,, \tag{2.26}$$

where the following relations are used:

$$\langle\Psi_0|E^{wi}_{km}E^{ln}_{yj}|\Psi_{\rm res}\rangle = 0\,, \tag{2.27}$$

$$\langle\Psi_0|E^{ik}_{ma}E^{nb}_{jl}|\Psi_{\rm res}\rangle = 0\,, \tag{2.28}$$

which are asserted by the killer condition associated with nonconservation of electron numbers in the operators. Using Eqs. (2.25) and (2.26), consequently, the highest rank of RDM required for FIC-MRCI can be reduced, without approximation, from five to four.

In Eqs. (2.25) and (2.26), the left-hand sides (lhs) and the second terms on the right-hand sides (rhs) are evidently symmetric, while the symmetries of the first terms on the rhs are not trivial. If the reference function does not satisfy the condition [Eq. (2.20)] exactly, the Hamiltonian blocks evaluated through the commutators, [Eqs. (2.25) and (2.26)], are no longer symmetric. This case also arises when 4-RDM is treated

approximately. In Sec. 2.2.5, we will discuss a cumulant approximation to 4-RDM. With this approximation, the symmetrization of the Hamiltonian matrix has to be performed to recover the symmetries of the first terms on the rhs of Eqs. (2.25) and (2.26).

2.2.5 Approximation to 4-RDM by cumulant reconstruction

Even with exact cancellation of the 5-RDM, there remains the 4-RDM in the tensor contraction formulas of the IC-MRCI Hamiltonian matrix. The $O(o^8)$ size of the 4-RDM rapidly becomes considerably large to store in fast memory. For example, with 20 active orbitals, the numerical array of the 4-RDM, without any use of permutation symmetry, occupies 190 gigabytes of memory. To circumvent this difficulty, we introduce an approximation to the FIC-MRCI method. In our implementation, the 4-RDM is reconstructed on-the-fly from lower-order (up to three-rank) RDMs on the basis of cumulant expansions of the 4-RDM. The approximation is made by neglecting the four-rank cumulants for the cumulant reconstruction of the 4-RDM.

The concept of cumulant expansions is used in statistical mechanics to provide hierarchical relationships among different orders of correlation functions. This concept has been extended to the quantum mechanics of fermionic many-body systems for direct determination of RDMs.[68, 69, 105, 106, 107, 108, 109] The cumulant decomposition of n-RDM (n = 1, 2, 3, and 4) can be written using the anti-symmetrized products among

the k-RDMs ($k = 1, 2, \ldots, n-1$) along with the n-rank cumulant (Δ), as follows,

$$D_i^j = \Delta_i^j, \tag{2.29}$$

$$D_{gh}^{ij} = \Delta_{gh}^{ij} + 4D_g^i \wedge D_h^j, \tag{2.30}$$

$$D_{ghi}^{jkl} = \Delta_{ghi}^{jkl} + 9D_{gh}^{jk} \wedge D_i^l - 12D_g^j \wedge D_h^k \wedge D_i^l, \tag{2.31}$$

$$\begin{aligned} D_{ghij}^{klmn} &= \Delta_{ghij}^{klmn} + 16D_{ghi}^{klm} \wedge D_j^n + 18D_{gh}^{kl} \wedge D_{ij}^{mn} \\ &\quad - 144D_{gh}^{kl} \wedge D_i^m \wedge D_j^n + 96D_g^l \wedge D_h^k \wedge D_i^m \wedge D_j^n \end{aligned} \tag{2.32}$$

where $\Delta_{\cdots}^{\cdots}$ refers to the fully-connected cumulant and is regard as perturbative in the cumulant approximation. The wedge symbol ($\wedge$) represents the anti-symmetrized products[109, 73]

$$(\mathbf{X}_n \wedge \mathbf{Y}_m)_{j_1,j_2,\cdots,j_{n+m}}^{i_1,i_2,\cdots,i_{n+m}} = \left(\frac{1}{(n+m)!}\right)^2 \sum_{\pi,\sigma} \epsilon(\pi)\,\epsilon(\sigma)\,\pi\,\sigma\, \left(\mathbf{X}_{j_1\cdots,j_n}^{i_1\cdots,i_n}\right) \left(\mathbf{Y}_{j_{n+1}\cdots,j_{m+n}}^{i_{n+1}\cdots,i_{m+n}}\right), \tag{2.33}$$

where $\mathbf{X}$ and $\mathbf{Y}$ are tensors whose ranks are n and m, respectively. In Eq. (2.33), π and σ permute all of the upper and lower indices, respectively, while ϵ returns the corresponding sign change to the given permutation. Eqs. (2.29) – (2.32) are expressed in spin-dependent form, but instead, we employ the spin-free variants of these formulas[71, 72, 73] for implementation. In our approximation to 4-RDM, the fully-connected cumulants Δ_{ghij}^{klmn} are neglected in Eq. (2.32). The FORTRAN subroutine to calculate spin-free 4-RDM on the basis of cumulant approximation is given as supplementary material.[110]

It is well known that the cumulant-approximated 4-RDM for the correlated reference is no longer N-representable.[111, 112, 113] It is thus found that, when used for evaluating

the IC-MRCI Hamiltonian matrix, it can lead to the serious breakdown of the variational nature of the IC-MRCI. Related to this, the elimination of four-rank cumulants may induce nonphysical interactions in the Hamiltonian matrix, producing spurious eigenstates, which may be much lower than the lowest state of IC-MRCI using exact 4-RDM. This means that specific numerical care has to taken of these issues to seek valid eigenstates, as discussed later. Our FIC-MRCI framework that uses a cumulant-approximated 4-RDM is referred to as FIC-cu(4)-MRCI.

2.2.6 Diagonalization

Because the IC bases are not orthogonal, the IC-MRCI equation takes the form of the generalized eigenequation,

$$\mathbf{HC} = \mathbf{SCE} \tag{2.34}$$

where the Hamiltonian ($\mathbf{H}$) and overlap ($\mathbf{S}$) matrix elements are given as,

$$H_{0,0} = E_0, \tag{2.35}$$

$$H_{0,R} = \langle \Psi_0 | H E_R | \Psi_0 \rangle, \tag{2.36}$$

$$H_{L,0} = \langle \Psi_0 | E^L H | \Psi_0 \rangle, \tag{2.37}$$

$$H_{L,R} = \langle \Psi_0 | E^L H E_R | \Psi_0 \rangle, \tag{2.38}$$

and

$$S_{0,0} = 1, \tag{2.39}$$

$$S_{0,R} = 0, \tag{2.40}$$

$$S_{L,0} = 0, \tag{2.41}$$

$$S_{L,R} = \langle \Psi_0 | E^L E_R | \Psi_0 \rangle. \tag{2.42}$$

In Eqs. (2.35) – (2.42), L and R refer to the excitation class in Eqs. (2.12) – (2.14). In the diagonalization process based on the block-Davidson algorithm,[114] the σ-vector (the matrix-vector product of Hamiltonian and trial CI wave function) has to be calculated for each iteration, as given by

$$\sigma_0 \leftarrow T^0 E_0 + T^R \langle \Psi_0 | H E_R | \Psi_0 \rangle, \tag{2.43}$$

$$\sigma_L \leftarrow T^0 \langle \Psi_0 | E^L H | \Psi_0 \rangle + T^R \langle \Psi_0 | E^L H E_R | \Psi_0 \rangle \tag{2.44}$$

where $\sigma = \{\sigma_0; \sigma_L\}$ and $\mathbf{T} = \{T^0; T^R\}$ are the σ-vector and trial Ritz vector in the non-orthonormal representation, respectively. Our primal development is to implement Eqs. (2.43) and (2.44) into efficient computer code. Their tensor contraction formulas, which are programmable mathematical expressions for computer implementation, can be derived systematically using Wick's theorem. However, the resulting formulae involve approximately as many as three thousand terms of tensor contraction. Such an exceedingly large number of terms cannot be easily derived and coded by hand. To resolve this difficulty, we developed a tensor generator that automates the manipulation of tensor terms and creates efficient computer code. These are rather straightforward, but definitely error-prone procedures.

A schematic diagram of the diagonalization procedure is shown in Fig. 2.1. The σ-vector in the non-orthonormal representation is transformed into the orthonormalized representation,

$$\tilde{\sigma}_P \leftarrow \frac{1}{\sqrt{\epsilon_P}} J_P^L \sigma_L \tag{2.45}$$

where $\mathbf{J}$ and ϵ are the unitary orthogonalization matrix and normalization factors, respectively. These are obtained as eigenvectors and eigenvalues of the overlap matrix $\mathbf{S}$ [Eq. (2.42)], respectively:

$$\mathbf{SJ} = \mathbf{J}\epsilon. \tag{2.46}$$

In forming $\mathbf{J}$ and ϵ from Eq. (2.46), the full diagonalization of the $\mathbf{S}$ matrix of the same size as the 3-RDM ($o^3 \times o^3$) is required for the semi-internal ($ooov$:E_{ik}^{ma}) and internal ($cooo$:E_{wi}^{km}) excitation blocks, demanding computational effort O(o^9). The redundant IC components associated with the eigenvectors with small eigenvalues are truncated in forming the orthonormalized IC bases. In the WK and CW ansatz, this o^9 procedure is avoided because the semi-internal and internal blocks are treated in the uncontracted basis.

2.2.7 The IC-ACPF and IC-AQCC

Lack of size-consistency is one of the primary drawbacks of the MRCI. This is due to the truncation of excitation classes at the level of single and double excitations.[115, 116, 117] Related to this, a size-consistency error is ascribed to the quadruple excitation manifolds, which are referred to as the exclusion principle violating (EPV) term and are

not considered in MRCI. Numerous attempts have been made to remedy this drawback of the MRCI. Generally, there are two strategies to recover this property without introducing further complexity: so-called *a posteriori* and *a priori* size-consistency corrections. The former type of the correction is referred to as the Davidson-type correction.[93, 94, 95, 96, 97] It can be obtained in a noniterative manner by rescaling the MRCI correlation energy at a cost of merely several flops. The latter type of correction is based on the correlation energy functional, including MR-ACPF and MR-AQCC proposed by Gdanitz and Ahrlichs[87, 88, 89] and by Szalay and Bartlett,[90, 91, 92] respectively, in which the correlation energy and CI amplitude are defined as the variational solution to minimize

$$F[C_0, \tilde{C}_P] := \frac{\langle \Psi_0 | \left(C_0 + E^{P'} \tilde{C}_{P'} \right) (H - E_0) \left(C^0 + \tilde{C}^P E_P \right) | \Psi_0 \rangle}{C_0 C^0 + \lambda \tilde{C}_P \tilde{C}^P} \tag{2.47}$$

and the wave function ansatz is given as

$$|\Psi\rangle := \left(C^0 + \tilde{C}^P E_P \right) |\Psi_0\rangle. \tag{2.48}$$

Here, the amplitude for the IC basis, $\tilde{C}^P$, is given in the orthonormalized representation. Several forms for the factor, λ in Eq. (2.47), have been derived so as to best approximate the effect of the EPV term on the basis of coupled-cluster or electron-pair theories.[118, 119] The explicit forms of λ are summarized in Table 2.3 for the functionals that are applicable with the IC framework. To the best of our knowledge, there are several other forms of functionals,[91, 120, 121, 122] including ACPF-2[88] and the total-energy-based functional for AQCC,[92] but they cannot be defined in the IC framework because their differences with the conventional ACPF and AQCC stem from the uncontracted representation of the variational space.

By differentiating the functional [Eq. (2.47)] with respect to C_0 and $\tilde{C_P}$ along with the stationary conditions,

$$\frac{\partial F}{\partial C_0} = 0, \frac{\partial F}{\partial \tilde{C_P}} = 0 \tag{2.49}$$

one readily obtains a set of projected equations

$$C^0 F = \tilde{C}^P \langle \Psi_0 | H E_P | \Psi_0 \rangle, \tag{2.50}$$

$$\lambda \tilde{C}^P F = C^0 \langle \Psi_0 | E^{P'} H | \Psi_0 \rangle + \tilde{C}^P \langle \Psi^0 | E^{P'} (H - E_0) E_P | \Psi_0 \rangle. \tag{2.51}$$

Then, expanding the amplitude as a linear combination of the Ritz vector,

$$\begin{pmatrix} C^0 \\ \tilde{C}^P \end{pmatrix} = \alpha^I \begin{pmatrix} T_I^0 \\ \tilde{T}_I^P \end{pmatrix} \tag{2.52}$$

the projected equations [Eqs. (2.50) and (2.51)] are transformed into the corresponding subspace equations

$$\alpha^I (E_0 T_I^0 + \langle \Psi_0 | H E_P | \Psi_0 \rangle \tilde{T}_I^P) = \alpha^I (E_0 + F) T_I^0, \tag{2.53}$$

$$\begin{aligned} \alpha^I (\langle \Psi_0 | E^{P'} H | \Psi_0 \rangle T_I^0 + \langle \Psi_0 | E^{P'} H + (1 - \lambda) F E_P | \Psi_0 \rangle \tilde{T}_I^P) \\ = \alpha^I (E_0 + F) \tilde{T}_I^P. \end{aligned} \tag{2.54}$$

By applying the transposed Ritz vector ($\tilde{\mathbf{T}}^J$) from the left side, the quasi-eigenvalue equation with respect to the Davidson mini-(or subspace-)Hamiltonian can be written as

$$\begin{aligned} \alpha^I \tilde{\mathbf{T}}^J \begin{pmatrix} E_0 & \langle \Psi_0 | H E_P | \Psi_0 \rangle \\ \langle \Psi_0 | E^{P'} H | \Psi_0 \rangle & \langle \Psi_0 | E^{P'} [H + (1 - \lambda) F] E_P | \Psi_0 \rangle \end{pmatrix} \tilde{\mathbf{T}}_I \\ = \alpha^I (E_0 + F), \end{aligned} \tag{2.55}$$

which apparently converges to that for the CISD equation if λ is set to unity. For the functionals other than the CISD type, Eq. (2.55) has to be solved iteratively due to the correlation energy dependence of the mini-Hamiltonian. The concomitant computational cost is negligibly small compared to that for constructing of the σ-vector.

2.3 Implementation

2.3.1 Automated tensor generation and implementation

The biggest difficulties in the development of the FIC-MRCI and its size-consistency-corrected variants (ACPF, AQCC, etc.) are the derivation and factorization of the σ-equations into a stream of binary contractions. They are translated into high-performance computer code, which can efficiently run on top of highly tuned matrix–matrix multiplication subroutines such as `DGEMM`. These procedures are rather straightforward but quite prone to errors. To address these issues, we developed an efficient tensor generator using the C++ language for rapid development of the complicated electronic structure theory.[123] Its predecessor, SQA, is available as supplemental material to Refs.[51, 52]. The following operations are processed by means of the newly developed tensor generator.

1. Expand σ-equations [Eqs. (2.43) and (2.44)] into programmable formulae according to Wick's theorem

2. Combine like terms (all the permutational symmetries are considered)

3. Factorize terms into a stream of binary contractions

4. Generate parallelized tensor contraction code

The first two steps are considerably easier compared with the last two because they are unambiguous. Nevertheless, the optimal way to factorize the tensor products into a sequence of binary contractions may depend on several external factors, such as speed of disk I/O, the kind of parallelization strategy, and the scheme of storage allocation of the tensor quantities. Hence, minimization of flop counts does not simply result in obtaining optimal tensor contraction patterns. Against this difficulty, we utilize heuristic algorithms so as to mimic the contraction patterns of our parallel CT code.[54] There are two points to be considered: loading the electron repulsion integrals (ERIs) from disk and constructing 4-RDM from lower-order ones. The latter always requires floating point manipulations, at least of $O(o^8)$ with huge prefactors for one time. In order to minimize these heavy manipulations by making them outermost procedures in loop-structures, priority weights are defined, and values of the weights for loading ERIs and for cumulant reconstruction of 4-RDM are set so those operations are always of top priority. In the resultant implementation, the floating-point operations of binary contractions involving 4-RDM formally scale as $O(co^8)$, $O(o^9)$ and $O(o^8v)$. In computing a single σ-vector, the cumulant construction of the 4-RDM is repeated a constant number of times, which is favorably independent of the number of orbitals. Further, tensors whose sizes are less than or equal to o^6 are stored in memory in the current implementation; these refer to 1-, 2-, 3-RDMs and other intermediate arrays. All tensor contractions involving the ERIs are parallelized on top of the message passing interface (MPI) with respect to the first MO index of four-index ERIs.

Let us here discuss the factorization pattern of the contractions for 4-RDM in some detail. This process is key to efficient implementation of tensor contractions for computing the σ-vector where 4-RDM is constructed on-the-fly with the cumulant approximation. It is difficult to develop efficient subroutines for cumulant reconstruction using a vectorized subroutine such as `DGEMM`, because of its direct-product nature. Hence, the performance of the tensor contraction code in constructing the σ-vector becomes quite sensitive to the loop structure used in this procedure. In the σ-equation of our FIC-cu(4)-MRCI, there are 38 tensor contraction terms that all involve 4-RDM. Among these, 26 terms require either $O(co^8)$, $O(o^9)$ or $O(o^8v)$ flop counts, involving cumulant reconstruction; these manipulations dominate the total required computational time for large active space calculations. We here introduce the contracted 4-RDMs,

$$(\Gamma_A)^{kl}_{gh} \leftarrow D^{klmn}_{ghij} V^{ij}_{mn}, \tag{2.56}$$

$$(\Gamma_B)^{klm}_{ghp} \leftarrow D^{klmn}_{ghij} V^{ij}_{pn}, \tag{2.57}$$

which can be calculated with $O(o^8)$ and $O(o^8 \times (c + o + v))$ flop counts, respectively. It is found that 32 out of the 38 binary contractions can replaced by these predefined tensors. The construction of Γ_A and Γ_B is performed once in a single FIC-cu(4)-MRCI calculation outside the iterative Davidson procedure, whereas it is the heaviest tensor contraction in the FIC-cu(4)-MRCI. The Γ_A tensor [Eq. (2.56)] is stored in memory while the Γ_B tensor [Eq. (2.57)] is written to disk for each value of the index p, which runs over all MOs, and read from disk when they are necessary. Due to this factorization, the number of the tensor contraction terms that actually involve 4-RDM in the σ-vector

calculation can be reduced to only six. In each of the these six contraction terms, the cumulant reconstruction involving $O(o^8)$ flop counts is carried out once for a single σ vector calculation, so that they are no longer the bottleneck in constructing the σ-vector.

The generated tensor contraction code to evaluate the σ-equations and diagonal preconditioner elements are interfaced to the hand-coded block-Davidson solver, which is a main routine in the FIC-cu(4)-MRCI program. In a setup procedure in the FIC-cu(4)-MRCI program, the data files containing the 1-, 2-, 3-RDMs are restored from hard drives. They serve as a joint between the DMRG and FIC-cu(4)-MRCI calculations; in the DMRG-cu(4)-MRCI procedure, the FIC-cu(4)-MRCI uses the RDM data provided by the preceding DMRG calculation. The DMRG-cu(4)-MRCI code is implemented in ORZ package, our in-house electronic-structure program suite. The explicit formulae of the FIC-cu(4)-MRCI are attached to this article as supplementary material[110].

Indices of the core MOs in the RDM are excluded by using the killer conditions, $a_w^\dagger|\Psi_0\rangle = 0$; thus, the RDMs are decomposed into a product of lower-rank one and Kronecker's deltas. For instance,

$$D_{iw}^{yj} = -\,\delta_w^y D_i^j, \tag{2.58}$$

$$D_{vkw}^{xyi} = D_k^i(\delta_v^y\delta_w^x - 2\,\delta_v^x\delta_w^y). \tag{2.59}$$

In addition, the RDM with external indices vanishes because of another killer condition, $a_a|\Psi_0\rangle = 0$. Therefore, in our implementation, only active indices are left in the RDM, providing computational efficacy by the exclusion of core indices.

2.3.2 Truncation of the IC basis: Avoidance of variational collapse

When the cumulant approximation is employed in the 4-RDM, serious variational collapses may occur in some cases; the lowest energy root of the IC-MRCI equation [Eq. (2.34)] is determined to be completely unlike the true solution for the ground state, and the value of C_0 (reference weight) almost vanishes. When the variational collapse occurs, the trial eigenvalue of the Hamiltonian continues to go down during the block-Davidson procedure, typically converging to a value that is lower than the energy of the reference state by one order magnitude or more. In some cases, with vanishing C_0, the obtained energy happens to be plausible for the solution of the MRCI. According to our experiences, when the value of C_0 results in near zero, one should suspect that the variational collapse occurs. This phenomenon arises from the fact that the cumulant-approximated RDM is no longer N-representable. Therefore, as long as the cumulant approximation is employed in framework of the variational theory such as MRCI, the variational collapse is essentially non-negligible. This problematic behavior can possibly be remedied by truncating the IC basis with small ϵ_P [Eq. (2.45)] less than a given cutoff threshold (which is denoted by τ). This truncation introduces extra errors in the values of the energy and wave function. We determined that the truncation threshold $\tau = 1.0 \times 10^{-2}$ would be sufficient to avoid variational collapses as long as one seeks the ground state wave function in the near-equilibrium geometry.

As demonstrated in Sec. 2.4.4 for stretched geometries, this value for the cutoff thresh-

old may be insufficient to avoid variational collapses. Then, a much stronger truncation with larger τ is needed to stabilize the solution, while the truncation in return gives rise to errors in CI space.

2.4 Benchmark sets and application

We performed several benchmark calculations on illustrative chemical systems. The scalability of DMRG-cu(4)-MRCI was assessed by employing a polyene chain as a benchmark set. The singlet and triple energies of the free-base porphyrin molecule were evaluated using DMRG-MRCI with CAS(26e,24o), which is the record of the largest reference space ever used in MRCI calculations. Errors caused by the FIC representation and neglect of four-rank cumulant in 4-RDM were examined in the calculation of bond dissociation of a nitrogen molecule. The WK- and CW-MRCI calculations were performed using MOLPRO program suite, version 2012.1,[23] in serial execution. The development version of the ORZ program package was used for DMRG-CASSCF, DMRG-cu(4)-MRCI, DMRG-cu(4)-ACPF and DMRG-CASPT2 calculations. All the data sets are available as supplementary material to this work[110].

2.4.1 Polyene: $\mathbf{C_nH_{n+2}}$, CAS(ne, no)

To demonstrate scalability of the FIC-cu(4)-MRCI, computational times for a polyene chain from C_6H_8 to $C_{24}H_{26}$ were measured. All π MOs were included in the active space, e.g. CAS(24e, 24o) for $C_{24}H_{26}$, for this benchmark. The 1s orbitals of C atoms

were frozen. Structures of these molecules were optimized by using the CAM-B3LYP density functional[124] with 6-31G* basis set.[125] All calculations were performed in C_{2h} symmetry by using 6-31G* basis set. Fig. 2.2 and Table 2.4 show the computational times per iteration for FIC-cu(4)-MRCI and for MRCI based on the WK and CW contraction schemes. Timings of construction of the contracted 4-RDM [Γ_B of Eq. (2.57)] are included in Table 2.4.

The FIC-cu(4)-MRCI calculations were performed on top of an MPI-based parallelization using three computer cluster nodes; each node has two Intel® Xeon® X5660 processors of 2.80 GHz and 96 gigabytes of memory. The WK- and CW-MRCI calculations were performed on the same machine. Computational timings for the WK- and CW-MRCIs were taken as the differences between the times at which the first and second iterations finished. The WK-MRCI could not be applied to polyenes larger than C_8H_{10} due to limitations on computer time. Moreover, memory capacity was insufficient for the CW-MRCI calculation on $C_{16}H_{16}$ or larger.

For this benchmark set, the computational times for the WK-MRCI were fit to an exponential function, revealing that the WK scheme scaled by $6.3 \times 10^{-4} \exp(2.26o)$ (in seconds); on transition from C_6H_8 to C_8H_{10}, the computational time increased by about a factor of 90. For $C_{10}H_{12}$, the first iteration of WK-MRCI took about 4×10^5 seconds even though in the first iteration several computational procedures were skipped. This leads to a drastic reduction in computational time compared with the second and third iterations. The CW-MRCI exhibited impressive performance when the active space was sufficiently small, about 8.5 times faster than FIC type for C_8H_{10}. Although for $C_{12}H_{14}$

the CW-MRCI remained substantially efficient, computational time rose quite steeply and its scaling was $4.4 \times 10^{-3} \exp(1.01o)$.

CW-MRCI surpassed FIC-MRCI in computational time for smaller cases up to $C_{12}H_{14}$. However, the WK- and CW-contracted types showed steep increases in computational times because of the exponential dependence that comes from the uncontracted treatment. In contrast, the computational time of the FIC-MRCI increased rather slowly in a polynomial order. The timing of FIC-MRCI was found to be $5.8 \times 10^{-3} o^{4.69}$ seconds in a range between C_6H_8 and $C_{12}H_{14}$, and $5.2 \times 10^{-6} o^{7.42}$ seconds in a range between $C_{14}H_{16}$ to $C_{24}H_{26}$. Construction of the contracted 4-RDM $[\mathbf{\Gamma_B}]$ (Eq. (2.57)) scaled by $1.6 \times 10^{-5} o^{6.73}$ (in seconds) from C_6H_8 to $C_{12}H_{14}$, and $6.2 \times 10^{-8} o^{9.00}$ (in seconds) from $C_{14}H_{16}$ to $C_{24}H_{26}$; this shows that the observed scaling converges to the formal one ($O(o^9)$). The scaling for constructing the σ-vector was found to converge to $O(o^{7.5})$, while its formal scaling is $O(o^9)$. We deduced that the true bottleneck of the calculation did not appear in this benchmark set.

2.4.2 The basis set dependence

In this section, dependence of computational time on the size of the basis set is presented using $C_{12}H_{14}$ and $C_{16}H_{18}$ molecules for benchmark test. We employed three different basis sets (6-31G*, 6-311G* and 6-311G**[126]). The computer cluster nodes described in Sec. 2.4.1 were used here. In Fig. 2.3 and Table 2.5, the computational time per iteration is shown for each number of the MOs. The setting of the calculations regarding frozen cores and active space was the same as configured in Sec. IV A. For the $C_{12}H_{14}$,

the figure shows that the computational time (in seconds) scales by $9 \times 10^{-7} N^{3.93}$, while for $C_{16}H_{18}$, the scaling is $1 \times 10^{-5} N^{3.64}$ where N refers to the number of total MOs. These results suggest that overall computational times are dominated by the tensor contractions that involve at least three external MO indices. In the σ-equations, binary contractions with the four external indices take the form of a product of the amplitude and ERIs,

$$W_{ik}^{ca} \leftarrow T_{ik}^{bd} V_{cd}^{ab} \tag{2.60}$$

or

$$W_{wy}^{ac} \leftarrow T_{wy}^{bd} V_{cd}^{ab} \tag{2.61}$$

where W represents the intermediate tensor; hence, these contractions require floating point operations of $O(c^2v^4)$, or $O(o^2v^4)$. In contrast, binary contractions with three external indices do not always appear as a product of the amplitude and ERIs,

$$W_{wy}^{ac} \leftarrow T_{yi}^{ba} W'^{cb}_{wi}. \tag{2.62}$$

The complexity of Eq. (2.62) is $O(c^2ov^3)$. In addition, there are several other types of contraction patterns, similar to Eq. (2.62) that scale as $O(c^3v^3)$, $O(co^2v^3)$ or $O(o^3v^3)$. Even though contractions such as Eqs. (2.60) – (2.62) can be parallelized throughout all nodes without any waste of CPU time in this computer configuration, they still serve as rate-determining steps.

To address this point, we are planning to extend our code generator so as to be able to use the so-called external exchange operator (EEO) type contraction technique that is implemented in MOLPRO suite[127]. In addition, use of density-fitting (DF) instead of

the ERIs themselves may possibly overcome these bottlenecks in tensor contractions[128, 129, 130, 131, 132].

2.4.3 Free-base porphyrin: Singlet–Triplet gap

To assess the accuracy of the DMRG-cu(4)-MRCI, we calculated the energy gap between the lowest singlet and triplet states of the free-base porphyrin molecule ($C_{20}H_{14}N_4$). All out-of-plane 2p orbitals of C and N were used in the active space (CAS(26e, 24o)). Because the observation of the S-T (single-triplet) gap was based on a phosphorescence assay, the relaxed geometry was employed for the triplet state. For both singlet and triplet states, geometry optimization was performed using the UB3LYP functional[133] and the 6-31G* basis set with the GAUSSIAN09 program package.[134] The symmetry of the lowest triplet state was taken as B_{2u}.

We also performed the S-T gap calculation with a smaller active space, CAS(8e, 8o), and compared the results to those from the full valence DMRG-cu(4)-MRCI calculations. The setting of this small CAS was (5-6b_{3u}; 2-3a_u; 3-4b_{1g}; 3-4b_{2g}). We confirmed that this reproduces the CAS treatment in Ref.[135].

The starting reference description with CAS(26e, 24o) was calculated using the DMRG-CASSCF method. In the DMRG procedure, a Pipek–Mezey localization[136] was applied to the out-of-plane 2p orbitals, which were then arranged to form the lattice sites of the DMRG state. The one-dimensional DMRG ordering of the localized MOs, as well as their shapes, are given as supplementary material.[110] In the orbital optimization and generation of the RDMs, 1024 DMRG states were used. In the MRCI, ACPF, and CASPT2

calculations, the C and N 1s orbitals were not correlated. Thus, the orbital space for the multireference calcualtions consisted of 44 core, 24 active and 272 virtual MOs. For the DMRG-cu(4)-MRCI and DMRG-cu(4)-ACPF treatments, the overlap truncation was used with the threshold of $\tau = 1.0 \times 10^{-2}$.

In Table 2.6, the total energies of the S_0 and T_0 states and the S-T gap are shown for the free-base porphyrin. For reference, the CASPT2 value from Roos et. al.[137] and the diffusion Monte Carlo (DMC) value from Aspuru-Guzik et. al.[138] are also shown; the former corresponds to the vertical excitation from S_0 to T_0. It is notable that by involving all out-of-plane 2p electrons and orbitals in the active space, the CASSCF and MRCI values descrease by 0.39 and 0.34 eV, respectively, relative to the CAS(8e, 8o) counterparts. In comparison, the difference in CASPT2 between two tested active spaces is 0.08 and 0.21 eV with and without the IPEA shift (0.25)[139], respectively. By increasing the size of the active space, CASPT2 was found to be in good agreement with the experimental value. However, when using 0.25 for the IPEA shift value, the CASPT2(26e,24o) result is away from the experimental value by approximately 0.15 eV. This odd behavior suggests that the considerably good agreement for the CASPT2 calculation is more of a coincidence rather than substantial. Note that use of this IPEA value is considered to be the present *de facto* standard in the CASPT2 methodology.

If the smaller active space is used, the MRCI value (1.75 eV) deviates from the experimental and DMC values by approximately 0.19 eV, and this discrepancy cannot be corrected by adding the Davidson correction. However, by including all out-of-plane 2p electrons and orbitals in the active space, the MRCI value is improved drastically,

resulting in 1.41 eV. The MRCI+Q (1.53 eV) and the ACPF (1.55 eV) produce values very similar to the experimental one (1.58 eV). Note that the solvent effect is not included in any of the theoretical methods in Table 2.6.

2.4.4 Comparison to WK-MRCI

The accuracy of FIC-MRCI correlation energy relative to the WK type was tested in the bond dissociation curve of a nitrogen molecule. In Fig. 2.4, the deviations are shown for FIC-MRCI and FIC-ACPF with CAS($6e$, $6o$). In the reference space, two σ and four π MOs formed from $2p$ orbitals were considered, and 2s orbitals were set to the correlated core MOs while the 1s orbitals remained frozen, namely uncorrelated. All calculations were performed in D_{2h} symmetry by using aug-cc-pVTZ.[140, 141] When the exact 4-RDM was used, we found that FIC-MRCI tends to produce slightly lower correlation energies (and higher total energies) than WK in a range of 1.0 – 1.5 mEh in accordance with the variational theorem. However, ACPF shows somewhat different behavior. The stationary functional of ACPF [Eq. (2.47)] does not always lead to an upper-bound on the true energy spectrum because the λ coefficient is basically an approximation to recover EPV terms. When the cumulant-based 4-RDM was used with a cutoff threshold ($\tau = 1.0\times10^{-2}$) for forming the IC basis, the errors caused by the cumulant approximation were negligibly small for bond length shorter than R_e (1.1208Å). However, for bond length longer than R_e, variational collapses occurred. By raising the threshold τ to 1.0×10^{-1}, the variational collapse was circumvented though the notable errors associated with the truncation of IC basis were observed at the near equilibrium bond distance. For bond

length longer than 2.6 Å, magnitudes of the errors associated with the cumulant reduction increased drastically for MRCI and ACPF, reaching approximately 12.00 and 21.14 mEh, respectively, with two tested cutoffs for τ.

Next, we added to the active space the two σ MOs from $2s$ orbitals of nitrogen, having CAS(8e, 8o). We then repeated the assessment with this reference. The results are plotted in the Fig. 2.5. The tendencies in Fig. 2.5 are similar to those in Fig. 2.4 for CAS(6e, 6o), but the magnitudes of the errors decreased, becoming about five times smaller. Note that the variational collapse was recovered at bond length from 1.3 to 1.6 Å. This indicates that enlargement of active space helps improve the accuracy and stability of the cumulant-approximated MRCI solutions.

2.4.5 Comparison to full CI energy

In Fig. 2.6, energy differences relative to full CI values are shown for a nitrogen molecule with the cc-pVDZ basis set. For this assessment, CAS(6e, 6o), the same active space as in Sec. 2.4.4, was used for FIC-MRCI and FIC-ACPF calculations. The full CI and uncontracted MRCI energies were taken from Ref.[142]. When using the exact 4-RDM, the FIC-MRCI calculations produced, for all the bond lengths, somewhat higher values than the uncontracted MRCI using Kállay's string-based `MRCC` program;[143, 143] this behavior is consistent with the variational theorem. Considering size-consistency corrections (+Q correction and ACPF), the errors from full CI almost vanish. The correlation energies of MRCI with the cumulant-approximated 4RDM fall below those of the uncontracted type with R(N-N) $\geq$ 2.225Å (4.2a$_0$), indicating that the they are not a variational

solution. With cumulant-based 4-RDM, the results of MRCI+Q and ACPF are similar to those of the MRCI within an error of 0.01 mEh.

2.5 Conclusion

In this study, we have formulated a multireference approach that combines the *ab initio* DMRG and MRCI methods. The utilization of the FIC scheme is a key to the smooth connection between these two methods. The five-rank (ten-index) RDM, taken into account in the semi-internal and the internal excitation blocks of the Hamiltonian, is eliminated exactly by means of a commutator-based reduction technique. As a consequence, tensor contractions involving the 5-RDM, whose size grows at the rate of o^{10}, are no longer necessary. The remaining 4-RDM is approximated by neglecting the cumulants of rank four; thus, the σ-vector can be represented using the 1–3 rank RDMs. However, it is impossible to manually derive and implement the working equations of the FIC-MRCI theory because those programmable expressions are composed of approximately three thousand monstrous tensor contractions. Therefore, we have adopted an automated technique for resolving this difficulty, just as in the previous development of the CW-MRCI method,[17] which rather uses a weaker contraction scheme than ours. We have developed an efficient code generator on the basis of normal ordering in terms of the spin-free unitary group generator.

This generator derives all working equations and then transforms them into parallelized tensor contraction code on top of vectorized linear algebra subroutines. Even

though there is still plenty of room for optimizing the generated code, we find that the existing code can already be used at the production level.

The computational time of FIC-MRCI is of polynomial order in the molecular size, whereas the WK and CW variants scale exponentially with increasing complexity of the variational space. In addition, the DMRG-cu(4)-MRCI, a combined approach of *ab initio* DMRG and FIC-MRCI using cumulant reconstruction of 4-RDM, was applied to calculate the singlet-triplet gap for the porphyrin molecule using full valence π orbitals, namely 24 orbitals, in CAS. To the best of our knowledge, this is the largest reference space ever used in the MRCI, MRCI+Q and MR-ACPF calculations. The Davidson-corrected DMRG-cu(4)-MRCI and DMRG-cu(4)-ACPF were found to give results in considerably reasonable agreement with experimental values measured by phosphorescence observation.

Our MRCI is an approximation to the conventional uncontracted MRCI in the sense that the four-rank cumulant is neglected and the wave function is constructed thoroughly from the IC basis. Errors caused by these approximations were assessed in illustrative calculations of a nitrogen molecule with various bond lengths; the magnitude of the errors were merely of milli-hartree order. Even so, because the neglect of the cumulants violates N-representability, the cumulant approximation to 4-RDM often causes a variational collapse. Near the equilibrium bond length, this phenomenon is shown to be readily avoidable using a relatively small value for the truncation threshold ($\tau = 1.0 \times 10^{-2}$). Also for the practical applications, error caused by the cumulant approximations is found to be negligibly small.

In conclusion, the DMRG-MRCI was shown to be a highly scalable MRCI theory. However, the ninth-power scaling with molecular size ($O(N^9)$) may still hinder its routine application to chemically interesting systems, such as the isomerization reactions of the Cu_2O_2 complexes which may require the 28 electrons and 32 MOs in the active space. For practical applications, use of the DF technique is under investigation for improving the efficacy of our code. In addition, the tensor generator, developed as a byproduct of this work, is designed to be applicable to any ansatz, including the perturbative, coupled-cluster, or canonical-transformation types.

Bibliography

[1] S. Wilson, *Electron Correlation In Molecules*, Dover Publications, New York, 1984.

[2] J. Simons and J. A. Nichols, *Quantum mechanics in chemistry*, Oxford University Press New York, 1997.

[3] J. Cizek, J. Chem. Phys. **45**, 4256 (1969).

[4] J. Paldus, J. Cizek, and I. Shavitt, Phys. Rev. A **5**, 50 (1972).

[5] R. J. Bartlett, Annu. Rev. Phys. Chem. **32**, 359 (1981).

[6] R. J. Bartlett and M. Musiał, Rev. Mod. Phys. **79**, 291 (2007).

[7] R. J. Buenker and S. D. Peyerimhoff, Theor. Chim. Acta. **35**, 33 (1974).

[8] R. J. Buenker and S. D. Peyerimhoff, Theor. Chim. Acta. **39**, 217 (1975).

[9] H. Lischka et al., Phys. Chem. Chem. Phys. **3**, 664 (2001).

[10] H. Lischka et al., WIREs. Comput. Mol. Sci. **1**, 191 (2011).

[11] P. G. Szalay, T. Müller, G. Gidofalvi, H. Lischka, and R. Shepherd, Chem. Rev. **112**, 108 (2012).

[12] A. Venkatnathan, A. B. Szilva, D. Walter, R. J. Gdanitz, and E. A. Carter, J. Chem. Phys. **120**, 1693 (2004).

[13] D. B. Krisiloff and E. A. Carter, Phys. Chem. Chem. Phys. **14**, 7710 (2011).

[14] H.-J. Werner and E. A. Reinsch, J. Chem. Phys. **76**, 3144 (1982).

[15] H.-J. Werner and P. J. Knowles, J. Chem. Phys. **89**, 5803 (1988).

[16] P. J. Knowles and H.-J. Werner, Chem. Phys. Lett. **145**, 514 (1988).

[17] K. R. Shamasundar, G. Knizia, and H.-J. Werner, J. Chem. Phys. **135**, 054101 (2011).

[18] T. Shiozaki, G. Knizia, and H.-J. Werner, J. Chem. Phys. **134**, 034113 (2011).

[19] T. Shiozaki and H.-J. Werner, J. Chem. Phys. **134**, 184104 (2011).

[20] F. Neese, J. Chem. Phys. **119**, 9428 (2003).

[21] M. Hanrath and B. Engels, Chem. Phys. **225**, 197 (1997).

[22] W. Meyer, *Modern Theoretical Chemistry*, Plenum, New York, 1977.

[23] H.-J. Werner, P. J. Knowles, G. Knizia, F. R. Manby, and M. Schütz, WIREs. Comput. Mol. Sci. **2**, 242 (2012).

[24] S. R. White, Phys. Rev. Lett. **69**, 2863 (1992).

[25] S. R. White, Phys. Rev. B **48**, 10345 (1993).

[26] S. R. White and R. L. Martin, J. Chem. Phys. **110**, 4127 (1999).

[27] A. O. Mitrushenkov, G. Fano, F. Ortolani, R. Linguerri, and P. Palmieri, J. Chem. Phys. **115**, 6815 (2001).

[28] G.-L. Chan and M. Head-Gordon, J. Chem. Phys. **116**, 4462 (2002).

[29] G. K.-L. Chan and M. Head-Gordon, J. Chem. Phys. **118**, 8551 (2003).

[30] J. Hachmann, W. Cardoen, , and G. K.-L. Chan, J. Chem. Phys. **125**, 144101 (2006).

[31] J. Hachmann, J. J. Dorando, M. Avilés, and G. K.-L. Chan, J. Chem. Phys. **127**, 134309 (2007).

[32] K. H. Marti, I. M. Ondík, G. Moritz, and M. Reiher, J. Chem. Phys. **128**, 014104 (2008).

[33] D. Zgid and M. Nooijen, J. Chem. Phys. **128**, 014107 (2008).

[34] Y. Kurashige and T. Yanai, J. Chem. Phys. **130**, 234114 (2009).

[35] G.-L. Chan and D. Zgid, Ann. Rep. Comput. Chem. **5**, 149 (2009).

[36] W. Mizukami, Y. Kurashige, and T. Yanai, J. Chem. Phys. **133**, 091101 (2010).

[37] G. K.-L. Chan and S. Sharma, Ann. Rev. Phys. Chem. **62**, 465 (2011).

[38] S. Sharma and G. K.-L. Chan, J. Chem. Phys. **136**, 124121 (2012).

[39] W. Mizukami, Y. Kurashige, and T. Yanai, J. Chem. Theory Comput. **9**, 401 (2013).

[40] D. Zgid and M. Nooijen, J. Chem. Phys. **128**, 144116 (2008).

[41] S. Sharma and G. K.-L. Chan, J. Chem. Phys. **136**, 124121 (2012).

[42] D. Zgid and M. Nooijen, J. Chem. Phys. **128**, 144115 (2008).

[43] D. Ghosh, J. Hachmann, T. Yanai, and G. K.-L. Chan, J. Chem. Phys. **128**, 144117 (2008).

[44] Y. Kurashige and T. Yanai, J. Chem. Phys. **135**, 094104 (2011).

[45] Y. Kurashige, J. Chalupský, T. N. Lan, and T. Yanai, *unpublished* .

[46] B. O. Roos, P. R. Taylor, and P. E. Siegbahn, Chem. Phys. **48**, 157 (1980).

[47] B. O. Roos, Adv. Chem. Phys. **69**, 399 (1987).

[48] T. Yanai, Y. Kurashige, D. Ghosh, and G. K.-L. Chan, Int. J. Quantum Chem. **109**, 2178 (2009).

[49] T. Yanai and G. K.-L. Chan, J. Chem. Phys. **124**, 194106 (2006).

[50] T. Yanai and G. K.-L. Chan, J. Chem. Phys. **127**, 104107 (2007).

[51] E. Neuscamman, T. Yanai, and G. K.-L. Chan, J. Chem. Phys. **130**, 124102 (2009).

[52] E. Neuscamman, T. Yanai, and G. K.-L. Chan, J. Chem. Phys. **130**, 169901 (2009).

[53] E. Neuscamman, T. Yanai, and G. K.-L. Chan, J. Chem. Phys. **132**, 024106 (2010).

[54] Y. Yanai, Y. Kurashige, E. Neuscamman, and G. K.-L. Chan, Phys. Chem. Chem. Phys. **14**, 7809 (2012).

[55] K. Andersson, P.-Å. Malmqvist, B. O. Roos, A. J. Sadlej, and K. Wolinski, J. Phys. Chem. **94**, 5483 (1990).

[56] K. Andersson, P.-Å. Malmqvist, and B. O. Roos, J. Chem. Phys. **96**, 1218 (1992).

[57] T. Yanai, Y. Kurashige, E. Neuscamman, and G. K.-L. Chan, J. Chem. Phys. **132**, 024105 (2010).

[58] P. E. M. Siegbahn and M. Svensson, Int. J. Quantum Chem. **41**, 153 (1992).

[59] P. Celani and H.-J. Werner, J. Chem. Phys. **112**, 5546 (2000).

[60] P. Celani and H.-J. Werner, J. Chem. Phys. **119**, 5044 (2003).

[61] T. Shiozaki, W. Győffy, P. Celani, and H.-J. Werner, J. Chem. Phys. **135**, 081106 (2011).

[62] W. Győffy, T. Shiozaki, G. Knizia, and H.-J. Werner, J. Chem. Phys. **138**, 104104 (2013).

[63] H.-J. Werner, Mol. Phys. **89**, 645 (1996).

[64] T. Shiozaki and H.-J. Werner, J. Chem. Phys. **133**, 141103 (2010).

[65] Personal communication with Prof. Dr. T. Shiozaki and Prof. Dr. K. R. Shamasundar.

[66] L. Kong and E. F. Valeev, J. Chem. Phys. **131**, 214105 (2011).

[67] W. Kutzelnigg and D. Mukherjee, J. Chem. Phys. **107**, 432 (1997).

[68] F. C. C. P. del Valle, , and C. Valdemoro, Phys. Rev. A **47**, 971 (1993).

[69] F. Colmenero and C. Valdemoro, Phys. Rev. A **47**, 979 (1993).

[70] D. Zgid, D. Ghosh, E. Neuscamman, and G. K.-L. Chan, J. Chem. Phys. **130**, 194107 (2009).

[71] K. R. Shamasundar, J. Chem. Phys. **131**, 174109 (2009).

[72] W. Kutzelnigg, K. R. Shamasundar, and D. Mukherjee, Mol. Phys. **108**, 433 (2010).

[73] M. Hanauer and A. Köhn, Chem. Phys. **401**, 50 (2012).

[74] S. Hirata, J. Phys. Chem. A **107**, 9887 (2003).

[75] S. Hirata, J. Chem. Phys. **121**, 51 (2004).

[76] S. Hirata, Theor. Chem. Acc. **116**, 2 (2006).

[77] A. Engels-Putzka and M. Hanrath, J. Chem. Phys. **134**, 124106 (2011).

[78] C. L. Janssen and H. F. Schaefer, Theor. Chim. Acta. **79**, 1 (1991).

[79] A. Köhn, J. Chem. Phys. **130**, 104104 (2009).

[80] A. Köhn, J. Chem. Phys. **130**, 131101 (2009).

[81] M. Hanauer and A. Köhn, J. Chem. Phys. **131**, 124118 (2009).

[82] M. Hanauer and A. Köhn, J. Chem. Phys. **134**, 20411 (2011).

[83] T. Shiozaki, M. Kamiya, S. Hirata, and E. F. Valeev, J. Chem. Phys. **129**, 071101 (2008).

[84] T. Shiozaki, M. Kamiya, S. Hirata, and E. F. Valeev, Phys. Chem. Chem. Phys. **10**, 3358 (2008).

[85] T. Shiozaki, M. Kamiya, S. Hirata, and E. F. Valeev, J. Chem. Phys. **130**, 054101 (2009).

[86] T. Shiozaki, M. Kamiya, S. Hirata, and E. F. Valeev, J. Chem. Phys. **131**, 044118 (2009).

[87] R. Gdanitz and R. Ahlrichs, Chem. Phys. Lett. **143**, 413 (1988).

[88] R. Gdanitz, Intern. J. Quantum Chem. **85**, 281 (2001).

[89] W. Cardoen and R. Gdanitz, Chem. Phys. Lett. **364**, 39 (2002).

[90] P. G. Szalay and R. J. Bartlett, Chem. Phys. Lett. **214**, 481 (1993).

[91] L. Füsti-Molnár and P. G. Szalay, J. Chem. Phys. **100**, 6288 (1996).

[92] P. G. Szalay, Chem. Phys. **349**, 121 (2008).

[93] S. R. Langnoff and E. R. Davidson, Intern. J. Quantum Chem. **8**, 61 (1974).

[94] E. R. Davidson and D. W. Silver, Chem. Phys. Lett. **52**, 403 (1977).

[95] K. A. Brueckner, Phys. Rev. **100**, 36 (1955).

[96] J. A. Pople and R. Krishnan, Intern. J. Quantum Chem. **S11**, 149 (1977).

[97] L. Meissner, Chem. Phys. Lett. **146**, 204 (1988).

[98] W. Kutzelnigg, J. Chem. Phys. **77**, 3081 (1982).

[99] W. Kutzelnigg and S. Koch, J. Chem. Phys. **79**, 4315 (1983).

[100] W. Kutzelnigg, J. Chem. Phys. **80**, 822 (1982).

[101] J. Paldus, J. Chem. Phys. **61**, 5321 (1974).

[102] I. Shavitt, Int. J. Quantum Chem. **S11**, 131 (1977).

[103] I. Shavitt, Int. J. Quantum Chem. **S12**, 5 (1978).

[104] W. Duch and J. Karwowski, Int. J. Quantum Chem. **22**, 783 (1982).

[105] F. Colmenero and C. Valdemoro, Int. J. Quantum Chem. **51**, 369 (1994).

[106] K. Yasuda and H. Nakatsuji, Phys. Rev. Lett. **76**, 1039 (1996).

[107] K. Yasuda and H. Nakatsuji, Phys. Rev. A **56**, 2648 (1997).

[108] D. A. Mazziotti, Phys. Rev. A **57**, 4219 (1998).

[109] D. A. Mazziotti, Chem. Phys. Lett. **298**, 419 (1998).

[110] See Supplementary Material Document No. XXXXXXX for the programmable equations of the full IC-MRCI, FORTRAN subroutine to calculate 4-RDM my using the spin-free cumulant expansion and for computational details.

[111] A. J. Coleman, Rev. Mod. Phys. **35**, 668 (1963).

[112] E. R. Davidson, *Reduced Density Matrices in Quantum Chemistry*, Academic Press, New York, 1976.

[113] A. J. Coleman and V. I. Yukalov, *Reduced Density Matrices: Coulson's Challenge*, Springer-Verlag, New York, 2000.

[114] E. R. Davidson, J. Comput. Phys. **17**, 87 (1975).

[115] R. J. Bartlett, J. Phys. Chem. **93**, 1697 (1989).

[116] R. J. Bartlett and G. D. Purvis, Intern. J. Quantum Chem. **S11**, 149 (1977).

[117] G. D. Purvis and R. J. Bartlett, J. Chem. Phys. **76**, 1910 (1982).

[118] R. Ahlrichs, P. Scharf, and C. Ehrhardt, J. Chem. Phys. **82**, 15 (1984).

[119] D. P. Chong and S. R. Langhoff, J. Chem. Phys. **84**, 15 (1984).

[120] J. P. Malrieu, J. P. Daudey, and R. Caballol, J. Chem. Phys. **101**, 8908 (1994).

[121] J. Meller, J. P. Malrieu, and J. L. Heully, Mol. Phys. **101**, 2029 (2003).

[122] R. Fink and V. Staemmler, Theor. Chim. Acta. **87**, 129 (1993).

[123] FEMTO :: An Integrated Toolset For The Automated Tensor Generation, Version 0.1.0, M. Saitow (https://github.com/msaitow).

[124] T. Yanai, D. P. Tew, and N. C. Handy, Chem. Phys. Lett. **393**, 51 (2004).

[125] P. C. Hariharan and J. A. Pople, Theor. Chim. Acta. **28**, 213 (1973).

[126] R. Krishnan, J. S. Binkley, R. Seeger, and J. A. Pople, J. Chem. Phys. **72**, 650 (1980).

[127] P. Knowles, M. Schütz, and H.-J. Werner, NIC Series **3**, 97 (2000).

[128] J. L. Whitten, J. Chem. Phys. **58**, 4496 (1973).

[129] B. I. Dunlap, J. W. D. Connolly, and J. R. Sabin, J. Chem. Phys. **71**, 3396 (1979).

[130] M. Feyereisen, G. Fiztgerald, and A. Komornick, Chem. Phys. Lett. **208**, 359 (1993).

[131] O. Vahtras, J. Almlöf, and M. W. Feyereisen, Chem. Phys. Lett. **213**, 514 (1993).

[132] R. A. Kendall and H. A. Früchtl, Theor. Chem. Acc. **97**, 158 (1997).

[133] A. D. Becke, J. Chem. Phys. **98**, 5648 (1993).

[134] M. J. Frisch et al., Gaussian 09 Revision C.1, Gaussian Inc. Wallingford CT 2009.

[135] M. Merchán, E. Ortí, and B. O. Roos, Chem. Phys. Lett. **226**, 27 (1994).

[136] J. Pipek and P. G. Mezey, J. Chem. Phys. **90**, 4919 (1989).

[137] L. Serrano-Andrés, M. Merchán, M. Rubio, and B. O. Roos, Chem. Phys. Lett. **295**, 195 (1998).

[138] A. Aspuru-Guzik, O. E. Akramine, J. C. Grossman, and W. A. Lester, J. Chem. Phys. **120**, 3049 (2004).

[139] G. Ghigo, B. O. Roos, and P.-Å. Malmqvist, Chem. Phys. Lett. **396**, 142 (2004).

[140] J. T. H. Dunning, J. Chem. Phys. **90**, 1007 (1989).

[141] R. A. Kendall, J. T. H. Dunning, and R. J. Harrison, J. Chem. Phys. **96**, 6796 (1992).

[142] G. K.-L. Chan, M. Kállay, and J. Gauss, J. Chem. Phys. **121**, 6110 (2004).

[143] M. Kállay and P. R. Surján, J. Chem. Phys. **115**, 2945 (2001).

[144] P. Widmark, P.-Å. Malmqvist, and B. O. Roos, Theor. Chim. Acta. **77**, 291 (1990).

[145] R. Pou-Amérigo, M. Merchán, I. Nebot-Gil, P. Widmark, and B. O. Roos, Theor. Chim. Acta. **92**, 149 (1995).

[146] M. Gouterman and G.-E. Khalil, J. Mol. Spectrosc. **53**, 88 (1974).

Table 2.1: Notation and abbreviations

Orbital indices	
p, q, r, s	Generic orbitals
v, w, x, y	Core (inactive) orbitals
g, h, i, j, k, l, m, n	Active orbitals
a, b, c, d	External (virtual) orbitals
Determinant indices	
I_μ	Reference space (N)
S_μ	Singles space (N-1)
D_μ	Pair space (N-2)
Abbreviations	
ACPF	Averaged Coupled-Pair Functional
AQCC	Averaged Quadratic Coupled-Cluster
CAS	Complete Active Space
CC	Coupled-Cluster Theory
CSF	Configuration State Function
CT	Canonical Transformation Theory
cu(4)	Neglect of 4-particle rank cumulant

Table 2.1: Notation and abbreviations (cont.)

Abbreviations (cont.)	
CW	Celani-Werner internal contraction
DMRG	Density-Matrix Renormalization Group
EPV	Exclusion Principle Violating
ERI	Electron-Repulsion Integral
FIC	Full-Internal Contraction (or Full-Internally Contracted-)
IC	Internal Contraction (or Internally Contracted-)
MO	Molecular Orbital
MPI	Message Passing Interface
MR	Multireference
MRCI	Multireference Configuration Interaction
n-RDM	n-particle rank Reduced-Density Matrix
SCF	Self-Consistent Field
SR	Single Reference
WR	Werner and Reinsch internal contraction
WK	Werner and Knowles internal contraction

Table 2.2: List of contraction schemes of IC-MRCI ansatz. The schemes are categorized by the basis representation of the reference Ψ_0, internal, semi-internal, and external excitation classes. Each of the classes is represented with either contracted (C) or uncontracted (U) basis. Excitation classes are labeled using c, o, and v, which refer to core, active and external orbital, respectively For instance, *oovv* denotes the class of (o, o)→(v, v) excitation from the reference function. The categorization checks the presence of five-rank RDM in formulae.

		Internal excitation		Semi-internal excitation		External excitation	
Ansatz	Ψ_0	*cooo*	*ccoo*	*ccov/coov/ocov*	*ooov*	*ccvv/covv/oovv*	Has 5-RDM ?
WR-MRCI [a]	C	C	C	C	C	C	Yes
WK-MRCI [b]	U	U	U	U	U	C	No
CW-MRCI [c]	U	U	C	C	U	C	No
FIC (present)	C	C	C	C	C	C	No

Table 2.3: Forms of the factor λ, used in the correlation energy functionals.

Functional type	Form of λ
CISD	1
ACPF	$\frac{2}{Ne}$
AQCC	$1 - \frac{(Ne-3)(Ne-2)}{Ne(Ne-1)}$
CEPA(0)	0

Table 2.4: Calculation times of a single iteration including the construction of a σ vector in benchmark MRCI calculations using the WK, CW, and FIC-cu(4) schemes for C_nH_{n+2} ($6 \leq n \leq 24$) with the CAS(ne,no) reference. Times for the construction of the intermediate $\mathbf{\Gamma_B}$ [Eq. (2.57)], which need be evaluated only once in the FIC-cu(4)-MRCI calculation, are also shown. All timings are given in seconds. All out-of-plane valence 2p orbitals were included in the CAS. All 1s orbitals of C and H were kept uncorrelated.

	σ-vector			
Molecule	WK-MRCI	CW-MRCI	FIC-cu(4)-MRCI	$\mathbf{\Gamma_B}$
C_6H_8	207	3	27	3
C_8H_{10}	18470	13	94	17
$C_{10}H_{12}$	–	58	277	79
$C_{12}H_{14}$	–	515	698	325
$C_{14}H_{16}$	–	12424	1805	1250
$C_{16}H_{18}$	–	–	4572	4618
$C_{18}H_{20}$	–	–	9566	11897
$C_{20}H_{22}$	–	–	19584	30863
$C_{22}H_{24}$	–	–	47340	73136
$C_{24}H_{26}$	–	–	104396	170238

Table 2.5: Calculation times (in seconds) of a single iteration including the construction of a σ vector in the FIC-cu(4)-MRCI calculations using three types of basis sets (6-31G*, 6-311G* and 6-311G**) for $C_{12}H_{14}$ with CAS(12e,12o) and for $C_{16}H_{18}$ with CAS(16e,16o). All out-of-plane valence 2p orbitals were included in the CAS. All 1s orbitals of C and H were kept uncorrelated.

Basis set	Number of MOs	σ-vector
	$C_{12}H_{14}$	
6-31G*	184	698
6-311G*	246	2350
6-311G**	288	3998
	$C_{16}H_{18}$	
6-31G*	244	4572
6-311G*	326	13571
6-311G**	380	22728

Table 2.6: Energies and their differences for S_0 and T_0 states of the free-base porphyrin molecule calculated using several methods with the CAS(8e,8o) and CAS(26e,24o) references. The total energies and the singlet–triplet gaps are given in E_h and eV, respectively.

Method	Basis set	S_0	T_0	Gap
		CAS(8*e*, 8*o*)		
CASSCF	6-31G*	-983.314 110	-983.253 405	1.65
CW-MRCI	6-31G*	-985.264 078	-985.199 718	1.75
CW-MRCI+Q[d]	6-31G*	-986.023 128	-985.958 101	1.77
CASPT2 (IPEA shift = 0.00)	6-31G*	-986.441 282	-986.392 060	1.34
CASPT2 (IPEA shift = 0.25)	6-31G*	-986.429 953	-986.363 526	1.81
		CAS(26*e*, 24*o*) with the DMRG		
CASSCF	6-31G*	-983.535 440	-983.489 008	1.26
FIC-cu(4)-MRCI	6-31G*	-985.410 545	-985.358 663	1.41
FIC-cu(4)-MRCI+Q[a]	6-31G*	-986.115 122	-986.060 678	1.48
FIC-cu(4)-MRCI+Q[e]	6-31G*	-986.504 297	-986.447 988	1.53
FIC-cu(4)-ACPF	6-31G*	-986.581 052	-986.524 167	1.55
CASPT2 (IPEA shift = 0.00)	6-31G*	-986.421 523	-986.364 533	1.55
CASPT2 (IPEA shift = 0.25)	6-31G*	-986.403 296	-986.339 726	1.73
CASPT2 (Roos et. al.)[f]	ANO[g]	–	–	1.52
DMC (Aspuru-Guzik et. al.)[h]	–	–	–	1.60
Experiment[i]	–	–	–	1.58

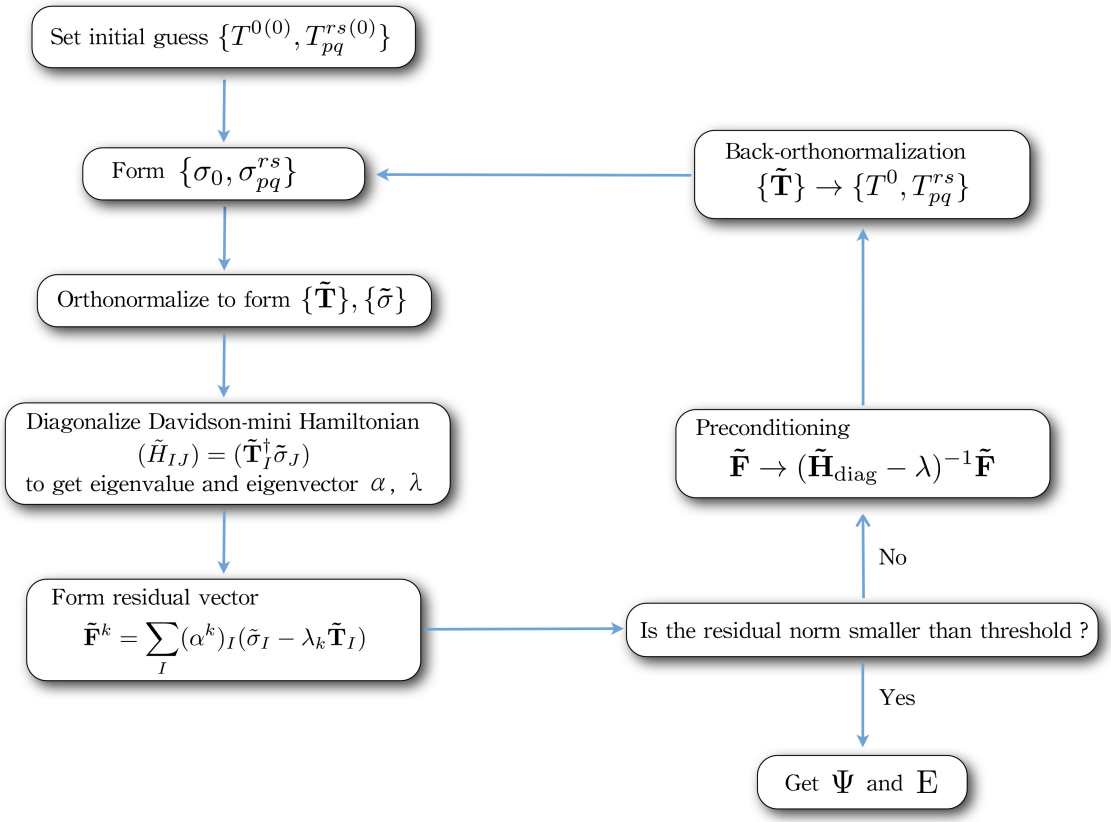

Figure 2.1: Flowchart of the iterative diagonalization procedure of the FIC-MRCI method.

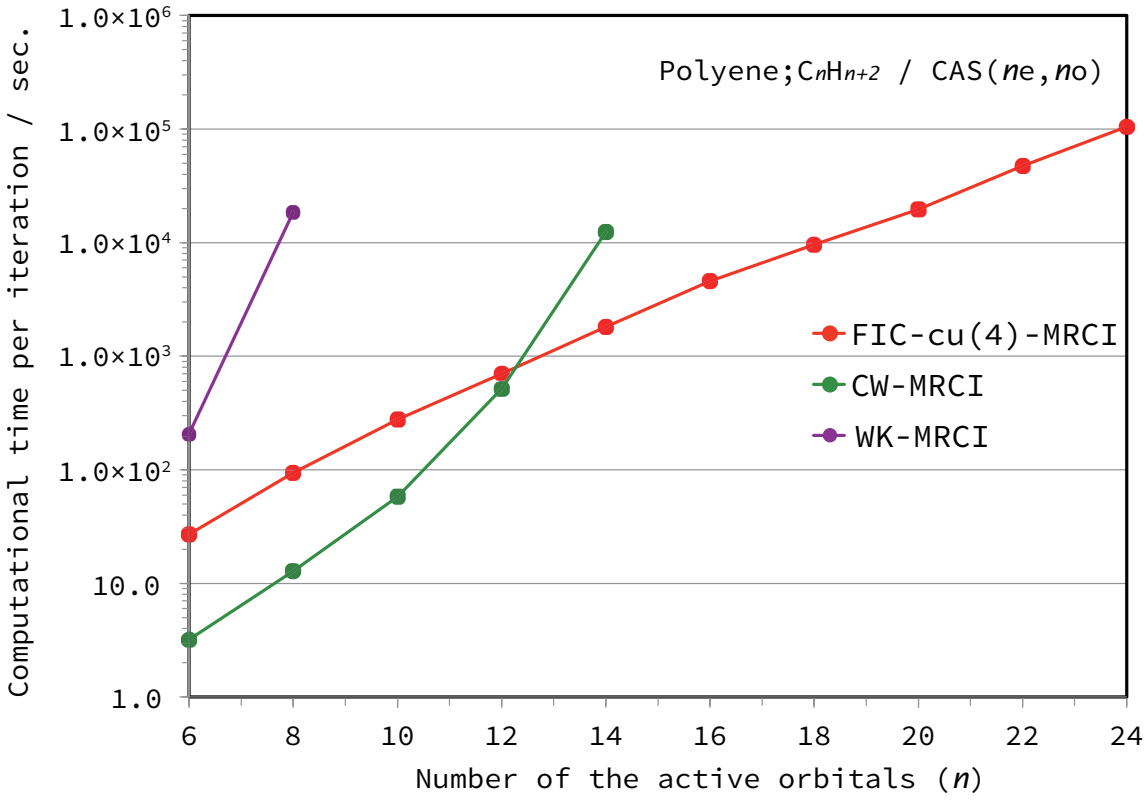

Figure 2.2: Calculation times (in seconds) of a single iteration including the construction of a σ vector in FIC-cu(4)-, CW-, WK-MRCI calculations for polyene molecules from C_6H_8 to $C_{24}H_{26}$ with the CAS(ne,no) reference. All out-of-plane valence 2p orbitals were included in the CAS. All 1s orbitals of C and H were kept uncorrelated.

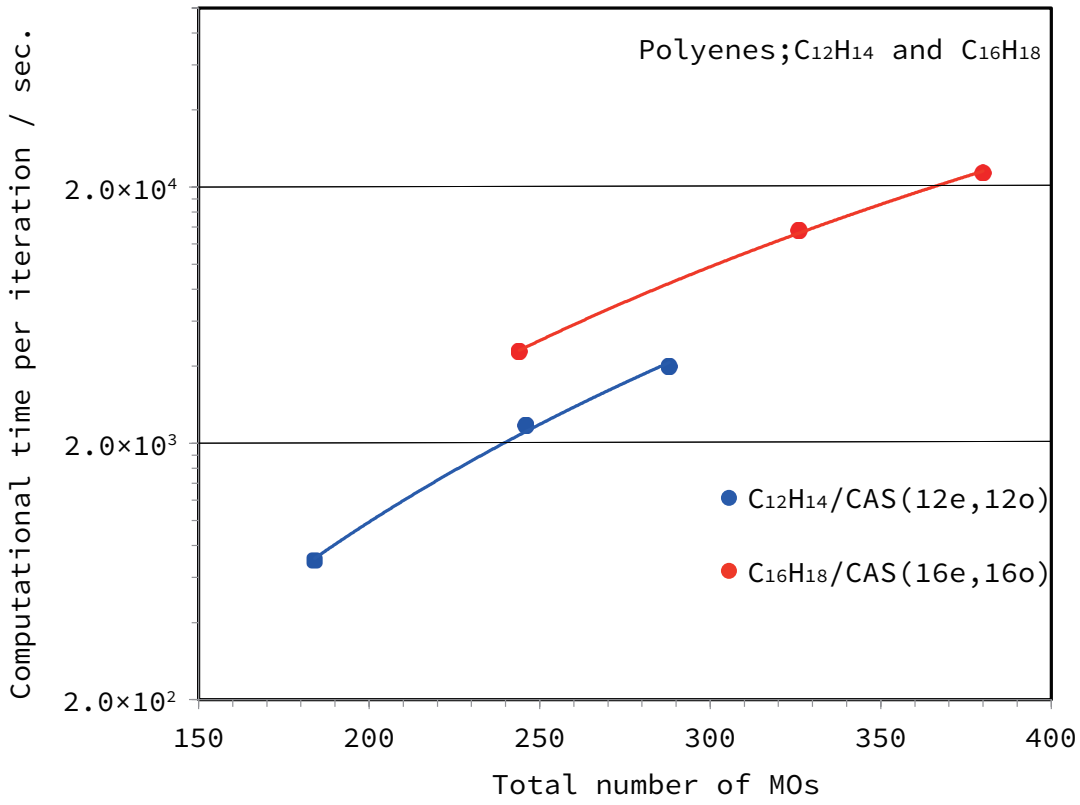

Figure 2.3: Dependence of the computational time of FIC-cu(4)-MRCI calculations per interation on the number of external MOs for C_nH_{n+2} with use of a given CAS(ne,no) reference for $n = 12$ and 16. Three types of the basis sets, 6-31G*, 6-311G* and 6-311G**, were employed. The active space consists of all out-of-plane π orbitals. All 1s orbitals of C and H were frozen.

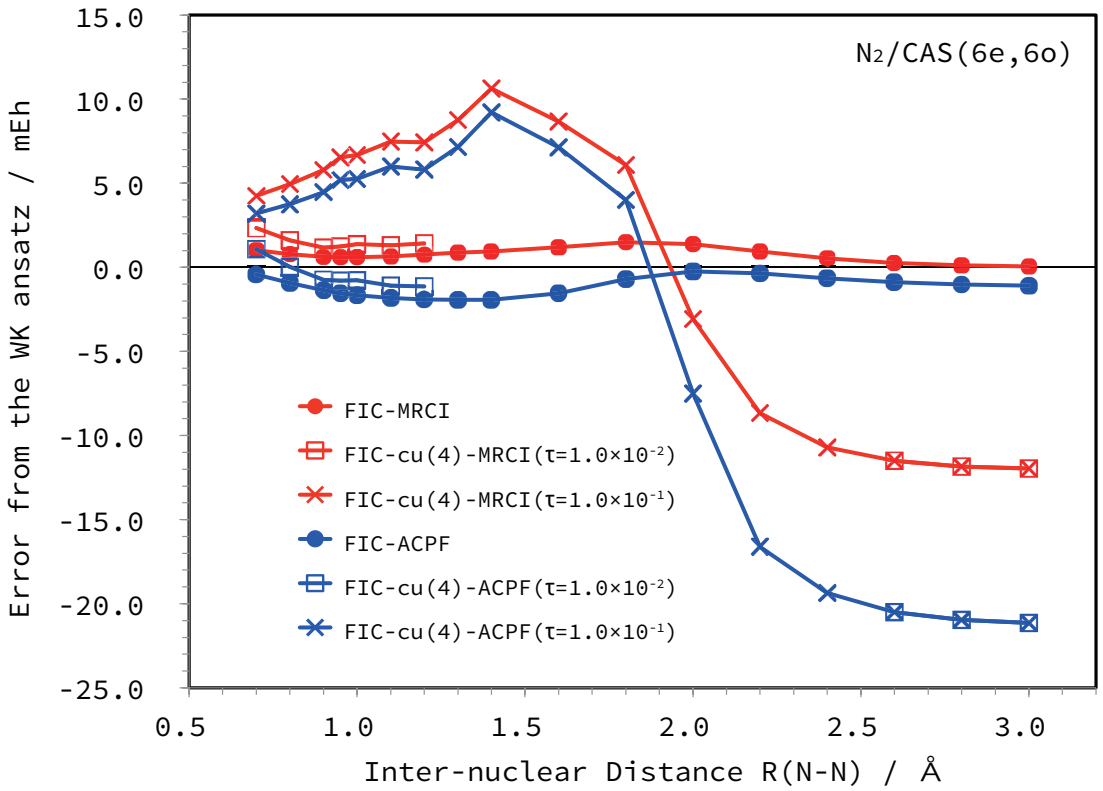

Figure 2.4: Errors in correlation energies of FIC-MRCI, FIC-ACPF and their cumulant-approximated variants relative to the WK counterparts for dissociation of the N_2 molecule. The CAS(6e, 6o) consisting of all 2p orbitals of the N atoms was used for the reference space while the 1s orbitals were frozen. The aug-cc-pVTZ basis set was used. The value of threshold for the overlap truncation (τ) used to avoid the variational collapse caused by the cumulant approximation is given in parentheses.

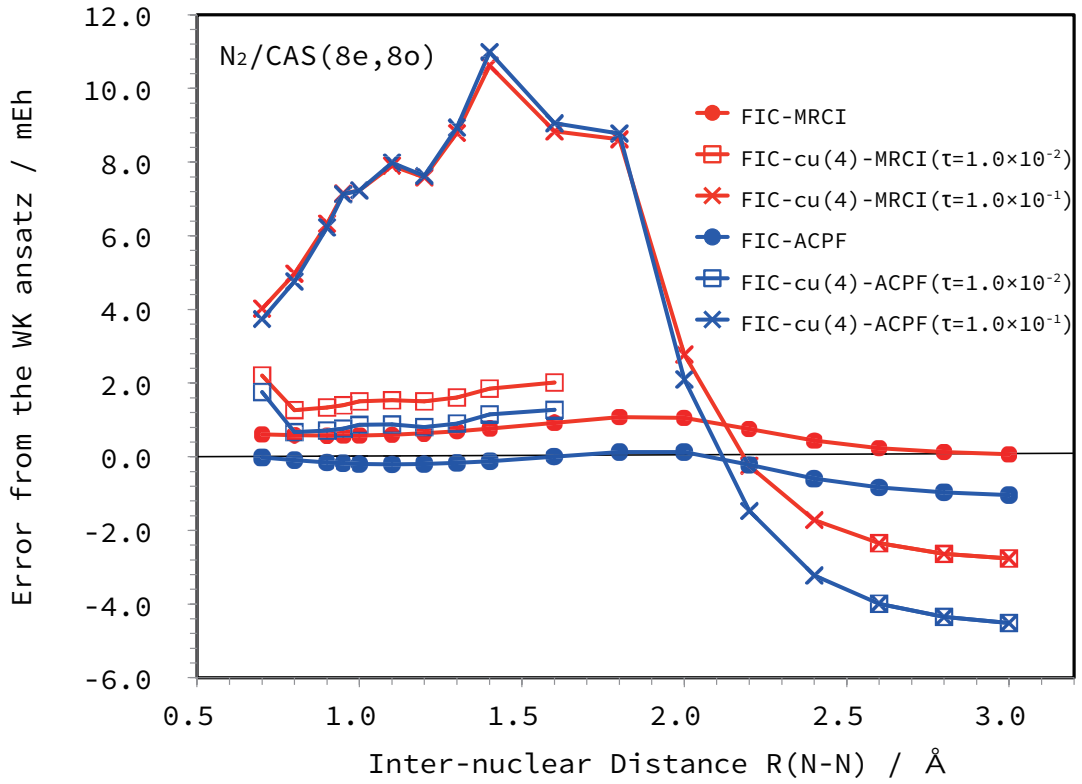

Figure 2.5: Errors in correlation energies of FIC-cu(4)-MRCI, FIC-cu(4)-ACPF and their cumulant approximated variants relative to the WK counterparts for dissociation of the N_2 molecule. The CAS($8e$, $8o$) consisting of all 2s and 2p orbitals of the N atoms was used for the reference while the 1s orbitals were frozen. The aug-cc-pVTZ basis set was used. The value of threshold for the overlap truncation (τ) used to avoid the variational collapse caused by the cumulant approximation is given in parentheses.

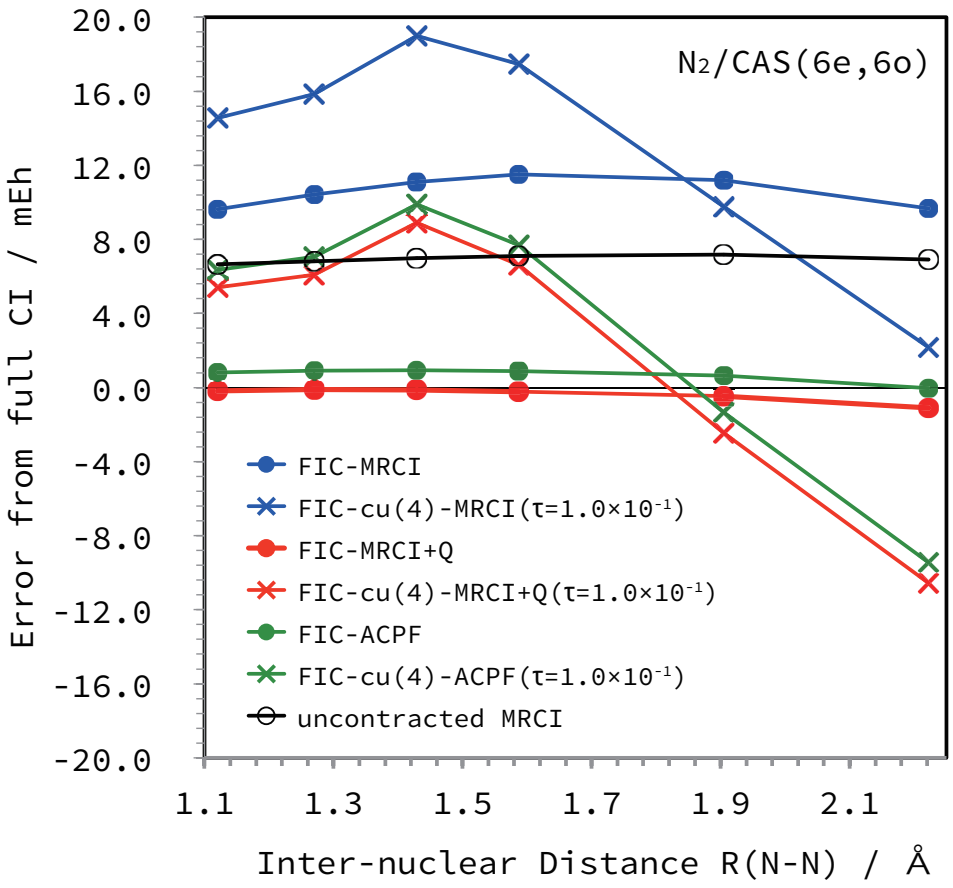

Figure 2.6: Energy differences from the full CI energies for dissociation of the N_2 molecule. All 2p orbitals of the N atoms were taken as the active space, resulting in CAS(6e, 6o). The cc-pVDZ basis set was employed. The MRCI+Q energies were evaulated on the basis of the renormalized Davidson correction.[93, 94, 95] The uncontracted MRCI values were taken from Ref. [142].

Chapter 3

The DMRG-MRCI Study of the Iron-Oxo Porphyrin Electromers

M. Saitow, Y. Kurashige, and T. Yanai, "Multireference theoretical stydy of the Iron-oxo porphyrin electromers on top of the ab initio density-matrix renormalization group reference function", *The Journal of Chemical Physics*, (in preparation).

3.1 Introduction

The cytochrome P450 is a large superfamily of the protein-bounded porphyrin complexes with the active oxygen that hydroxylates the substrate. Due to the highly active nature of the oxygen, the cytochrome P450 catalyzes the conversion of a variety of chemical compounds by inserting the oxygen atom into an inert C-H bond of the substrate[1, 2]. The reactive intermediate in cytochrome P450 catalytic reaction is postulated to be an iron-oxo porphyrin radical cation, which is often referred to as *Compound I* (Cpd I)[3], and is considered to participate the oxygen-transfer reactions[4]. While the neutral iron(III)-oxo porphyrin derivatives are relatively stable, a more oxidized iron(IV)-oxo porphyrin radical cation is known to be a highly reactive oxidant in an *in vivo* context. This is because of the extremely electrophilic nature of the Fe^{IV}-O group, and therefore the oxidation state of iron in the Cpd I is thought to be iron(IV). For the ground state Cpd I and the synthetic analogues, the spectroscopic consensus has been drawn that supports this assumption[5, 6, 7, 8, 9, 10]. However, recent advances in the laser flash photolysis (LFP) technique have suggested the existence of the low-lying and thermally-accessible iron(V)-oxo porphyrin electronic isomer (electromer)[11, 12]. For the Fe^{V}-O synthetic analogues, it has been reported that the coordination of the corrole, which would be a much stronger electron donor than the porphyrin, stabilized the highly oxidative Fe^{V}-O group, and consequently the iron(V)-oxo corrole was spectroscopically detected in real time[13]. Stabilization of the (+V) oxidation state of iron is also observed under the existence of the other strong electron donor in several iron-oxo compounds[14, 15].

Therefore, it may be plausible for the thermally-accessible iron(V)-oxo compounds with the porphyrin ligands to really exist in the biological context. It was reported that the synthetic iron(V)-oxo porphyrin transient reacted 4 – 5 orders of magnitude faster than the corresponding iron(IV)-oxo electromers[16]. If such a compound exists in an *in vivo* enzymatic cycle, it would be a remarkably strong oxidant.

Aiming to provide the theoretical issue to the existence of the hypothetical iron(V)-oxo electomer of the Cpd I, Pierloot *et al.* recently performed the restricted active space second order perturbation (RASPT2)[17, 18, 19, 20, 21] and the density-functional theoretical (DFT) calculations[22] to examine the stability relative to the iron(IV)-oxo electromer, which is supposedly a ground state. In the RASPT2 calculations, they included 16 π MOs of the porphyrin, all the $3d$ orbitals of iron, $2p$ orbitals of oxygen and further 3 double shell d orbitals, resulting in the active space with 29 electrons distributed in the 28 MOs, and a fairly large basis set was used. Contrary to the experimental consensus, their extraordinarily large-scale multireference calculations suggested that the iron(V)-oxo porphyrin may presumably be stabler than its iron(IV)-oxo electromer *in vacuo*, which is, however, considered to be the ground state. The reason of the inconsistency between the experiments and the large-scale multireference calculation was speculated to consist in an existence of the solvent: In the presence of the polarizable continuum, it was observed by the DFT calculation that iron(IV)-oxo porphyrin was stabilized relative to the iron(V)-oxo electromer. It was further suggested that in the second order perturbartive treatment the dynamic correlation for the high-spin pentaradicaloid form of the iron(IV)-oxo electromer might be overestimated. Accodring to the various spectroscopic

techniques[5, 6, 7, 8, 9, 10], the triradicaloid iron(IV)-oxo was suggested to be the ground state.

For giving a more thorough rationale for the stability of the iron(V)-oxo porphyrin with respect to the iron(IV)-oxo electromer, these two requirements would have to be fulfilled: (1) Use of the Complete-Active Space (CAS) methodology[23, 24, 25] instead of the RAS analogue and (2) use of a much more robust treatment of the dynamic correlation than the second order perturbation, i.e. the MultiReference Configuration Interaction (MRCI)[26, 27, 28, 29, 30, 31, 32, 33, 34, 35, 36, 37, 38, 39, 40, 41, 42, 43], Coupled-Cluster (MRCC)[44, 45, 46, 47, 48, 49, 50, 51, 52, 53, 54, 55, 56, 57, 58, 59], or Canonical Transformarion (CT)[60, 61, 62, 63, 64, 65] ansatz. Nonetheless, such a large active space is far beyond the reach of any conventional CAS-based multireference methodologies. In the CAS-CI framework, the static correlation in the active space is solved by means of the Full Configuration Interaction (FCI) while the RAS analogue uses the truncated CI for the active space correlation. The computational effort of the CAS-CI method explicitly depends on the dimension of the Hilbert space and so, it scales exponentially (or factorially) with respect to the size of the molecule. Therefore, the applicability of the usual CAS method is limited to the active space utmost with 16 electrons distributed in the 16 molecular orbitals (MOs).

The recent advances in the *ab initio* Density-Matrix Renormalization Group (DMRG) have opened a new possibility for overcoming this inherent limitations of the CAS-based multireference methodologies[66, 67, 68, 69, 70, 71, 72, 73, 74, 75, 76, 77, 78, 79, 80, 81]. The DMRG algorithm is an efficient alternative to the conventional FCI and the compact

parameterization of the wave function achieves a drastic reduction in the computational cost. By means of the DMRG treatment, the exact diagonalization of the active-space Hamiltonian with approximately 30 – 40 active MOs is no longer an obstacle for the multireference quantum chemistry[69, 74, 82, 76, 83]. The Complete-Active Space Self-Consistent Field (CASSCF) that uses the DMRG as an engine to diagonalize the active-space Hamiltonian has been proposed by Zgid and Nooijen[84] and by Chan *et al.*[85]. By means of the joint approach of the DMRG and CASSCF, which is referred to as DMRG-CASSCF, recently, the multireference calculation on the Mn_4CaO_5 cluster, a catalytic metalloenzyme in photosystem II has performed using a fairly large basis set and active space with 44 electrons in the 35 active MOs[86]. Use of the active space DMRG is a key to perform such an extremely large scale CAS treatment, which is far beyond the reach of the conventional CAS methodologies. So far, inclusion of the dynamic correlation on top of the DMRG reference function is possible by means of three approaches; (1) the multireference second order perturbation [DMRG-CASPT2][87, 88], (2) the multireference CT theory [DMRG-CT][63] and (3) the MRCI and its size-consistency corrected variants such as averaged coupled-pair functional (ACPF)[89, 90, 91], averaged quadratic coupled-cluster (AQCC)[92, 93, 94, 95], which we call DMRG-MRCI, DMRG-ACPF and DMRG-AQCC[43], respectively. All of these multireference dynamic correlation methods have been developed in the *internally-contracted* (IC) framework to achieve the compact wave function representation[96, 97, 98, 28, 29].

The objective of this research is to ascertain the stability of the hypothetical iron(V)-oxo electromer of the Cpd I by means of the high-level electron correlation theory based

on the DMRG multireference methodologies. The high-performance computer implementation of the DMRG-MRCI methods enables us to perform the extraordinaliry large-scale calculations on both iron(IV)-oxo and iron(V)-oxo prophyrin electromers of the Cpd I. In these calculations, we included further 2 double-shell d orbitals into the Pierloot's active space, leading to the active space with 29 electrons distributed in the 30 active MOs. For achieving such large-scale MRCI calculations, cumulant-approximated form of the 4-particle rank reduced-density matrix (4-RDM)[43] is decomposed explicitly and factorized into a stream of the binary contractions. Due to this, the formal scaling of the DMRG-MRCI calculation is reduced to O(N^8) from the previous one (O(N^9)) where N refers to the magnitude of the molecular size. A computer-aided approach was employed on the symbolic optimization of the tensor equation and on the translation of the equations into the parallilized and efficiently-vectorized computer code.

3.2 Theory

3.2.1 The DMRG-MRCI

In the DMRG-MRCI theory, the wave function is written in the IC framework as

$$|\Psi_{\mathrm{MRCI}}\rangle := \left(C_0 + \sum_{pqrs} C_{pq}^{rs} E_{rs}^{ps} \right) |\Psi_0\rangle \tag{3.1}$$

where **C** and **E** refer to the MRCI amplitude and the spin-free excitation operator, respectively, while Ψ_0 represents the DMRG- or conventional CASSCF reference function. The indices $wxyz$, $ijkl$.. and $abcd$.. represent the core, active and virtual MOs, respec-

tively, while the others ($prqs$) are used for the generic MOs. Note that the (E^{rs}_{pq}) covers the eight types of the excitation in total, except the intra-active excitation (E^{kl}_{ij}) from the consideration[31, 32, 43]. In Eq. (3.1), the action of the E-operator to the reference generates the IC basis, an alternative many-body basis to the Slater determinant; $|e^{rs}_{pq}\rangle \leftarrow E^{ps}_{rs}|\Psi_0\rangle$. Since the IC excitation function is a non-orthonormal and overcomplete basis, the DMRG-MRCI equation takes form of the generalized eigenvalue equation

$$\mathbf{HC} = \mathbf{SCE} \tag{3.2}$$

where **H** and **S** represent the Hamiltonian and overlap matrices, respectively. At each step of the block-Davidosn procedure[99, 100] to solve Eq. (3.2), the σ-equation (Hamiltonian–Vector product) is calculated;

$$\sigma^L = \sum_R \langle e^L|H|e_R\rangle T^R \tag{3.3}$$

where L (R) refers to either of the eight types of the IC basis and **T** represents the Ritz vector that constitutes the MRCI amplitude (**C** in Eq. (3.1)). The molecular electronic Hamiltonian in the spin-free formulation is used

$$H = \sum_{pq} h^q_p E^p_q + \frac{1}{2}\sum_{pqrs} V^{rs}_{pq} E^{pq}_{rs}. \tag{3.4}$$

The explicit form of the spin-free working equation is derived from Eqs. (3.3) and (3.4) by invoking the normal ordering of the spin-free E-operator[101]. For this purose, the symbolic manipulation programs have been developed by the several groups[102, 62, 103, 64, 104, 43]. Each term of the MRCI σ-equation is expressed as a product of one **T**-amplitude, one molecular integral (**h** or **V** in Eq. (3.4)) and one RDM. Note that the

RDM is an expectation value of the E-operator with respect to the reference function, i.e. $D^{kl..}_{ij..} = \langle\Psi_0|E^{kl..}_{ij..}|\Psi_0\rangle$.

As originally proposed by Werner and Reinsch[28], when Eq. (3.3) is evaluated straightforwardly, the lengthy 5-RDM, which is a ten-index tensor, stems from the semi-internal excitation (E^{ai}_{jk}) block of the σ equation, resulting in the substantially large computational scaling of O(N^{11}). To eliminate this quantity, we express the semi-internal Hamiltonian elements by using the multiple commutators[105, 43] as

$$\sigma^{jk}_{ai} = \Big(\langle\Psi_0|[[E^{jk}_{ai}, H], E^{nb}_{lm}]|\Psi_0\rangle + E_0\langle\Psi_0|E^{jk}_{ai}E^{nb}_{lm}|\Psi_0\rangle\Big)\, T^{nb}_{lm} \tag{3.5}$$

where E_0 represents the reference energy. The non-trivial conversion from Eq. (3.3) to Eq. (3.5) is responsible for eliminating the presence of the 5-RDM without any approximation. As a consequence, the DMRG-MRCI σ-equation becomes expressible only by 1 – 4 RDMs and then, its concomittant computational scaling is reduced to O(N^9). The proof of this tranformation is given in Ref. [43].

Novertheless, the eight-index 4-RDM still hinders the aplication of the DMRG-MRCI to the systems with approximately 20 – 30 active MOs or more. By neglecting the 4-particle rank cumulant in the 4-RDM, the relatively large 4-RDM is decomposed into a sum of an anti-symmetrized product of the lower-rank RDMs[106, 107, 108, 109, 110, 111, 112, 113, 114, 115, 116, 117]. The definition of the cumulant-decomposition for the spin-free RDM is not as evident as that in the spin-dependent case[114, 115, 116]. Our formulation on the spin-free cumulant-decomposed 4-RDM is given, in the supplimentary

material of Ref. [43], as

$$\begin{aligned} D^{klmn}_{ghij} \rightarrow D^{klm}_{ghi} D^{n}_{j} + \ & (15 \text{ terms}) \\ - D^{kl}_{gh} D^{mn}_{ij} + \ & (26 \text{ terms}) \\ + \frac{1}{3} \Gamma^{kl}_{gh} \Gamma^{mn}_{ij} + \ & (26 \text{ terms}) \end{aligned} \tag{3.6}$$

where $\mathbf{\Gamma}$ represents the spin-free cumulant, i.e. $\Gamma^{rs}_{pq} = D^{rs}_{pq} - D^{r}_{p} D^{s}_{q} + \frac{1}{2} D^{s}_{p} D^{r}_{q}$.

The full-form of the σ-vector (Eq. (3.3)) and the diagonal preconditioner required in the block-Davidson procedure are composed of approximately as many as 3000 tensor contraction terms in total. The derivation and implementation of such a tremendous amount of terms are somewhat straightforward, but quite prone to errors. To this end, we have developed a tensor generator to expand the many-fermionic ansatz into the tensor-contracted forms and to trasnlate them to the efficiently vectorized tensor contraction code[104]. The generated program can use more than hundreds of computer nodes on the basis of the Message-Passing Interface (MPI) parallelism.

3.2.2 Symbolic optimization of the cumulant-approximated 4-RDM

In the earlier algorithm implemented in our tensor generator, the largest number of the tensors consisting of a single tensor-contracted term is assumed to be three. Since the typical term in the DMRG-MRCI σ-equation is written as $\sigma \leftarrow \mathbf{V} \cdot \mathbf{T} \cdot \mathbf{D}$, this postulate is true. However, when the cumulant decomposition (Eq. 3.6) is invoked in the spin-free 4-RDM, the terms with the 4-RDM takes form as $\sigma \leftarrow \mathbf{V} \cdot \mathbf{T} \cdot \mathbf{D}_{m} \cdot \mathbf{D}_{(4-m)}$ where m refers

to the particle rank of the RDM and is either of 1, 2 or 3. In the previous implementation of the DMRG-MRCI, the 4-RDM is constructed on-the-fly from the lower order RDMs to ensure the postulate. In this scheme, the cumulant reconstruction of the 4-RDM and the associated tensor contraction require the floating-point operations (FPOs) of $O(N^8)$ and $O(N^9)$, respectively. Due to the direct-product nature of the cumulant reconstruction scheme, the $O(N^8)$ manipulations cannot be vectorized by means of the efficient matrix multiplication subroutines such as `DGEMM`.

For the systems with approximately 30 active MOs, it was found that the unvectorized $O(N^8)$ manipulation causes a substantial amount of cache-miss. Therefore, explicit decomposition of the cumulant-approximated 4-RDM and factorization of them into a stream of binary tensor contraction are imperative tasks on. To this end, we have rewritten the symbolic manipulation part of our tensor generator so as to minimize the FPO and to eliminate the demanding unvectorized step from the calculation. The newly developed symbolic program can deal with the tensor-contracted term with the arbitrary number of tensor factors by taking into account all the possible way to form the binary contractions. Moreover, the program, which is written in Haskell language[118] on the basis of the purely-functional programming, optimizes the binary contraction with respect to the minimization of the FPO, permutational symetry of the tensor and the parallelization aspect. As a consequence, the formal scaling of the DMRG-MRCI is reduced to $O(N^8)$ from previous order of $O(N^9)$ and the unvectorized $O(N^8)$ operations for the cumulant reconstruction of the 4-RDM is eliminated from the construction of the σ-equation.

For a fairly large system, it was also observed that the sorting of each tensor in the

binary contraction, as a preprocess to perform the Matrix–Matrix multiplication, may become crucial. The inefficient sorting algorithm often causes a drastic mount of cache-miss, leading to extreme decrease in the computational throughput. An optimization algorithm for the presorting of the tensor has been implemented in the code generator. Due to these modifications, the new DMRG-MRCI program shows a drastic speedup relative to the previous version and is routinely applicable even to the systems with more than 30 active MOs.

Hereafter, in this Section, we briefly sketch the basic design of our tensor contraction program used for the construction of the σ-vector. Since we are aiming at execution of the DMRG-MRCI for the systems with approximately 30 active and 500 virtual MOs, loop-fusion among the binary contractions is a necessary requirement to reduce the size of the intermediate arrays that should be allocated on the fast memory. If the term has only three tensor factors, the term is decomposed into two binary contractions and there are only three possibilities to form them; $((\mathbf{V}\cdot\mathbf{D})\cdot\mathbf{T})$, $((\mathbf{V}\cdot\mathbf{T})\cdot\mathbf{D})$ and $((\mathbf{D}\cdot\mathbf{T})\cdot\mathbf{V})$. In this case, factorization of the term into the binary contraction and fusion of the loops shared with both binary contractions are rather simple. However, if the number of the tensor factors is four, the number of the unique combinations to form the binary contractions is as many as fifteen[119]. Amongst them, twelve patterns form the *sequential* contractions, i.e. for instance $(((\mathbf{V}\cdot\mathbf{D}_m)\cdot\mathbf{T})\cdot\mathbf{D}_{(4-m)})$, while the remaining three are the *non-sequential* contraction patterns such as $((\mathbf{V}\cdot\mathbf{D}_m)\cdot(\mathbf{T}\cdot\mathbf{D}_{(4-m)}))$. The algorithm to fuse the common loops amongst the binary contractions also becomes much more complicated than that for the loop-fusion of the two binary contractions. By the virtue of the Haskell as a

functional programming language, the computer code for such an abstract optimization algorithm can be implemented relatively easily in comparison to the implementation with the usual procedural programming languages such as Python, C/C++ and FORTRAN.

3.3 Results and discussion

As a model molecule for the active intermediate in the Cpd I, we used neutral FeO(P)(Cl) where P stands for porphyrin. As shown in Ref. [22], Pierloot's RASPT2 calculations produced much lower total energies for the two states ($^6A_1$ and ^2E) than the $^4A_2$ state, which has a tetravalent Fe^{IV} iron; however, the $^4A_2$ state is experimentally suggested to be the ground state. The electronic structures for $^6A_1$ and ^2E states are consider to be $(^5Fe^{IV})(^2P^{\cdot})Cl$ and $(^2Fe^{V})(^1P)Cl$, respectively, while that for the $^4A_2$ ground state is $(^3Fe^{IV})(^2P^{\cdot+})Cl$. We performed the DMRG-CASSCF/MRCI calculations for these three states. The same geometries were used as in Pierloot's calculation, which were optimized by means of the BP86 density functional[120, 121] for each state. The DMRG-CASSCF/MRCI calculations were performed with the development version of the ORZ package, our in-house quantum chemistry program suite, using the second order Douglas-Kroll Hamiltonian[122, 123, 124] for the quasi-relativistic treatment. The ANO-RCC basis set[125] was used on all the atoms, contracted to $[7s6p5d3f2g1h]$ on Fe, to $[4s3p1d]$ on Cl, to $[4s3p2d1f]$ on O, to $[3s2p1d]$ on N and C, and to $[2s]$ on H, leading to approximately 500 basis functions in total. All the calculations were performed with C_{2v} symmetry.

In Figs. 3.1, the natural orbitals (NOs) obtained from the DMRG-CASSCF are shown in the one-dimensional DMRG ordering. In Fig. 3.1, NO1 – NO16 are 16 π MOs of P formed from the $2p$ orbitals on the carbon atoms while the remaining NOs are formed from the $3d$ orbitals on iron. Note that NO20 and NO21 are double-shell orbitals ($3d'_{xy}$ and $3d'_{z^2}$), which were missed in the Pierloot's active space setting. For the ^{2}E state, only the π^*_{xz} orbital (NO26) in the Fe–O bond is singly-occupied while for the pentaradicaloid $^6A_1$ state, non-bonding $d_{x^2-y^2}$ orbital (NO18), the highest occupied π orbital (NO3) in the porphyrin, π^*_{xz} and π^*_{yz} orbitals (NO26 and NO29, respectively) are singly-occupied as shown in Fig. 3.2. The triradicaloid $^4A_2$ state is considered to be the ground state that has three open-shell orbitals; π^*_{xz}, π^*_{yz} orbitals and the highest occupied π orbital in the porphyrin. We set the initial super-block matrix elements for the DMRG sweep in a manner such that these spin-states are allowed to be constructed.

For carrying out the DMRG-MRCI calculation on the FeO(P)Cl using active space with 29 electrons distributed in the 30 orbitals, we incorporated an extra optimization into our implementation. To measure how much the performance of our program was improved, we performed a benchmark calculation on the $[H_4Fe_2O_7]^{2+}$, a hypothetical differate intermediate that catalyzes the water to form the O–O bond[126], using ANO-RCC basis set. The differate system is composed of 19 closed, 32 active and 279 virtual orbitals. The calculation was performed on top of a MPI-based parallelization using six computer nodes; each of which has two Intel® Xeon® X5660 processors of 2.80 GHz and 96 gigabytes of memory. As a preliminary steps to diagonalize the DMRG-MRCI Hamiltonian, two intermediate tensors [$\mathbf{\Gamma_A}$ and $\mathbf{\Gamma_B}$ in Ref. [43]] have to be constructed

whose associated tensor contraction require FPOs of O(N^8) and O(N^9), respectively. Both $\mathbf{\Gamma_A}$ and $\mathbf{\Gamma_B}$ are formed by contracting the 4-RDM and electron repulsion integral ($\mathbf{V}$ in Eq. (3.4)) as

$$(\Gamma_{\mathrm{A}})^{kl}_{gh} \leftarrow \sum_{ijmn} D^{klmn}_{ghij} V^{ij}_{mn} \tag{3.7}$$

and

$$(\Gamma_{\mathrm{B}})^{klm}_{ghp} \leftarrow \sum_{ijn} D^{klmn}_{ghij} V^{ij}_{pn}. \tag{3.8}$$

By using the previous DMRG-MRCI code, the construction of $\mathbf{\Gamma_A}$ and $\mathbf{\Gamma_B}$ were observed to take 4311 and 1141585 seconds, respectively, in wall time. In the current implementation, the 4-RDM in both Eqs. (3.7) and (3.8) is explicitly decomposed into the cumulant-approximation and factorized into binary tensor contractions. Because of this, the largest FPOs for construction of $\mathbf{\Gamma_A}$ and $\mathbf{\Gamma_B}$ are reduced from O(N^8) and O(N^9) to O(N^7) and O(N^8), respectively. In the current implementation, constructions of the $\mathbf{\Gamma_A}$ and $\mathbf{\Gamma_B}$ were observed to take 16 and 1569 seconds, respectively, in wall time on the same cluster configuration. Owing to the explicit decomposition of the 4-RDM in the σ-equation (Eq. (3.3)), the computational scaling is reduced to O(N^8) from the previous one (O(N^9)). The actual computational timings for a single σ-vector evaluated with the previous and current implementations was measured to be 869959 and 125095 seconds, respectively, in wall time. In consequence of the reduction in the computational scaling and of the elimination of the unvectorized cumulant reconstruction, a drastic acceleration was achieved in the construction of both the σ-vector and the preliminary intermediates.

3.4 Concluding remark

To theoretically give an answer to the argument on the hypothetical iron(V)-oxo electromer of the Cpd I, we used a more thorough active space setting than the work of Pierloot *et al.*; in our CAS treatment, 2 double-shell $3d$ orbital of iron were additionally included, resulting in the active space with 29 electrons distributed in the 30 orbitals. On top of this CAS setting, a series of the extremely-large scale DMRG-CASSCF/MRCI calculations are carried out for the problematic two cases; for the high-spin $(^5\mathrm{Fe}^{\mathrm{IV}})(^2\mathrm{P}^{\cdot})\mathrm{Cl}$ and $(^2\mathrm{Fe}^{\mathrm{V}})(^1\mathrm{P})\mathrm{Cl}$, which were assigned to $^6\mathrm{A}_1$ and $^2\mathrm{E}$ states, respectively. Pierloot's RASPT2 calculation (*in vacuo*) predicted an inconsistent consequence with the experimental consensus; the $^6\mathrm{A}_1$ and $^2\mathrm{E}$ states were calculated to be much stabler than the triradicaloid ground state ($^4\mathrm{A}_2$ state).

The execution of such large DMRG-MRCI calculations required an extreme improvements in our computer implementation. To this end, we have developed a symbolic program to optimize the tensor-contracted equations of the DMRG-MRCI. To reduce the inefficient sorting algorithm of the intermediate tensor, which often deteriorates the computational throughput, we have added an optimization algorithm of the loop-structure to our tensor generator. Due to these modifications, the computational performance of the DMRG-MRCI has presently proven to be approximately seventh time faster than the previous implementation for a benchmark system with the 32 active orbitals: The construction of a single σ-equation, which took approximately ten days by means of the previous implementation, is now achievable in nearly one day.

Bibliography

[1] C. Jung, Biochimica et Biophysica Acta **1814**, 46 (2011).

[2] P. R. Ortiz de Montellano, *Cytochrome P450: Structure, Mechanism, and Biochemistry, 3rd Ed.*, Kluwer Academic/Plenum Publishers, New York, 2005.

[3] S. Shaik, D. Kumar, S. de Visser, A. Altun, and W. Thiel, Chem. Rev. **105**, 2279 (2005).

[4] Z. Pan, R. Zhang, and M. Newcomb, J. Inorg. Biochem. **100**, 524 (2006).

[5] A. Gold and R. Weiss, J. Porph. Phthal. **4**, 344 (2000).

[6] R. Weiss, V. Bulach, A. Gold, and J. Terner, J. Biol. Inorg. Chem. **6**, 831 (2001).

[7] J. T.Groves, J. Inorg. Biochem. **100**, 434 (2006).

[8] S. H. Kim, R. Perera, L. P. Hager, J. H. Dawson, and B. M. Hoffman, J. Am. Chem. Soc. **128**, 5598 (2006).

[9] W. Nam, Acc. Chem. Res. **40**, 522 (2007).

[10] J. Rittle and M. T. Green, Science **330**, 933 (2010).

[11] K. Yamaguchi, Y. Watanabe, and I. Morishita, J. Chem. Soc., Chem. Commun. , 1721 (1992).

[12] T. Murakami, K. Yamaguchi, Y. Watanabe, and I. Morishita, Bull. Chem. Soc. Jpn **71**, 1343 (1998).

[13] D. Harischandra, G. Lowery, R. Zhang, and M. Newcomb, Org. Lett. **11**, 2089 (2009).

[14] F. Tiago de Oliveira et al., Science (New York, N.Y.) **315**, 835 (2007).

[15] S. Lee et al., Chemistry (Weinheim an der Bergstrasse, Germany) **13**, 9393 (2007).

[16] Z. Pan, Q. Wang, X. Sheng, J. Horner, and M. Newcomb, Journal of the American Chemical Society **131**, 2621 (2009).

[17] K. Andersson, P.-Å. Malmqvist, B. O. Roos, A. J. Sadlej, and K. Wolinski, J. Phys. Chem. **94**, 5483 (1990).

[18] K. Andersson, P.-Å. Malmqvist, and B. O. Roos, J. Chem. Phys. **96**, 1218 (1992).

[19] K. Andersson, Theor. Chim. Acta. **91**, 31 (1995).

[20] G. Ghigo, B. O. Roos, and P.-Å. Malmqvist, Chem. Phys. Lett. **396**, 142 (2004).

[21] P.-Å. Malmqvist et al., J. Chem. Phys. **128**, 204109 (2008).

[22] M. Radoń, E. Broclawik, and K. Pierloot, J. Chem. Theory Comput. **7**, 898 (2011).

[23] B. O. Roos, P. R. Taylor, and P. E. Siegbahn, Chem. Phys. **48**, 157 (1980).

[24] B. O. Roos, Adv. Chem. Phys. **69**, 399 (1987).

[25] K. Ruedenberg, L. M. Cheung, and S. T. Elbert, Int. J. Quantum Chem. **16**, 1069 (1979).

[26] R. J. Buenker and S. D. Peyerimhoff, Theor. Chim. Acta. **35**, 33 (1974).

[27] R. J. Buenker and S. D. Peyerimhoff, Theor. Chim. Acta. **39**, 217 (1975).

[28] H.-J. Werner and E. A. Reinsch, J. Chem. Phys. **76**, 3144 (1982).

[29] P. E. M. Siegbahn and M. Svensson, Int. J. Quantum Chem. **41**, 153 (1992).

[30] H.-J. Werner and P. J. Knowles, J. Chem. Phys. **89**, 5803 (1988).

[31] P. J. Knowles and H.-J. Werner, Chem. Phys. Lett. **145**, 514 (1988).

[32] K. R. Shamasundar, G. Knizia, and H.-J. Werner, J. Chem. Phys. **135**, 054101 (2011).

[33] P. G. Szalay, T. Müller, G. Gidofalvi, H. Lischka, and R. Shepherd, Chem. Rev. **112**, 108 (2012).

[34] H. Lischka et al., Phys. Chem. Chem. Phys. **3**, 664 (2001).

[35] H. Lischka et al., WIREs. Comput. Mol. Sci. **1**, 191 (2011).

[36] F. Neese, J. Chem. Phys. **119**, 9428 (2003).

[37] M. Hanrath and B. Engels, Chem. Phys. **225**, 197 (1997).

[38] T. Martinez and E. Carter, J. Chem. Phys. **102**, 7564 (1995).

[39] A. Venkatnathan, A. B. Szilva, D. Walter, R. J. Gdanitz, and E. A. Carter, J. Chem. Phys. **120**, 1693 (2004).

[40] D. B. Krisiloff and E. A. Carter, Phys. Chem. Chem. Phys. **14**, 7710 (2011).

[41] T. Shiozaki, G. Knizia, and H.-J. Werner, J. Chem. Phys. **134**, 034113 (2011).

[42] T. Shiozaki and H.-J. Werner, J. Chem. Phys. **134**, 184104 (2011).

[43] M. Saitow, Y. Kurashige, and T. Yanai, J. Chem. Phys. **139**, 044118 (2013).

[44] D. Mukherjee, R. Moitra, and A. Mukhopadhyay, Mol. Phys. **33**, 955 (1977).

[45] B. Jeziorski and H. J. Monkhorst, Phys. Rev. A **24**, 1668 (1981).

[46] U. S. Mahapatra, B. Datta, and D. Mukherjee, Mol. Phys. **94**, 157 (1998).

[47] M. Hanrath, J. Chem. Phys. **123**, 084102 (2005).

[48] A. Banerjee and J. Simons, Intern. J. Quantum Chem. **19**, 207 (1981).

[49] W. D. Laidig, P. Saxe, and R. J. Bartlett, J. Chem. Phys **86**, 887 (1987).

[50] M. Hanauer and A. Köhn, J. Chem. Phys. **137**, 131103 (2012).

[51] M. Hanauer and A. Köhn, J. Chem. Phys. **136**, 204107 (2012).

[52] F. Evangelista, M. Hanauer, A. Köhn, and J. Gauss, J. Chem. Phys. **136**, 204108 (2012).

[53] F. Evangelista and J. Gauss, J. Chem. Phys. **134**, 114102 (2011).

[54] T.-C. Jagau, E. Prochnow, F. Evangelista, and J. Gauss, J. Chem. Phys. **132**, 144110 (2010).

[55] T.-C. Jagau and J. Gauss, Chem. Phys. , 73 (2012).

[56] T.-C. Jagau and J. Gauss, J. Chem. Phys. **137**, 044115 (2012).

[57] T.-C. Jagau and J. Gauss, J. Chem. Phys. **137**, 044116 (2012).

[58] V. V. Ivanov and L. Adamowicz, J. Chem. Phys. **112**, 9258 (2000).

[59] D. Datta, L. Kong, and M. Nooijen, J. Chem. Phys. **134**, 214116 (2011).

[60] T. Yanai and G. K.-L. Chan, J. Chem. Phys. **124**, 194106 (2006).

[61] T. Yanai and G. K.-L. Chan, J. Chem. Phys. **127**, 104107 (2007).

[62] E. Neuscamman, T. Yanai, and G. K.-L. Chan, J. Chem. Phys. **130**, 124102 (2009).

[63] T. Yanai, Y. Kurashige, E. Neuscamman, and G. K.-L. Chan, J. Chem. Phys. **132**, 024105 (2010).

[64] E. Neuscamman, T. Yanai, and G. K.-L. Chan, J. Chem. Phys. **132**, 024106 (2010).

[65] Y. Yanai, Y. Kurashige, E. Neuscamman, and G. K.-L. Chan, Phys. Chem. Chem. Phys. **14**, 7809 (2012).

[66] S. R. White, Phys. Rev. Lett. **69**, 2863 (1992).

[67] S. R. White, Phys. Rev. B **48**, 10345 (1993).

[68] S. R. White and R. L. Martin, J. Chem. Phys. **110**, 4127 (1999).

[69] A. O. Mitrushenkov, G. Fano, F. Ortolani, R. Linguerri, and P. Palmieri, J. Chem. Phys. **115**, 6815 (2001).

[70] G.-L. Chan and M. Head-Gordon, J. Chem. Phys. **116**, 4462 (2002).

[71] G. K.-L. Chan and M. Head-Gordon, J. Chem. Phys. **118**, 8551 (2003).

[72] J. Hachmann, W. Cardoen, , and G. K.-L. Chan, J. Chem. Phys. **125**, 144101 (2006).

[73] J. Hachmann, J. J. Dorando, M. Avilés, and G. K.-L. Chan, J. Chem. Phys. **127**, 134309 (2007).

[74] K. H. Marti, I. M. Ondík, G. Moritz, and M. Reiher, J. Chem. Phys. **128**, 014104 (2008).

[75] D. Zgid and M. Nooijen, J. Chem. Phys. **128**, 014107 (2008).

[76] Y. Kurashige and T. Yanai, J. Chem. Phys. **130**, 234114 (2009).

[77] G.-L. Chan and D. Zgid, Ann. Rep. Comput. Chem. **5**, 149 (2009).

[78] W. Mizukami, Y. Kurashige, and T. Yanai, J. Chem. Phys. **133**, 091101 (2010).

[79] G. K.-L. Chan and S. Sharma, Ann. Rev. Phys. Chem. **62**, 465 (2011).

[80] S. Sharma and G. K.-L. Chan, J. Chem. Phys. **136**, 124121 (2012).

[81] W. Mizukami, Y. Kurashige, and T. Yanai, J. Chem. Theory Comput. **9**, 401 (2013).

[82] D. Zgid and M. Nooijen, J. Chem. Phys. **128**, 144116 (2008).

[83] S. Sharma and G. K.-L. Chan, J. Chem. Phys. **136**, 124121 (2012).

[84] D. Zgid and M. Nooijen, J. Chem. Phys. **128**, 144115 (2008).

[85] D. Ghosh, J. Hachmann, T. Yanai, and G. K.-L. Chan, J. Chem. Phys. **128**, 144117 (2008).

[86] Y. Kurashige, G. Chan, and T. Yanai, Nat. Chem. **5**, 660 (2013).

[87] Y. Kurashige and T. Yanai, J. Chem. Phys. **135**, 094104 (2011).

[88] Y. Kurashige, J. Chalupský, T. N. Lan, and T. Yanai, *unpublished* .

[89] R. Gdanitz and R. Ahlrichs, Chem. Phys. Lett. **143**, 413 (1988).

[90] R. Gdanitz, Intern. J. Quantum Chem. **85**, 281 (2001).

[91] W. Cardoen and R. Gdanitz, Chem. Phys. Lett. **364**, 39 (2002).

[92] P. G. Szalay and R. J. Bartlett, Chem. Phys. Lett. **214**, 481 (1993).

[93] L. Füsti-Molnár and P. G. Szalay, J. Chem. Phys. **100**, 6288 (1996).

[94] P. G. Szalay, Chem. Phys. **349**, 121 (2008).

[95] P. G. Szalay, T. Müller, and H. Lischka, Phys. Chem. Chem. Phys. **2**, 2067 (2000).

[96] W. Meyer, *Modern Theoretical Chemistry*, Plenum, New York, 1977.

[97] W. Meyer, J. Chem. Phys. **64**, 2901 (1976).

[98] P. Pulay, S. Saebø, and W. Meyer, J. Chem. Phys. **81**, 1901 (1984).

[99] E. R. Davidson, J. Comput. Phys. **17**, 87 (1975).

[100] B. Liu, *Report on the Workshop: Numerical Algorithms in Chemistry: Algebraic Methods*, Lawrence Brekeley Lab., Univ. of California, California, 1978.

[101] W. Kutzelnigg and D. Mukherjee, J. Chem. Phys. **107**, 432 (1997).

[102] C. L. Janssen and H. F. Schaefer, Theor. Chim. Acta. **79**, 1 (1991).

[103] E. Neuscamman, T. Yanai, and G. K.-L. Chan, J. Chem. Phys. **130**, 169901 (2009).

[104] FEMTO :: An Integrated Toolset For The Automated Tensor Generation, Version 0.1.0, M. Saitow (https://github.com/msaitow).

[105] L. Kong and E. F. Valeev, J. Chem. Phys. **131**, 214105 (2011).

[106] F. C. C. P. del Valle, , and C. Valdemoro, Phys. Rev. A **47**, 971 (1993).

[107] F. Colmenero and C. Valdemoro, Phys. Rev. A **47**, 979 (1993).

[108] F. Colmenero and C. Valdemoro, Int. J. Quantum Chem. **51**, 369 (1994).

[109] K. Yasuda and H. Nakatsuji, Phys. Rev. Lett. **76**, 1039 (1996).

[110] K. Yasuda and H. Nakatsuji, Phys. Rev. A **56**, 2648 (1997).

[111] D. A. Mazziotti, Phys. Rev. A **57**, 4219 (1998).

[112] D. A. Mazziotti, Chem. Phys. Lett. **298**, 419 (1998).

[113] J. E. Harrison, Phys. Rev. A **65**, 052507 (2002).

[114] K. R. Shamasundar, J. Chem. Phys. **131**, 174109 (2009).

[115] W. Kutzelnigg, K. R. Shamasundar, and D. Mukherjee, Mol. Phys. **108**, 433 (2010).

[116] M. Hanauer and A. Köhn, Chem. Phys. **401**, 50 (2012).

[117] A. J. Coleman, Rev. Mod. Phys. **35**, 668 (1963).

[118] The Haskell Programming Language, http://www.haskell.org/.

[119] In case of the tensor-contracted term with five factors, the number of the unique ways to construct the binary contraction increases to 105(!). For the term with the arbitrary number of the tensor factors, a sophisticated algorithm to form the binary contraction and to factorize the common intermediate tensor is developed on the basis of the binary-tree data structure. Because of the recursive nature of this, the algorithm can be implemented straightforwardly by using the functional programming language. This will be described in detail elsewhere.

[120] A. D. Becke, Phys. Rev. A **38**, 3098 (1988).

[121] J. P. Perdew, Phys. Rev. B **33**, 8822 (1986).

[122] M. Reiher and A. Wolf, J. Chem. Phys. **121**, 2037 (2004).

[123] M. Reiher and A. Wolf, J. Chem. Phys. **121**, 10945 (2004).

[124] A. Wolf and M. Reiher, J. Chem. Phys. **124** (2006).

[125] B. Roos, R. Lindh, P. Malmqvist, V. Veryazov, and P. Widmark, J. Phys. Chem. A **109**, 6575 (2005).

[126] Y. Kurashige, M. Saitow, J. Chalupský, and T. Yanai, Phys. Chem. Chem. Phys. , (submitted).

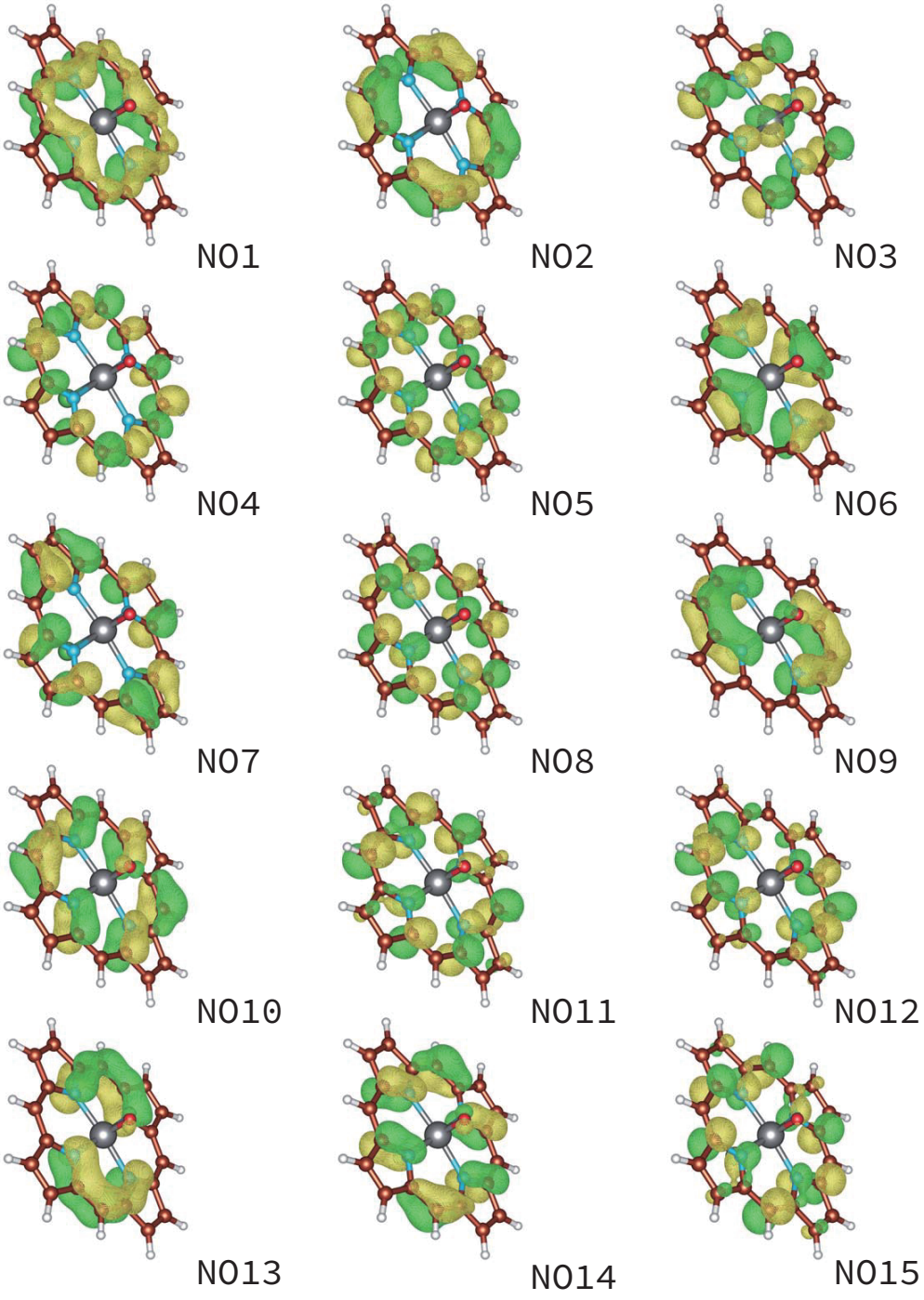

Figure 3.1: The one-dimensional DMRG ordering of the natural orbitals (NOs), which were used to form the lattice sites of the DMRG state. These MOs were depicted by using the CHARMOL, a program for molecular graphics (`http://sourceforge.net/projects/charmol/`)

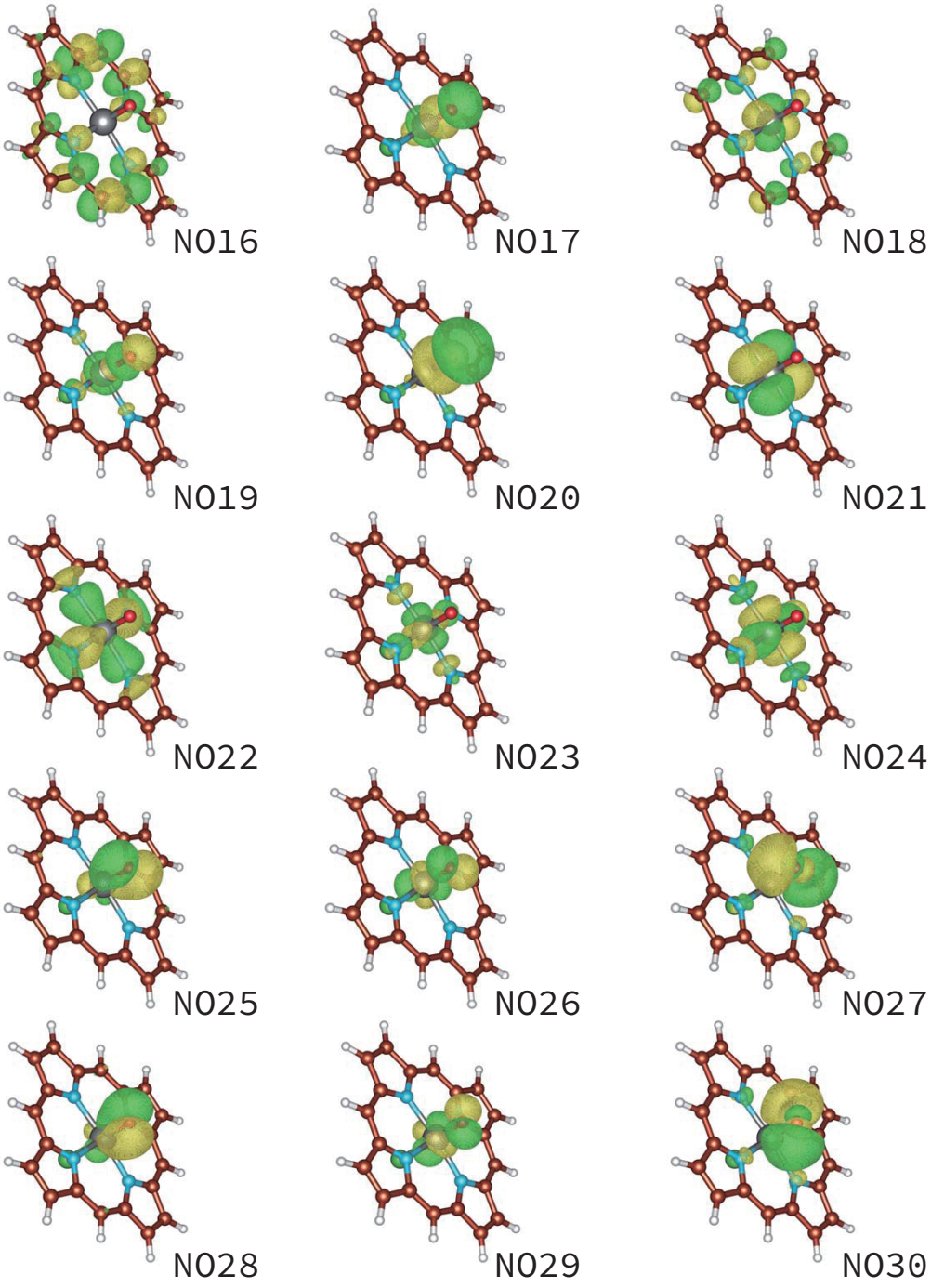

Figure 3.1: (*Continued.*)

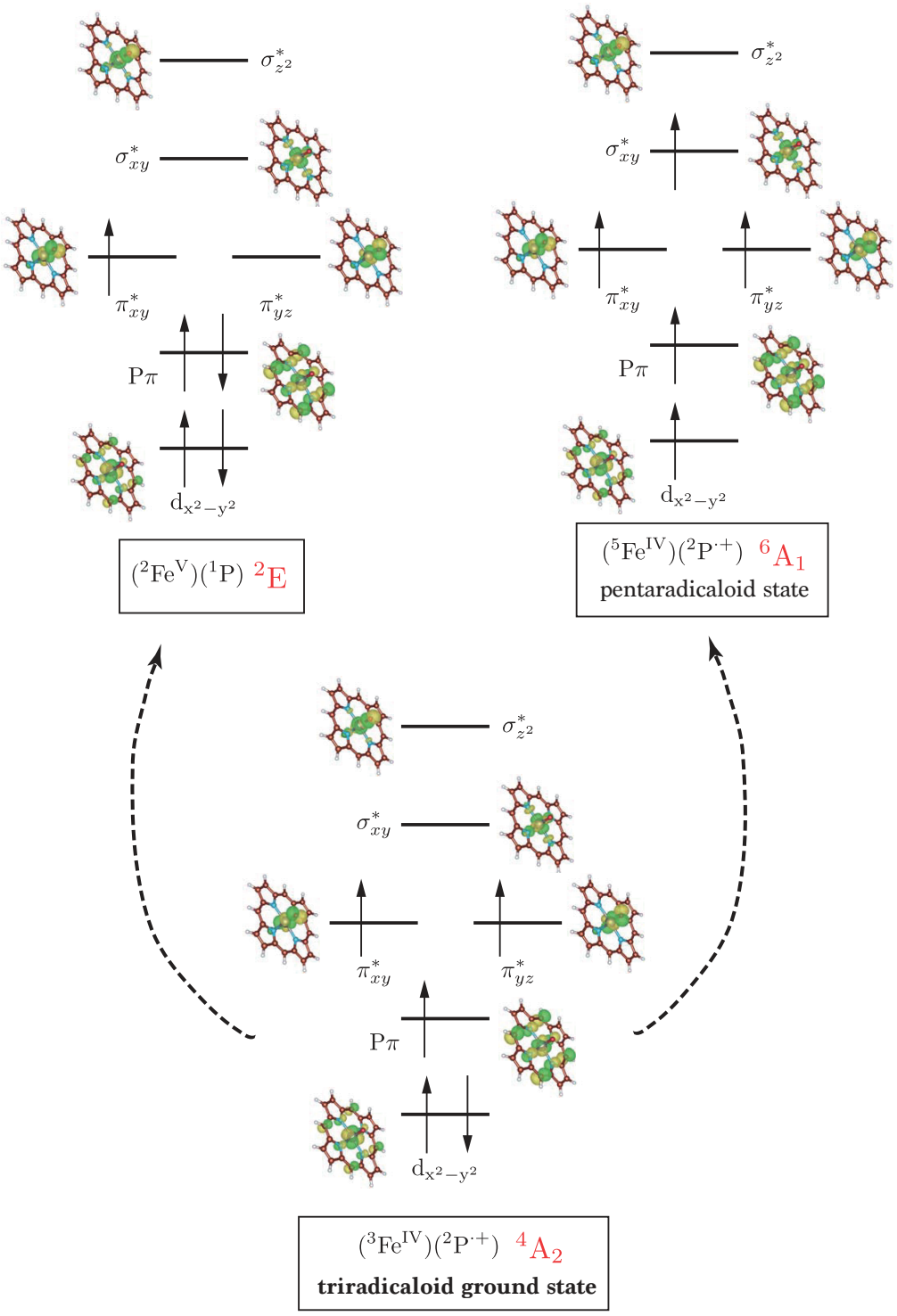

Figure 3.2: The elctronic occupations for the iron-oxo porphyrin electromers where triradicaloid iron(IV)-oxo is recognized as the ground state by experimental means. The other two states ($^6A_1$ and ^2E states) are the two lowest lying excited state.

Chapter 4

Radical O-O coupling reaction in diferrate-mediated water oxidation studied with multireference wave function theory

Y. Kurashige, M. Saitow, J. Chalupský, and T. Yanai, "Radical O-O coupling reaction in diferrate-mediated water oxidation studied with multireference wave function theory", *Physical Chemistry Chemical Physics*, (under review).

4.1 Introduction

Solar-driven catalysis of water splitting has been a subject of intensive investigation for many years; the focus has been mainly on understanding the biological process of photosynthesis to evolve atmospheric oxygen[1, 2] as well as developing its artificial analog using synthetic systems for solar energy conversion and storage.[3, 4, 5, 6, 7, 8] This catalytic process mediates two reactions, H_2 formation and water oxidation, which involve a multi-electron transference coupled to proton migration. The oxidation of water to O_2 is considered to be a rate-limiting step, which is largely responsible for a multi-electronic process to form the O-O bonding, prior to release of O_2, through the buildup of high redox potentials. Detailed characterization of the O-O bond formation is thus imperative for improving catalyst design while it generally remains elusive despite extensive theoretical and experimental investigations.[9, 10, 11, 12, 13, 14, 15, 16, 17, 18, 19, 20]

Two classes of the reaction mechanisms of the O-O bonding event have been proposed: (i) oxo or oxyl aggregation associated with direct radical coupling and (ii) nonradical acid-base mechanism triggered by nucleophile attack. In the radical coupling mechanism (i), the O-O bond is formed between two cofacial metal-bound radicaloid oxo or oxyl (M-O) units through the combination of two singly-occupied M-O π orbitals; this process has been widely implicated in the design of multi-center water oxidation catalysts. The acid-base mechanism (ii) embraces attack of hydrolytic water to an electrophilic M-O group, in which the formation of the O-O σ bond is conjugated with the breaking of the M-O π bond via the reduction of the metal center.

Over the past decades, there have been a large degree of theoretical and experimental efforts devoted to the design of efficient water oxidation catalysts. Numerous types and variants of synthetic systems to catalyze the water-splitting reaction have been developed and characterized, ranging from single-center transition metal complexes,[21, 22, 23, 24, 25, 26] dimeric or dimetalic coordination systems,[27, 28, 29, 30] tetra-nuclear clusters[31, 32] to solid-state metal-oxide systems.[33, 34] Although high-performance catalytic systems that operate under homogeneous condition have been synthesized, many of the most efficient catalysis to date relies on the use of expensive and earth-scare transition metals such as ruthenium[16, 24, 17, 25, 32, 5, 27, 26, 6] and iridium[21, 22, 23].

An increasingly important challenge arising in recent years is to develop economically-viable water oxidation catalysts using earth-abundant materials,[35, 36] e.g., cobalt,[37, 38, 4] manganese,[13] iron,[39, 40] and copper[41] based systems; however, the $3d$ metal-based catalysis remains much less established. As desirable catalysts using the first-row transition metals, iron-based systems are most valued in the sense that iron is the most abundant and environmentally benign. Recent studies led to the discovery of promising catalysts of iron-mediated water oxidation, such as iron-centered complexes bearing tetraamido macrocyclic ligands[39] or tetradentate N-donor ligands;[40] they show marked catalytic ability in the presence of an excess of some sacrificial oxidant. Theoretical and experimental characterizations of these systems are at present under active investigation.[42, 43, 44, 45]

Water oxidation is catalyzed in nature by Mn_4Ca cofactor embedded within the oxygen-evolving complex (OEC) in photosystem II.[1, 2] Determination of the exact

molecular details of the biological water-splitting reaction has been a challenging goal for experimental[1, 2, 46, 47, 48, 49, 50, 51, 52, 53, 54, 55] and computational studies[56, 57, 58, 59, 60, 61, 62] of the OEC. It is considered to eventually inspire us with the basic design of efficient synthetic catalysts based on abundant metals like OEC. Recently, atomistic details of the crystal structure of PSII with OEC in the dark-stable S1 state of Kok's catalytic cycle was reported by Shen and Kamiya groups, dissecting the topological structure of the Mn cluster at a resolution of 1.9 Å.[1] This work paves the way for illuminating the physical chemical details of OEC through electronic structure simulation as well as spectroscopic analysis. Earlier computational studies on the Mn_4Ca were conducted entirely within the mean-field electronic structure approaches based on density functional theory (DFT),[56, 57, 58, 59, 60, 61] which is a workhorse method of quantum chemistry that has been widely applied to various catalytic systems despite the cost of uncontrolled functional.

Formidable difficulties in quantum mechanical modeling of the electronic character of the tetra-nuclear Mn complex lie in the fact that the Mn ions each permit a multi-valency ascribed to a partially-filled $3d$ shell and there are diverse types of the Mn-O and Mn-Mn chemical interactions. In the picture based on the configuration interaction (CI) theory, such complex electronic states can be in a rigorous sense interpreted as a superposition of multiple electron configurations. For each Mn, the description of $3d$ electrons that quantum-mechanically fluctuate in the $3d$ shell within a narrow energy range requires multiple energetically-competing configurations. This near-degeneracy can be attributed to electron correlation in many-body theory, and such correlated nature is referred to as

multireference, which cannot be in principle properly handled with the mean-field or one-electron theory including DFT. In the Mn_4Ca cluster, the full set of such configuration, arising from the Mn $3d$ orbitals and the μ-oxo $2p$ bridges, involves an active space of 44 electrons in 35 orbitals, denoted (44e,35o), resulting in over 10^{18} configurations.[62] This thus involves a large degree of quantum entanglement of electrons, which is out of reach of the conventional approaches.

In the previous study,[62] we tackled this nontrivial complexity of the Mn cluster using the quantum simulation based on the density matrix renormalization group (DMRG) algorithm.[63, 64, 65, 66, 67, 68, 69, 70, 71, 72, 73, 74, 75] The DMRG allowed us to efficiently describe the entanglement structure of a large-dimensional wave function in a space of (44e,35o) at the near full CI level of accuracy by reducing it to the special structure of low energy physical states. In addition, our recent development[76, 77, 78] enables the orbital optimization to be coupled with active space DMRG calculations in the same manner as the complete active space self-consistent field (CASSCF) calculations.[79, 80] This level of theoretical descriptions, corresponding to CASSCF(44e,35o), has been a long-standing demand of quantum chemists. Our DMRG calculations confirmed that at the Shen-Kamiya X-ray diffraction geometry, the Mn cluster model is reduced relative to the widely-accepted biological S1 state, supporting the recent hypothesis about potential X-ray damage to Mn ions.[81, 58] We further identified multiple low-lying energy surfaces associated with the structural deformation seen using X-ray crystallography, highlighting "spin-independent" multi-state reactivity in transition metal chemistry. In addition, the relations between bonding nature and changes in orbital entanglements were illustrated

across Kok's S1 to S4 states. We here note these calculations did not take into account dynamic correlation, which is irrelevant to the qualitative accuracy in determining reference electronic structures but is known to have a certain quantitative impact on relative energies.

In this work, using the DMRG method, we investigate the electronic-level mechanism of the O-O bond formation mediated by 3*d*-block transition metal complex. Recently, Roth and colleagues reported a joint experimental-computational analysis to unravel the mechanism of a bench-top water oxidation catalyzed by potassium ferrate ($K_2Fe^{VI}O_4$).[9] In the study, comparisons of experimental and DFT-based free energy as well as oxygen-18 kinetic isotope effects[82] were made, showing that the intramolecular radical O-O coupling within the dimerized ferrate, or diferrate, occurs in preference to intermolecular water attack ascribed to the acid-base mechanism. This finding renders diferrate attractive for basic study as a model of 3*d* metal-based water-splitting oxidants. The feature of the O-O bond formation deduced for the diferrate complex bears a structural resemblance to that hypothesized for the Mn cluster of the OEC,[83, 84, 57] in that the both undergo the reaction that couples two terminal O ligands over the coordinated metal centers. A difference may arise from the electronic-level understanding of these O-O couplings. The determination of oxo (M=O) versus oxyl ($M-O^{\bullet}$) coupling is of considerable interest. It was shown by Roth *et al.* experimentally and computationally that the O-O bond formation in diferrate originates from the coupling of the adjacent oxo moieties (Fe(VI)=O).[9]

The object of this study is to carry out detailed quantum chemical analysis on the

above-mentioned direct oxo-coupling reaction using multireference theory. We employ various levels of active space to evaluate the potential energy profiles, in which the reaction energies and redox behavior of diferrate are monitored as a function of the O-O bond distance. As described earlier, the multireference treatment is highly desirable (but also challenging) for electronic structure calculations of multi-center transition metal complexes. The bonding nature of Fe-O has been extensively investigated in earlier theoretical studies on the chemistry of heme and nonheme oxygen activating iron enzymes.[85, 86, 87] These studies coped with difficulties in characterizing the Fe-O bonding nature because it has remarkable electronic flexibility associated with multivalent and variously-oxidizable nature of the iron ion. The importance of multireference understanding arises again from this flexible electronic structure in the Fe-O bond. In the present study, the multireference character of two interacting Fe-O moieties is described using an entangled many-electron wave function in a high-dimensional active space, which can be computed only with *ab initio* DMRG. Another challenge of this study lies in the quantitatively accurate determination of relative energies, where dynamic correleation effects also play a major role. We attempt to account for dynamic correlation energies on top of the active space DMRG wave function through complete active space second-order perturbation (CASPT2) theory[88, 89] and multireference configuration interaction (MRCI) theory.[90, 91] The joint theory to combine DMRG with CASPT2 and MRCI was developed recently by our group, referred to as DMRG-CASPT2[92, 93] and DMRG-MRCI,[94] respectively. It has been recognized that the inclusion of the second (higher-lying) valence shell into active space treatment, the so-called "double shell" correction,[85, 86, 95] plays

a critical role in complementing the performance of the simple PT2 treatment. These unprecedented computational settings allow us to gain a deeper insight into chemical bonds of Fe-O and dimeric coupling.

This paper is organized as follows. In Sec. 2, we provides a brief review of quantum chemical DMRG and associated dynamic correlation methods. Computational details are given in Sec. 3. The results from our calculations are displayed along with discussion in Sec. 4. Finally, Sec. 5 concludes our work.

4.2 Theoretical methods

Although general algorithmic aspects of the present *ab initio* (or quantum chemical) DMRG approaches are given in detail in our previous work,[76, 72, 94, 92, 93] their basic ideas and background are recapitulated in this section in order to introduce the notations and give a self-contained description of our methods.

4.2.1 *Ab initio* density matrix renormalization group

The DMRG theory, introduced by White,[63, 64] is originally a numerical method of condensed-matter physics to study strongly correlated quantum phenomena. In the DMRG algorithm, the wave function of highly correlating electrons is encoded into the special entanglement structure that is present in low-lying physical quantum states. Quantum chemical DMRG is formulated by assigning orbitals to the lattice.[65, 66, 67, 68, 69, 70, 72, 71, 73, 74, 75] The resulting description is represented in a compact, re-

duced form that is based on a contracted product of tensors, the so-called matrix product state ansatz,[71, 73, 74] given as

$$|\Psi^{\mathrm{DMRG}}\rangle = C^{n_1}_{i_1} C^{n_2}_{i_1 i_2} \cdots C^{n_{k-1}}_{i_{k-2} i_{k-1}} C^{n_k}_{i_{k-1}} |n_1 n_2 \cdots n_k\rangle, \tag{4.1}$$

where the Einstein summation convention is imposed and $|n_1 n_2 \cdots n_k\rangle$ denotes the Slater determinant in an occupation number form; n_μ is the occupation of the orbital μ, and the total number of orbitals is k. The tensorial objects $C^{n_\mu}_{ij}$ in eqn (4.1) are each optimized one after the other in a variational fashion through the DMRG sweep procedure, in which the Hamiltonian is repeatedly diagonalized in the model space with renormalized basis. The dimension of the renormalized Hilbert space is quadratically dependent on the user-specified integer parameter, hereafter denoted M, which is equal to the dimension of the auxiliary indices $i_1, i_2, \cdots i_{k-1}$. The level of the approximation is thus determined by M and is typically chosen to be in the range of a few hundreds to thousands for molecular electronic structure calculations. With increasing M, the solution variationally approaches the full configuration interaction (FCI) accuracy.

The DMRG method is by nature particularly efficient for describing 1D many-body systems, as eqn (4.1) succinctly highlights the 1D nature of the DMRG representation. Despite the specialized ansatz, a capability of treating high dimensional problems has been shown in some systems studied in condensed-matter physics, such as 2D Kagome lattice antiferromagnet.[96] In a very similar sense, the non-1D complexity of correlation nature arises in electron structures of inorganic coordination molecules. Applicability of DMRG to multinuclear transition metal compounds has been revealed in recent studies

using the quantum chemical (or *ab initio*) DMRG approach.[69, 70, 72, 97, 92, 93, 75, 62] Challenging applications to such complex chemical systems can be found in the previous DMRG studies on dicopper-dioxygen isomers,[69, 72, 97] tetranuclear manganese cluster,[62] and 2Fe-2S ferredoxins.[75] This capability considerably exceeds the limitation of the conventional approaches.

In this study, the electronic structure of the dimeric ferrate molecule is characterized using the DMRG method. In general, extra complexity for calculation setups arises in the *ab initio* DMRG approach; users are required to specify the shapes of the orbitals and the arrangement of their order on the 1D lattice. The accuracy of the DMRG depends much on them. A set of localized molecular orbitals (MOs) obtained by the Pipek-Mezey transformation[98] or other variants is a natural choice for shaping the orbitals. The use of these atomic-orbital (AO)-like MOs likely improves the feasibility of the orbital ordering. The bonding topology in the molecule serves as a clue to seize the correlation network among the orbitals. It is, however, not so obvious to reduce the topology of transition metal compounds, like diferrate, onto 1D because their molecular structures are generally rich in dimension. Finding the best ordering is technically a hard problem, but in fact in many cases reasonable ordering that give sufficient accuracy can be obtained by heuristic approaches. Variational nature of the DMRG energy is helpful for the determination of the shapes and order of the orbitals.

4.2.2 Active space DMRG model

It is suitable to use the DMRG for the treatment of the correlation problem in active space, which is a central model space to describe the static (or strong) correlation ascribed to the overlap of near-degenerate valence atomic states. We employ the complete active space (CAS) model[79, 80] to construct the active space. In the CAS approach, the set of MOs in quantum chemical calculations is divided into two sections, referred to as active and external orbitals, respectively, and the static correlation is accounted for using the active orbitals through the exact or near-exact diagonalization. The DMRG enables us to handle exceedingly larger-size CAS.

The active space DMRG method is carried out in conjunction with the orbital optimization procedure, resulting in a highly-scalable analog of the complete active space self-consistent field (CASSCF) method. This integrated approach is referred to as the DMRG-CASSCF method.[76, 77, 78] The orbital optimization is a key ingredient for the active space treatment of the transition metal systems because it enables the identification of the active orbitals in a systematic fashion. The DMRG-CASSCF calculations deliver the optimal active orbitals that are determined self-consistently by energy minimization.

4.2.3 DMRG-CASPT2 and DMRG-MRCI methods

The way of characterizing electron correlation in terms of static and dynamic correlations separately is a well-established concept, and the active space approaches treat these types of correlation on the separated physical scales. Given that static correlation

is accounted for by DMRG-CASSCF, the rest of correlation, namely dynamic correlation, arises from electronic interactions between active space orbitals and external (core and virtual) orbitals. Their description can be efficiently obtained with a lower level theory, such as configuration interaction,[90, 91, 99, 100] perturbation theory,[79, 80] exponential-based transformation,[97, 101] etc. In this study, the complete active space second-order perturbation (CASPT2)[92, 93] and multireference configuration interaction (MRCI)[94] theories are used on top of the DMRG-CASSCF reference to achieve qualitative accuracy of correlation energies. Dynamic correlation effects are considered to be crucial for transition metal systems where marked short-range Coulombic interaction arises from a number of electrons that are locally packed in atomic *d*-block space of metal sites.

The CASPT2 was introduced by Roos *et al.*[79, 80] as the multireference extension of the second-order Møller-Plesset theory. Given the DMRG-CASSCF description as the zeroth order wave function $|\Psi^{(0)}\rangle$, the DMRG-CASPT2 method determines the first-order perturbative correction to it, denoted $|\Psi^{(1)}\rangle$, as given by,

$$|\Psi\rangle = |\Psi^{(0)}\rangle + |\Psi^{(1)}\rangle \,. \tag{4.2}$$

The first order wave function $|\Psi^{(1)}\rangle$ is expanded into the configuration basis within the single and double excitation space:

$$|\Psi^{(1)}\rangle = \sum_{pqrs} c_{pqrs}\, \hat{E}_{pq}\hat{E}_{rs}|\Psi^{(0)}\rangle = \sum_{\mu} c_{\mu}|\mu\rangle \,, \tag{4.3}$$

where the fourfold compound index $pqrs$ is labeled as μ (and ν afterward). The first

order equation to obtain c_μ is written as:

$$\sum_\nu [\langle\mu|\hat{H}_0|\nu\rangle - E_0\langle\mu|\nu\rangle]\, c_\nu = -\langle\mu|\hat{V}|\Psi^{(0)}\rangle\,, \tag{4.4}$$

where the zeroth order part $\hat{H}_0$ and perturbation $\hat{V}$ constitute the Hamiltonian $\hat{H}$, as given by $\hat{H} = \hat{H}_0 + \hat{V}$. The definition of $\hat{H}_0$ is given in detail in ref. [92, 93]. The zeroth order energy E_0, the equivalent of the DMRG-CASSCF energy, is then written as $E_0 = \langle 0|\hat{H}_0|0\rangle$, and the DMRG-CASPT2 energy $E_{\mathrm{DMRG-CASPT2}}$ is obtained as:

$$E_{\mathrm{DMRG-CASPT2}} = E_0 + E_2\,, \tag{4.5}$$

with the second-order energy given by $E_2 = \langle\Psi^0|V|\Psi^1\rangle = \sum_\mu \langle\Psi^{(0)}|\hat{V}|\mu\rangle\, c_\mu$. The most computational intensive part of DMRG-CAPST2 calculations lies in the evaluations of the 3- and 4-particle rank reduced density matrices (RDMs) from the active space DMRG wave function. They are mainly used to form the first order equation (eqn (4.4)).

The MRCI method has been widely used as a powerful means for achieving highly accurate solutions for multireference electronic systems.[90, 91, 99, 100] The basic algorithm of MRCI can be simply conceived as diagonalizing Hamiltonian in CI space, which is represented with a liner combination of configurations. The DMRG-MRCI wave function is linearly expanded into singly- and doubly-excited internally-contracted configurations relative to DMRG reference space $|\Psi^{(0)}\rangle$, as given by

$$|\Psi\rangle = (c_0 + \sum_{pqrs} c_{pqrs}\, \hat{E}_{pq}\hat{E}_{rs})|\Psi^{(0)}\rangle\,. \tag{4.6}$$

The CI coefficients $\{c_\mu\}$ including c_0 are determined by the eigen-equation:

$$\mathbf{Hc} = E_{\mathrm{DMRG-MRCI}}\mathbf{Sc}\,, \tag{4.7}$$

where $\mathbf{H}_{\mu\nu} = \langle\mu|\hat{H}|\nu\rangle$, $\mathbf{S}_{\mu\nu} = \langle\mu|\nu\rangle$, and the eigenvalue corresponds to the DMRG-MRCI energy (see also ref [94]). Our DMRG-MRCI implementation entails the *a posteriori* size-consistency correction, also known as Davidson (+Q) correction,[102, 103, 104, 105] which can be computed from $\mathbf{c}$.

4.3 Computational details

4.3.1 Density functional theory (DFT) calculations

Spin-polarized (or spin-unrestricted) DFT calculations were performed on the dimeric ferrate molecule (μ-1,2-oxo-bridged diferrate) with the GAUSSIAN 09 package,[106] employing the def2-TZVP basis sets.[107] The geometry optimizations for reactant and product states, transition state (TS) search, and potential energy surface (PES) scan were carried out using the B3LYP exchange-correlation functional[108] under C_{2v} molecular symmetry. In the PES scan calculations, the O-O bond distance was used as the scanning variable, which was set to constant values, allowing the other geometric parameters to be relaxed; the scanned O-O bond length was chosen to be in the range between 1.3 and 1.8 Å by a step size of 0.1 Å and between 2.0 and 3.0 Å by 0.2 Å for monitoring the O-O bond formation. Upon the molecular geometries obtained by B3LYP, which are referred to as the B3LYP geometries, we performed single-point energy calculations using the meta-hybrid functional TPPSh.[109] In these DFT calculations, antiferromagnetic order arising from the two localized Fe spin sites was described with the spin-polarized (or broken-symmetry) treatment. The net charge of the system was set to +2, and the num-

bers of α and β electrons were assumed to be equal. Relativistic effects were neglected for the DFT calculations. In this study, consideration of environment effects was left out of scope.

4.3.2 DMRG-CASSCF/CASPT2/MRCI calculations

Multireference calculations using the DMRG-CASSCF, DMRG-CASPT2, and DMRG-MRCI methods were performed on the B3LYP geometries with the system isolated in the gas phase. We used the atomic natural orbital (ANO) basis sets[110] corresponding to Fe: $[21s15p10d6f4g]$ / $(6s5p3d2f1g)$, O: $[10s9p4d3f]$ / $(4s3p2d1f)$, and H: $[8s4p]$ / $(2s1p)$ contractions. Scalar relativistic effects were included using the second-order Douglas-Kroll-Hess (DKH) Hamiltonian.[111, 112, 113] The PES of the O-O bond formation was calculated in the singlet state with the same molecular charge as used in the DFT calculations.

The active space for the DMRG treatment was composed of the following orbitals in the AO representation: (i) all the valence $3d$ orbitals for the two Fe atoms, (ii) all the $2p$ orbitals of the two adjacent O ligands associated with the O-O bonding, (iii) three higher-lying O $2p'$ (or $3p$) orbitals for the double-shell treatment of each of the Fe-oxo moieties, and (iv) two $2p$ orbitals for each of the remaining five O atoms. This CAS setting resulted in an active space of 36 electrons distributed in 32 ($= 5\times2 + [3 + 3]\times2 + 2\times5$) orbitals, denoted as CAS(36e,32o), which is tractable with the DMRG approach.

The active orbitals used in the DMRG calculations were localized with "split-localized" procedure,[114] subject to the reduced C_s symmetry constraints, to transform them into

efficient local sites that can be mapped to the DMRG 1D lattice. The localized orbitals obtained by the DMRG-CASSCF calculation for the reactant structure is shown in Fig. S1† in order of our DMRG orbital ordering. Different sets of orbital ordering were used for three segments of the reaction path as a function of the O-O distance: R(O-O) $\leq$ 1.8 Å, 1.8 $\leq$ R(O-O) $\leq$ 2.2 Å, and R(O-O) $\geq$ 2.2 Å; we confirmed that the difference in the orbital ordering at the joints, i.e., R(O-O)=1.8 and 2.2 Å, altered the energies only to a negligible degree. The active space DMRG wave functions were determined with $M = 512$ and 1024 spin-adapted[70, 75] renormalized basis, and the natural orbitals and associated occupancies were obtained from the density matrices.

The dynamic correlation was evaluated with DMRG-CASPT2 and DMRG-MRCI+Q on top the preceding DMRG-CASSCF description. In the DMRG-CASPT2 calculations, the modification to the zeroth-order Hamiltonian was employed with the ionization potential/electron affinity (IPEA)[115] specified to be 0.25 a.u. along with an imaginary denominator shift (IS) of 0.2 a.u. The DMRG-MRCI+Q calculations employed the overlap truncation with the threshold of $\tau = 5 \times 10^{-2}$ (see also ref [94] for the definition of τ). The seventeen core orbitals were frozen. The three-particle rank RDM was evaluated directly using the DMRG wave function, while the four-particle rank RDM was evaluated in an approximate fashion using lower-particle rank RDMs through the cumulant reconstruction neglecting the connected four-rank cumulants.[94, 116]

4.3.3 Conventional CASPT2/MRCI calculations

We examined the dependence of accuracy of the multireference treatments on the size of active space. The CASSCF, CASPT2 and MRCI+Q calculations were performed with another two sets of active space: CAS(4e,4o) and CAS(20e,14o). The MOLPRO[117] and MOLCAS[118] packages were used for the multireference calculations with CAS(4e,4o) and CAS(20e,14o), respectively. MRCI+Q(20e,14o) was not considered in this study. The supersymmetry was invoked in CASSCF(20e,14o) to avoid mixing of inner-shell orbitals and active-space orbitals. The IPEA and IS parameters were set to the same as used in the DMRG-CASPT2 calculations.

4.4 Results and Discussions

The O-O bonding reaction is the primal focus of the present study. Fig. 4.1 shows the molecular structures of the diferrate molecule that were optimized with the B3LYP calculations for the reactant, transition intermediate, and product states, labeled by **R**, **TS**, and **P**, respectively. The bond distance between the two O atoms associated with the O-O bonding, denoted R(O-O), was 3.226, 1.893, and 1.347 Å for **R**, **TS**, and **P**, respectively. The O-O forming reaction proceeds as a function of R(O-O). With decreasing R(O-O), the bond between the Fe ion and O ligand and is increasingly stretched: R(Fe-O)= 1.584, 1.647, and 1.757 for **R**, **TS**, and **P**, respectively. The B3LYP geometries considered in this study are all provided in ESI.†

Comparisons are made in the potential energy profiles between the DFT and DMRG

results (Fig. 4.2) and between the DMRG and conventional multireference results (Fig. 4.3). Fig. 4.2 and 4.3 show the energies relative to the **R** state. Activation barriers ($\Delta E(\mathbf{R} \rightarrow \mathbf{TS})$) and reaction energies ($\Delta E(\mathbf{R} \rightarrow \mathbf{P})$) are summarized in Table 4.1. Total energies at the calculated points were shown in Table S1.† DMRG-CASSCF, DMRG-CASPT2, and DMRG-MRCI+Q all commonly predicted that the active barrier and reaction energy are positive and negative, respectively, and the O-O coupling reaction should be more or less facile. This qualitative trend is basically in accord with the DFT potential energy profiles as well as the results of the earlier study of Roth *et al.*[9] Some marked differences in quantitative features were observed among DMRG and DFT results. The activation barrier obtained by DMRG-CASSCF was estimated to be ca. 5 kcal/mol higher than those by DMRG-CASPT2 and DMRG-MRCI+Q. The reaction energy of DMRG-MRCI+Q was ca. 4 kcal/mol lower than those of DMRG-CASSCF and DMRG-CASPT2. From general theoretical point of view, the errors of the results should be MRCI+Q $<$ CASPT2 $<$ CASSCF. A notable difference between the DFT and DMRG results arises from the reaction energies (Fig. 4.2). The DFT predictions provided a rather stabilized **P**, which was lower in energy by ca. 9-11 and 5-7 kcal/mol relative to the DMRG-CASPT2 and DMRG-MRCI+Q results, respectively. This should lead to important differences in the understanding of the chemical process subsequent to **P**, which is followed by O_2 release. Note that the use of the DFT(B3LYP) geometries for the DMRG calculations should be validated in future work.

As shown in Fig. 4.3, the minimal active space treatment modeled by CAS(4e,4o) caused a complete failure with and without dynamic correlation correction, yielding

chemically invalid potential energy profiles. The relative energies of CASSCF(20e,14o) on the reaction coordinate **R** → **TS** showed a good agreement with DMRG-CASSCF energy profile; however, the relative energy of **P** was underestimated to a great extent by CASSCF(20e,14o) with an error of ca. 15 kcal/mol relative to that of DMRG-CASSCF. The CASPT2 correction to CASSCF(20e,14o) gave rise to a questionable potential energy profile, in which minima were observed at the intermediates of the reaction pathway. The CASPT2 and MRCI+Q results for the present diiron system were shown to depend largely on the active space.

We next proceed to qualitative characterization of the role of electrons in the O-O bonding formation. On the basis of natural orbital (NO) analysis, relative change in electron populations was monitored along the reaction coordinate. The active space wave functions obtained by the DMRG-CASSCF and conventional CASSCF calculations were used to derive the NOs and associated occupation numbers (NOONs), which range from 0 (unoccupied) to 1 (singly occupied) and 2 (doubly occupied). In the natural orbital based picture, electron populations determined by the conventional CASSCF were found to be more or less similar to those by DMRG-CASSCF using large active space. Therefore, unless otherwise noted, our description of the natural orbitals in the O-O bonding process is given hereafter at the CASSCF(20e,14o) level of theory.

In the multireference calculations, the **R** state was shown to be an antiferromagnetic state formed by four near-singly-occupied orbitals (**9**–**12** in Fig. 4.4). They are localized on the two Fe-O units, as shown in Fig. 4.4 as well as Fig. S4[†] [DMRG-CASSCF(36e,32o)]. The bonding nature of the Fe-O units for **R** is characterized in detail as follows:

1. In our calculation for **R**, the oxidation states of the Fe and O ions are confirmed to be +6 and −2, respectively.
2. Fe(VI) ions each have two singly-occupied $3d$ orbitals, which are related to the two-fold degenerate e orbitals arising from the tetrahedral complex and having a lower-energy level relative to the t_2 counterparts. This reflects the fact that the monomeric ferrate can be seen approximately as a tetrahedral coordination complex.
3. As shown in Fig. 4.5, the singly-occupied $3d_{xz}$ ($3d_{yz}$) of each Fe is coupled to the doubly-occupied $2p_x$ ($2p_y$) orbital of the associated O ligand. This orbital coupling between Fe d and O p orbitals gives rise to the bonding and antibonding π orbitals, which are designated as ψ_{d+p} and ψ_{d-p}, respectively, and evaluated to be doubly and singly occupied, respectively. This interaction picture shows that the O atom coordinates Fe as the oxo ligand and the two spins are built up at each oxo group.
4. The four singly-occupied NOs in Fig. 4.4 (**9**–**12**) are regarded as formed by the σ and π interactions between two units of ψ_{d-p} arising in the dimeric Fe(VI)=O. As shown in Fig. 4.6, they are interpreted as bonding σ_{d-p} (**9**) and π_{d-p} (**11**) orbitals as well as anti-bonding σ^*_{d-p} (**10**) and π^*_{d-p} (**12**) orbitals. Note that the singlet state is totally formed with these open shells, meaning the spins on them are coupled antiferromagnetically. The similar orbital interactions take place between two units of ψ_{d+p}, leading to σ_{d+p} (**5**), σ^*_{d+p} (**6**), π_{d+p} (**7**), and π^*_{d+p} (**8**) orbitals, which are all doubly occupied.

Table 4.2 shows the occupancies of the σ_{d-p}, σ^*_{d-p}, π_{d-p}, and π^*_{d-p} orbitals as a function

of the reaction coordinate, **R**, **TS**, and **P**. Natural orbitals and occupancies are shown for **TS** and **P** of (20e,14o) in Fig. Fig. S2, and S3,† respectively, and for **TS** and **P** of (36e,32o) in Fig. S5, and S6,† respectively.

Varying occupancies associated with antiferromagnetic (or radical) coupling in two iron sites were mainly observed in these orbitals. As the reaction proceeds from **R** to **TS**, the strength of the O-O interaction rises to the degree that the occupancies of σ_{d-p} and σ^*_{d-p} approach 1.64 and 0.51, respectively, for CAS(20e,14o) and 1.70 and 0.42, respectively, for CAS(36e,32o), which are rather away from fully singly-occupied nature of these orbitals for **R**. The presence of the approximately doubly-occupied σ_{d-p} orbital indicates that the σ type bond is formed to an appreciable extent. The π_{d-p} and π^*_{d-p} orbitals were found to remain more or less singly occupied in the domain from **R** to **TS**. These occupancies indicate that the adjacent Fe-O species of **TS** form transiently a peroxo bridge.

As the reaction finally turns into **P**, the transfer ratio of one electron from σ^*_{d-p} to σ_{d-p} exceeds 90%, indicating a tight formation of the σ bond in O-O. In addition, we observed a rise in electron populations associated with the forming of π-type O-O bond; the corresponding π_{d-p} and π^*_{d-p} orbitals have an occupancy of ca. 1.7–1.8 and 0.5, respectively.

In Fig. 4.7, an overall mechanism of the electronic process in the diferrate-mediated O-O bonding reaction is schematized. We here introduce the bond order of O-O and Fe-O, denoted as n(O-O) and n(Fe-O), respectively. Let them be estimated using the following formulas in conjunction with the results (Table 4.2) from the natural orbital

analysis:

$$n(\text{O-O}) = (f(\sigma_{d-p}) - f(\sigma^*_{d-p}) + f(\pi_{d-p}) - f(\pi^*_{d-p}))/2 \tag{4.8}$$

$$n(\text{Fe-O}) = 2 - n(\text{O-O}) \tag{4.9}$$

where $f(\tau)$ refers to the NOON of the orbital τ. Table 4.3 shows the estimations of n(O-O) and n(Fe-O). They are reflected by the bond orders of the chemical structures shown in Fig. 4.7.

The prominent feature of this O-O bond formation lies in the dual bonding character associated with σ and π orbital interactions. The formation rate of the σ bond was found to be much faster than that of the π bond. As indicated in our scheme (Fig. 4.7), the metal-oxo bonds are homolitically cleaved and the oxidation states of the Fe ions each decrease. When the O-O bond is formed (**P**), O-O has a bond order of 1.5, exceeding a single bond, and remains coordinated to Fe ions with a bond order of 0.5 (Table 4.3). It was thus indicated that the Fe ions of **P** formally have a non-integer oxidation states, +4.5, i.e. between +4 and +5. In the reaction scheme proposed by Roth *et al.*,[9] the O-O bond of the **P** intermediate was characterized as a single bond, which serves as a bridge connecting the two Fe(V)$-$O$^\bullet$ groups. These descriptions highlight a marked difference between our study and that of Roth *et al.*, which should be quite critical for evaluating the viability of the subsequent O_2 release. Our non-integer picture of electron occupancies arises from the theoretical treatment based on a quantum superposition of electron configurations beyond the single-determinant DFT picture. The discovery of these remarkable chemical bonds in the O-O bond formation was enabled by the quantitative

description of bonding characters, which was properly obtained by the multireference approaches.

4.5 Conclusions

It is of great importance to corroborate the role of electrons that come into play in the O-O bond formation on the basis of quantum chemical theory. The electronic-level elucidation serves as a core foundation to understand the overall mechanism of the water oxidation mediated by artificial or native catalysts. However, the quantum chemical treatment of the catalytic systems involving multiple metal centers poses great challenges. A correct qualitative description of transition metal chemistry can be provided by accounting for all quantum valence degrees of freedom of the electronic wave function. For theoretical analysis of multi-center catalysts having numerous elections that participate in the reaction, such rigorous calculations have been considered to be formidable because of its exponentially growing complexity.

In our previous work,[62] using the DMRG method, we determined many-electron wave functions of the water-splitting Mn_4CaO_5 cluster with the accuracy of the model corresponding to the CASSCF(44e,35o) level of theory; in this active space, $3d$ shells of four Mn atoms as well as $2p$ shells of five oxo bridges were all considered of as highly relevant to identifying the oxidation states of the Mn cluster. In the present study, we displayed the DMRG calculations for the O-O bond formation reaction taking place in the diferrate (two-center) catalyst model, which was previously studied by Roth and

colleagues by means of experiment and DFT simulation.[9] Roth *et al.* provided the scheme of the direct radical coupling of the adjacent oxo ligands in the formation of the O-O bond. We examined this O-O coupling scheme in detail with multireference treatments using large-size active spaces up to CAS(36e,32o) in conjunction with dynamic correlation correction. This work presented the first application of the DMRG-CASPT2 and DMRG-MRCI methods using double shell (i.e. $2p$ and $3p$) active space, which is responsible for the redox behavior of the two oxo units, to the qualitative determination of the potential energy profiles.

Comparisons were made between the potential energy profiles determined by various electronic structure methods. The active space description obtained by the DMRG-CASSCF method which accounts for static correlation alone was quite valuable and robust for getting a qualitative insight into the highly-correlated electronic structure of the system. The contribution of the dynamic correlation to it through DMRG-CASPT2 and DMRG-MRCI was shown to be an indispensable factor for studying potential energy profiles, which are considerably affected by the associated quantitative corrections. Inclusion of double shells in active space plays an important role in obtaining reliable results from CASPT2 calculations. The importance of this double-shell effects has frequently been pointed out by earlier studies;[85, 86, 95] however, handling them with conventional approaches is not computationally feasible, especially for multinuclear complexes.

Overall, our calculations of the potential energy profile confirmed a viability of the O-O bond formation as a result of the coupling of the two Fe-oxo (Fe(VI)=O) units. A marked difference between DFT and DMRG results lies in the relative energy of the

product state with respect to the reactant state. The DFT predictions provided a rather stabilized product state, which was lower in energy by ca. 9-11 and 5-7 kcal/mol compared to the DMRG-CASPT2 and DMRG-MRCI relative energies, respectively. This seems to likely give rise to critical difference in quantitative characterization of the viability of the pathway for O_2 release, which occurs after the O-O bonding step and is thought to be triggered by additional water insertion. Using natural orbital analysis, we offered the intriguing suggestion that the resultant O-O bond is intermediate between single and double or a 1.5 bond, characterized by the formation of a single σ bonding and a substantial portion of a π bonding.

Computational investigations into water oxidation have so far mostly been carried out within the simplifying electronic structure framework of DFT, which uses a one-electron wavefunction picture. Recent technological advances in *ab initio* DMRG and associated dynamic correlation methods open up the possibility for practical, reliable multireference treatments of multinuclear transition metal complexes. Complementing the DFT picture, they provide a more complete and desirable picture at the entangled quantum many-electron level, which should expedite the deeper and accurate understanding of catalytic water oxidation processes. The water attack mechanism, which is thought to be another pathway of the O-O bond formation in diferrate, is out of scope in this study, but needs be investigated using the DMRG approaches in future work.

Bibliography

[1] Y. Umena, K. Kawakami, J.-R. Shen, and N. Kamiya, Nature **473**, 55 (2011).

[2] W. Lubitz, E. J. Reijerse, and J. Messinger, Energy Environ. Sci. **1**, 15 (2008).

[3] X. Li, G. Chen, S. Schinzel, and P. E. M. Siegbahn, Dalton T **40**, 11296 (2011).

[4] Q. Yin et al., Science **328**, 342 (2010).

[5] S. W. Gersten, G. J. Samuels, and T. J. Meyer, J. Am. Chem. Soc. **104**, 4029 (1982).

[6] L. Duan et al., Nat. Chem. **4**, 418 (2012).

[7] R. K. Hocking et al., Nat. Chem. **3**, 461 (2011).

[8] D. Wang and J. T. Groves, P Natl Acad Sci Usa **110**, 15579 (2013).

[9] R. Sarma, A. M. Angeles-Boza, D. W. Brinkley, and J. P. Roth, J. Am. Chem. Soc. **134**, 15371 (2012).

[10] X. Yang and M.-H. Baik, J. Am. Chem. Soc. **128**, 7476 (2006).

[11] X. Yang and M.-H. Baik, J. Am. Chem. Soc. **130**, 16231 (2008).

[12] X. Liu and F. Wang, Coord. Chem. Rev. **256**, 1115 (2012).

[13] G. C. Dismukes et al., Acc. Chem. Res. **42**, 1935 (2009).

[14] F. Bozoglian et al., J. Am. Chem. Soc. **131**, 15176 (2009).

[15] X. Sala et al., Angew. Chem. Int. Ed. **49**, 7745 (2010).

[16] A. E. Clark and J. K. Hurst, *Progress in Inorganic Chemistry*, pages 1–54, John Wiley & Sons, Inc., 2011.

[17] L.-P. Wang, Q. Wu, and T. Van Voorhis, Inorg. Chem. **49**, 4543 (2010).

[18] L.-P. Wang and T. Van Voorhis, J. Phys. Chem. Lett. **2**, 2200 (2011).

[19] E. M. Sproviero, J. A. Gascón, J. P. McEvoy, G. W. Brudvig, and V. S. Batista, Coord. Chem. Rev. **252**, 395 (2008).

[20] K. Tanaka, H. Isobe, S. Yamanaka, and K. Yamaguchi, P Natl Acad Sci Usa **109**, 15600 (2012).

[21] N. D. McDaniel, F. J. Coughlin, L. L. Tinker, and S. Bernhard, J. Am. Chem. Soc. **130**, 210 (2008).

[22] J. F. Hull et al., J. Am. Chem. Soc. **131**, 8730 (2009).

[23] A. Savini et al., Chem. Comm. **46**, 9218 (2010).

[24] J. J. Concepcion et al., Acc. Chem. Res. **42**, 1954 (2009).

[25] H.-W. Tseng, R. Zong, J. T. Muckerman, and R. Thummel, Inorg. Chem. **47**, 11763 (2008).

[26] S. Masaoka and K. Sakai, Chem. Lett. **38**, 182 (2009).

[27] T. Wada, K. Tsuge, and K. Tanaka, Angew. Chem. Int. Ed. **39**, 1479 (2000).

[28] J. A. Gilbert et al., J. Am. Chem. Soc. **107**, 3855 (1985).

[29] C. Sens et al., J. Am. Chem. Soc. **126**, 7798 (2004).

[30] R. Zong and R. P. Thummel, J. Am. Chem. Soc. **127**, 12802 (2005).

[31] R. Brimblecombe, G. F. Swiegers, G. C. Dismukes, and L. Spiccia, Angew. Chem. Int. Ed. **47**, 7335 (2008).

[32] A. Sartorel et al., J. Am. Chem. Soc. **130**, 5006 (2008).

[33] A. Fujishima, Nature **238**, 37 (1972).

[34] Z. Zou, J. Ye, K. Sayama, and H. Arakawa, Nature **414**, 625 (2001).

[35] H. Yamazaki, A. Shouji, M. Kajita, and M. Yagi, Coord. Chem. Rev. **254**, 2483 (2010).

[36] P. Du and R. Eisenberg, Energy Environ. Sci. **5**, 6012 (2012).

[37] M. W. Kanan and D. G. Nocera, Science **321**, 1072 (2008).

[38] D. Shevchenko, M. F. Anderlund, A. Thapper, and S. Styring, Energy Environ. Sci. **4**, 1284 (2011).

[39] W. C. Ellis, N. D. McDaniel, S. Bernhard, and T. J. Collins, J. Am. Chem. Soc. **132**, 10990 (2010).

[40] J. L. Fillol et al., Nat. Chem. **3**, 807 (2011).

[41] S. M. Barnett, K. I. Goldberg, and J. M. Mayer, Nat. Chem. **4**, 498 (2012).

[42] E. E. Kasapbasi and M.-H. Whangbo, Inorg. Chem. **51**, 10850 (2012).

[43] M. Z. Ertem, L. Gagliardi, and C. J. Cramer, Chem. Sci. **3**, 1293 (2012).

[44] G. Chen, L. Chen, S.-M. Ng, W.-L. Man, and T.-C. Lau, Angew. Chem. Int. Ed. **52**, 1789 (2013).

[45] R.-Z. Liao, X.-C. Li, and P. E. M. Siegbahn, Eur. J. Inorg. Chem. , n/a (2013).

[46] J. Messinger et al., J. Am. Chem. Soc. **123**, 7804 (2001).

[47] L. V. Kulik, B. Epel, W. Lubitz, and J. Messinger, J. Am. Chem. Soc. **129**, 13421 (2007).

[48] J. Yano and V. K. Yachandra, Photosynth Res **92**, 289 (2007).

[49] K. Sauer, J. Yano, and V. K. Yachandra, Coord. Chem. Rev. **252**, 318 (2008).

[50] J. Yano and V. K. Yachandra, Inorg. Chem. **47**, 1711 (2008).

[51] Y. Pushkar, J. Yano, K. Sauer, A. Boussac, and V. K. Yachandra, P Natl Acad Sci Usa **105**, 1879 (2008).

[52] H. Nagashima and H. Mino, BBA Bioenerg. **1827**, 1165 (2013).

[53] M. Asada et al., BBA Bioenerg. **1827**, 438 (2013).

[54] T. Noguchi, Biomedical Spectroscopy and Imaging **2**, 115 (2013).

[55] T. Noguchi, Coord. Chem. Rev. **252**, 336 (2008).

[56] P. E. M. Siegbahn, Chem. Phys. Chem. **12**, 3274 (2011).

[57] P. E. Siegbahn, Phys. Chem. Chem. Phys. **14**, 4849 (2012).

[58] S. Luber et al., Biochemistry **50**, 6308 (2011).

[59] M. Shoji et al., Catal. Sci. Technol. **3**, 1831 (2013).

[60] W. Ames et al., J. Am. Chem. Soc. **133**, 19743 (2011).

[61] D. A. Pantazis, W. Ames, N. Cox, W. Lubitz, and F. Neese, Angew. Chem. Int. Ed. **51**, 9942 (2012).

[62] Y. Kurashige, G. K.-L. Chan, and T. Yanai, Nat. Chem. **5**, 660 (2013).

[63] S. R. White, Phys. Rev. Lett. **69**, 2863 (1992).

[64] S. R. White, Phys. Rev. B **48**, 10345 (1993).

[65] S. R. White and R. L. Martin, J. Chem. Phys. **110**, 4127 (1999).

[66] A. O. Mitrushenkov, G. Fano, F. Ortolani, R. Linguerri, and P. Palmieri, J. Chem. Phys. **115**, 6815 (2001).

[67] G.-L. Chan and M. Head-Gordon, J. Chem. Phys. **116**, 4462 (2002).

[68] G. K.-L. Chan and M. Head-Gordon, J. Chem. Phys. **118**, 8551 (2003).

[69] K. H. Marti, I. M. Ondík, G. Moritz, and M. Reiher, J. Chem. Phys. **128**, 014104 (2008).

[70] D. Zgid and M. Nooijen, J. Chem. Phys. **128**, 014107 (2008).

[71] G.-L. Chan et al., An introduction to the density matrix renormalization group ansatz in quantum chemistry, in *Frontiers in Quantum Systems in Chemistry and Physics*, edited by S. Wilson, P. Grout, J. Maruani, G. Delgado-Barrio, and P. Piecuch, volume 18 of *Progress in Theoretical Chemistry and Physics*, pages 49–65, Springer Netherlands, 2008.

[72] Y. Kurashige and T. Yanai, J. Chem. Phys. **130**, 234114 (2009).

[73] G.-L. Chan and D. Zgid, Ann. Rep. Comput. Chem. **5**, 149 (2009).

[74] G. K.-L. Chan and S. Sharma, Ann. Rev. Phys. Chem. **62**, 465 (2011).

[75] S. Sharma and G. K.-L. Chan, J. Chem. Phys. **136**, 124121 (2012).

[76] D. Ghosh, J. Hachmann, T. Yanai, and G. K.-L. Chan, J. Chem. Phys. **128**, 144117 (2008).

[77] D. Zgid and M. Nooijen, J. Chem. Phys. **128**, 144115 (2008).

[78] T. Yanai, Y. Kurashige, D. Ghosh, and G. K.-L. Chan, Int. J. Quantum Chem. **109**, 2178 (2009).

[79] B. O. Roos, P. R. Taylor, and P. E. M. Siegbahn, Chem. Phys. **48**, 157 (1987).

[80] B. O. Roos, Adv. Chem. Phys. **69**, 399 (1987).

[81] J. Yano et al., P Natl Acad Sci Usa **102**, 12047 (2005).

[82] A. M. Angeles-Boza and J. P. Roth, Inorg. Chem. **51**, 4722 (2012).

[83] P. E. M. Siegbahn and R. H. Crabtree, J. Am. Chem. Soc. **121**, 117 (1999).

[84] M. Lundberg and P. E. M. Siegbahn, Chem. Phys. Lett. **401**, 347 (2005).

[85] S. Shaik and H. Chen, J. Bio. Inorg. Chem. **16**, 841 (2011).

[86] M. Radoń, E. Broclawik, and K. Pierloot, J. Chem. Theo. Comp. **7**, 898 (2011).

[87] M. Srnec, S. D. Wong, J. England, L. Que, and E. I. Solomon, P Natl Acad Sci Usa **109**, 14326 (2012).

[88] K. Andersson, P.-Å. Malmqvist, B. O. Roos, A. J. Sadlej, and K. Wolinski, J. Phys. Chem. **94**, 5483 (1990).

[89] K. Andersson, P.-Å. Malmqvist, and B. O. Roos, J. Chem. Phys. **96**, 1218 (1992).

[90] H.-J. Werner and E. A. Reinsch, J. Chem. Phys. **76**, 3144 (1982).

[91] P. E. M. Siegbahn and M. Svensson, Int. J. Quantum Chem. **41**, 153 (1992).

[92] Y. Kurashige and T. Yanai, J. Chem. Phys. **135**, 094104 (2011).

[93] Y. Kurashige, Mol. Phys. **0**, 1 (0).

[94] M. Saitow, Y. Kurashige, and T. Yanai, J. Chem. Phys. **139**, 044118 (2013).

[95] P. E. Siegbahn and M. R. Blomberg, Chem. Rev. **100**, 421 (2000).

[96] S. Yan, D. A. Huse, and S. R. White, Science **332**, 1173 (2011).

[97] T. Yanai, Y. Kurashige, E. Neuscamman, and G. K.-L. Chan, J. Chem. Phys. **132**, 024105 (2010).

[98] J. Pipek and P. G. Mezey, J. Chem. Phys. **90**, 4919 (1989).

[99] H.-J. Werner and P. J. Knowles, J. Chem. Phys. **89**, 5803 (1988).

[100] K. R. Shamasundar, G. Knizia, and H.-J. Werner, J. Chem. Phys. **135**, 054101 (2011).

[101] E. Neuscamman, T. Yanai, and G. K.-L. Chan, J. Chem. Phys. **132**, 024106 (2010).

[102] S. R. Langnoff and E. R. Davidson, Intern. J. Quantum Chem. **8**, 61 (1974).

[103] E. R. Davidson and D. W. Silver, Chem. Phys. Lett. **52**, 403 (1977).

[104] K. A. Bruekner, Phys. Rev. **100**, 36 (1955).

[105] J. A. Pople and R. Krishnan, Intern. J. Quantum Chem. Symp. **8**, 61 (1977).

[106] M. J. Frisch et al., Gaussian 09 Revision C.1, Gaussian Inc. Wallingford CT 2009.

[107] F. Weigend and R. Ahlrichs, Phys. Chem. Chem. Phys. **7**, 3297 (2005).

[108] A. D. Becke, J. Chem. Phys. **98**, 5648 (1993).

[109] J. Tao, J. P. Perdew, V. N. Staroverov, and G. E. Scuseria, Phys. Rev. Lett. **91**, 146401 (2003).

[110] P. Widmark, P.-Å. Malmqvist, and B. O. Roos, Theor. Chim. Acta. **77**, 291 (1990).

[111] M. Douglas and N. M. Kroll, Ann. Phys. (N.Y.) **82**, 89 (1974).

[112] B. A. Heß, Phys. Rev. A **33**, 3742 (1986).

[113] G. Jansen and B. A. Heß, Phys. Rev. A **39**, 6016 (1989).

[114] L. Bytautas, J. Ivanic, and K. Ruedenberg, J. Chem. Phys. **119**, 8217 (2003).

[115] G. Ghigo, B. O. Roos, and P.-Å. Malmqvist, Chem. Phys. Lett. **396**, 142 (2004).

[116] W. Kutzelnigg and D. Mukherjee, J. Chem. Phys. **107**, 432 (1997).

[117] H.-J. Werner, P. J. Knowles, G. Knizia, F. R. Manby, and M. Schütz, WIREs. Comput. Mol. Sci. **2**, 242 (2012).

[118] G. Karlström et al., Comp. Mat. Sci. **28**, 222 (2003).

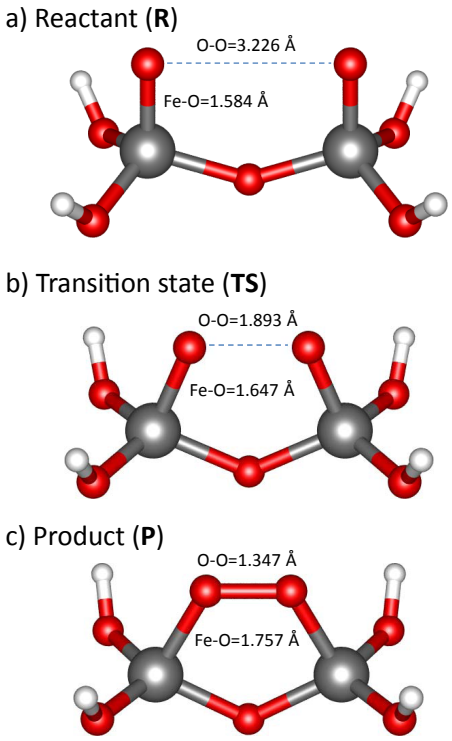

Figure 4.1: Optimized structures for reactant (**R**), transition state (**TS**), and product (**P**) of diferrate, $[H_4Fe_2O_7]^{2+}$.

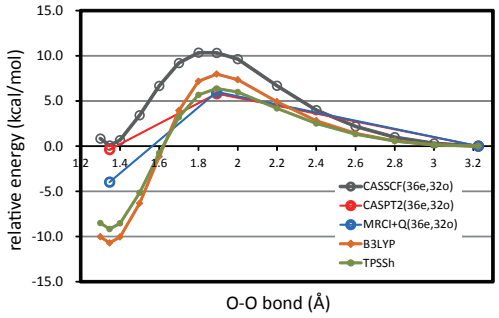

Figure 4.2: Relative energies of $[H_4Fe_2O_7]^{2+}$ obtained by DFT calculations with B3LYP and TPSSh functionals and multireference DMRG-CASSCF/CASPT2/MRCI calculations with a (36e,32o) active space along the O-O bonding reaction coordinate. All energies (in kcal/mol) are measured relative to that of **R** (R(O-O)= 3.226 Å). $M = 1024$ was used for DMRG calculations.

Table 4.1: Activation barriers ($\Delta E(\mathbf{R} \rightarrow \mathbf{TS})$) and reaction energies ($\Delta E(\mathbf{R} \rightarrow \mathbf{P})$) of $[H_4Fe_2O_7]^{2+}$ obtained by various methods (in kcal/mol). The B3LYP geometries were used for the energy calculations of **R**, **TS**, and **P**. DMRG results were taken from the DMRG calculations with $M = 1024$.

Method	Activation barrier $\Delta E(\mathbf{R} \rightarrow \mathbf{TS})$	Reaction energy $\Delta E(\mathbf{R} \rightarrow \mathbf{P})$
B3LYP	7.98	-10.71
TPSSh	6.37	-9.17
DMRG-CASSCF(36e,32o)	10.33	0.08
DMRG-CASPT2(36e,32o)	5.82	-0.37
DMRG-MRCI+Q(36e,32o)	6.01	-3.98
CASSCF(20e,14o)	9.72	-15.23
CASPT2(20e,14o)	-13.16	-3.91
CASSCF(4e,4o)	-14.59	-83.27
CASPT2(4e,4o)	-16.01	-60.43
MRCI+Q(4e,4o)	-15.65	-79.13

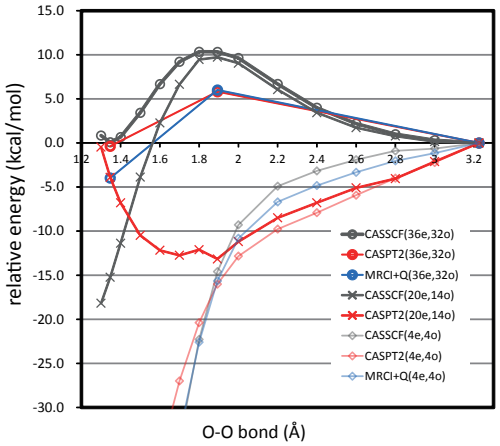

Figure 4.3: Relative energies of $[H_4Fe_2O_7]^{2+}$ obtained by multireference calculations using various levels of active space, (4e,4o), (20e,14o), and (36e,32o), along the O-O bonding reaction coordinate. Optimized orbitals from CASSCF procedure were used. CASPT2 and MRCI methods were further used to include dynamic correlation energies where possible. All energies (in kcal/mol) are measured relative to that of **R** (R(O-O)= 3.226 Å). The active space (36e,32o) was treated by the DMRG method $M = 1024$.

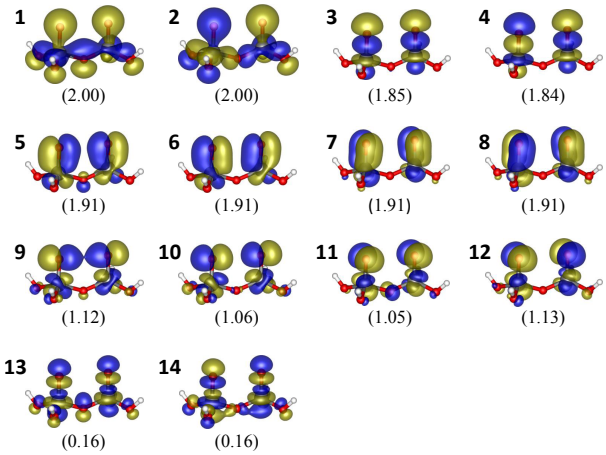

Figure 4.4: Natural orbitals and electron occupancies (in parentheses) of active space from CASSCF(20e,14o) calculation for diferrate in **R** state.

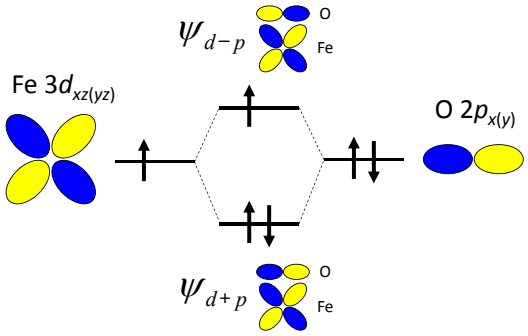

Figure 4.5: Orbital interaction diagram for the valence Fe-O orbital nature in monomeric ferrate. The coupling between the singly-occupied Fe $3d_{xz}$ (or $3d_{yz}$) and doubly-occupied $2p_x$ (or $2p_y$) orbitals leads to the bonding and antibonding Fe-O orbitals, designated as ψ_{d+p} and ψ_{d-p}.

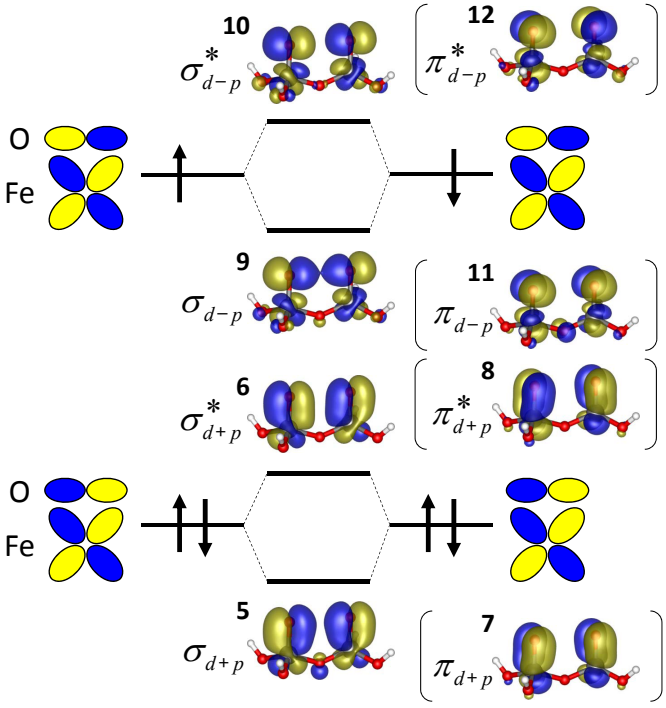

Figure 4.6: Orbital interaction diagram for valence orbitals formed by the dimerized Fe-O units in diferrate. The two adjacent sets of $\psi_{d\pm p}$ each arising in the Fe-O unit (shown in Fig. (4.5)) are coupled via the σ (or π) interaction, leading to bonding $\sigma_{d\pm p}$ [**5** and **9**] and antibonding $\sigma^*_{d\pm p}$ [**6** and **10**] (or $\pi_{d\pm p}$ [**7** and **11**] and $\pi^*_{d\pm p}$ [**8** and **12**]).

Table 4.2: Electron occupancies for natural orbitals σ_{d-p}, σ^*_{d-p}, π_{d-p}, and π^*_{d-p} highly relevant to the O-O coupling in diferrate for **R**, **TS**, and **P**. They are obtained by the CASSCF calculations with (4e,4o), (20e,14o), and (36e,32o) active space for diferrate.

Size of CAS	geometry	σ_{d-p}	σ^*_{d-p}	π_{d-p}	π^*_{d-p}
CAS(4e,4o)					
	R	1.03	0.97	0.98	1.02
	TS	1.53	0.47	1.20	0.80
	P	1.94	0.06	1.79	0.21
CAS(20e,14o)					
	R	1.12	1.06	1.05	1.13
	TS	1.64	0.51	1.33	0.88
	P	1.92	0.07	1.76	0.49
CAS(36e,32o) [a)]					
	R	1.05	1.08	1.01	1.11
	TS	1.70	0.42	1.21	0.90
	P	1.94	0.07	1.67	0.48

a) DMRG $M = 512$.

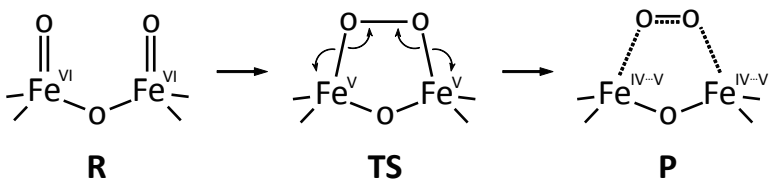

Figure 4.7: Schematic representation of bond structure of diferrate and oxidation states of Fe ions determined by the multireference electronic structure calculations for the intramolecular O-O bond formation.

Table 4.3: Bond orders of O-O and Fe-O, denoted n(O-O) and n(Fe-O), respectively, for **R**, **TS**, and **P** of diferrate. They are evaluated using eqn (4.8) and (4.9) with the electron occupancies shown in Table 4.2.

Size of CAS	geometry	n(O-O)	n(Fe-O)
CAS(4e,4o)			
	R	0.0	2.0
	TS	0.7	1.3
	P	1.7	0.3
CAS(20e,14o)			
	R	0.0	2.0
	TS	0.8	1.2
	P	1.6	0.4
CAS(36e,32o) [a)]			
	R	-0.1	2.1
	TS	0.8	1.2
	P	1.5	0.5

a) DMRG $M = 512$.

Chapter 5

General Conclusion

In the present study, we have formulated a MultiReference Configuration Interaction (MRCI) theory that can use the *ab initio* Density-Matrix Renormalization Group (DMRG) wave function as a reference. Due to the compactly parameterized ansatz of the DMRG wave function, the joint approach, which we call the DMRG-MRCI, is liberated from the exponentially-growing complexity and proven to possess an exceptional performance to deal with the large-scale multireference correlation to account for both static and dynamic correlations. The extraordinarily complicated working equations for the DMRG-MRCI are derived and implemented into the high-performance computer program by means of the automation technique. The computational effort of the DMRG-MRCI has been shown to scale polynomially with respect to the size of system and the dimension of the active space. The DMRG-MRCI has been applied to several multireference systems, which have never been calculated by means of such a accurate quantum chemical method. The results obtained in this study are summarized as follows.

In Chapter 2, the derivation and the implementation of the DMRG-MRCI into an efficiently vectorized program are given. The connectivity of the *ab initio* DMRG and the MRCI are borne by the *Internally-Contracted* (IC) representation of the wave function. Nonetheless, when the MRCI wave function is expanded by means of the IC basis, the straightforward evaluation of the Hamiltonian matrix elements required 5-particle rank reduced density-matrix (5-RDM), a ten-index tensor quantity. Due to the presence of this, the computational scaling of the DMRG-MRCI was estimated to be, at least, of $O(N^{11})$ where N refers to a magnitude of the system size. To this end, we reformulate the MRCI Hamiltonian elements in a multiple-commutator form so as for the lengthy

5-RDM to be cancelled out. As a consequence, in our formalism, the construction of the Hamiltonian requires only 1 – 4 RDMs. The exceedingly complicated MRCI equations in the tensor-contracted form are derived and implemented by means of an automated tensor generator, which was developed by us using the object-oriented C++ language. The DMRG-MRCI with the cumulant-approximated 4-RDM was applied to the dissociation curve of the nitrogen molecule and then, the errors caused by use of the IC basis and by neglect of the cumulant were estimated to be negligibly small. The S_0–T_0 gap for the free-base porphyrin was calculated by means of the DMRG-MRCI with the full π valence orbitals included in the active space and was shown to be in good agreement with the experimental and the Diffusion Monte-Carlo (DMC) results.

In Chapter 3, the stability of the hypothetical iron(V)-oxo porphyrin compound, which is a typical model molecule for the active intermediate in the *in vivo* enzyme so-called *Compound I* (Cpd I), was calculated by means of the DMRG-based multireference theories including the DMRG-MRCI. According to the spectroscopic consensus, in the ground state Cpd I, the oxidation state of iron in the active intermediate is recognized as iron(IV). However, recent advances in the laser-flash photolysis (LFP) suggest the presence of the low-lying and thermally-accessible iron(V)-oxo porphyrin electronic isomer (electromer). In an earlier theoretical study, a large-scale multireference perturbation (RASPT2) and the density-functional theoretical (DFT) calculations were performed on both iron(IV)-oxo and iron(V)-oxo electromers by Pierloot *et. al.*. The RASPT2 study reached a conclusion: The iron(V)-oxo electromer might be much stabler than the iron(IV)-oxo *in vacuo*.

To perform such a large calculation on the iron-oxo porphyrin at the DMRG-MRCI level of theory, a further optimization in our computer implementation was needed. For this purpose, we have rewritten the symbolic manipulation component in our tensor generator to eliminate the unvectorized cumulant-reconstruction step and to optimize the sorting algorithm. The performance of the DMRG-MRCI program has been greatly improved by these optimizations and so its applicability was drastically extended. Presently, the MRCI calculation that uses approximately 30 active orbitals or more is routinely executable on the usual PC clusters.

In Chapter 4, we have performed a series of the multireference calculations on the O–O (oxygen–oxygen) bond formation process catalyzed by a differate catalyst. This process is conceived as a key step of the catalytic reaction of the dioxygen formation from water molecule. Recently, kinetic isotope effect analysis was carried out on the O–O bond formation catalyzed by a potassium ferrate compound (K_2FeO_4), revealing the intermolecular oxo-coupling mechanism within a di-iron(VI)intermediate. The study also involved a series of the Density-Functional Theoretical (DFT) calculations, supporting the experimental results. However, the strong multireference correlation effect in a general sense plays an important role in the electronic structure of multi-metal reaction. Therefore, we performed the large-scale multireference calculations on top of the DMRG reference function; the active space with 36 electrons distributed in the 32 orbitals was used. The second order multireference perturbation (DMRG-CASPT2) and DMRG-MRCI calculations revealed that the DFT overstabilized the reaction energy.

Apart from the development and application of the DMRG-MRCI, Appendices A

and B are devoted to the derivation of the second order polarization propagator in the algebraic-diagrammatic construction framework, which is referred to as ADC(2). In Appendix A, the partially-renormalized ADC(2) [PR-ADC(2)] is developed and implemented as a part of the `PSI4` quantum chemistry program suite. We performed the PR-ADC(2) calculations on the free-base and metallo-porphyrins and as a consequence, their characteristic peaks in the UV/vis spectra called B- and Q-bands were reproduced accurately relative to the experimental and Symmetry-Adopted Cluster and Configuration Interaction (SAC/SAC-CI) values. Since the computational scaling of the PR-ADC(2) is of $O(N^5)$, while that for SAC/SAC-CI is of $O(N^6)$, the PR-ADC(2) has been proven a useful method to calculate excitation energy, overcoming a fairly large quasi-degeneracy in electronic structure. In Appendix B, the self-energy shifting is introduced in the ADC(2) theory, referred to as ADC(2)$_{SS}$. The ADC(2)$_{SS}$ was applied to the several small to medium size molecules and yielded better results than the by the usual ADC(2) for both valence and Rydberg excitations. We have observed that the ADC(2)$_{SS}$ produces the excitation energy for both valence and Rydberg state as accurately as the Coupled-Cluster with Singles and Doubles (CCSD). The computational efforts for the ADC(2)$_{SS}$ and CCSD scale $O(N^5)$ and $O(N^6)$, respectively. Therefore, we conclude that the ADC(2)$_{SS}$ is useful and reliably applicable approach.

Appendix A

Partially-Renormlized Polarization Propagator

M. Saitow, and Y. Mochizuki, "Excited state calculation for free-base and metalloporphyrins with the partially renormalized polarization propagator approach", *Chemical Physics Letters*, **525**, 144 (2012).

1. Introduction

Porphyrin derivatives are involved in various biological processes including photosynthesis and transportation of oxygen molecules in blood and so forth. These functions of the chemical species originate from rich and highly stable π electrons perpendicularly lying on the tetrapyrrole ring. Free-base (H_2P) and metalloporphyrins including zinc- (ZnP) and magnesium- (MgP) porphyrins (hereafter porphyrin is occasionally abbreviated as P) are also attracting chemical attentions with respect to their particular spectral behavior, showing two characteristic peaks at 450 and 600 nm called B- and Q-bands, respectively in the electronic spectra. In addition, B-band possesses very large intensity with the molar absorption coefficient, which reaches almost 10^6 M/cm[1] while Q-band exhibits very small intensity contrastingly. The peak positions and widths vary depending on the environmental effect caused by peripheral residues in proteins, or the functional groups bonded to the ring itself. Due to this fact, a series of chlorophyll can absorb almost whole range of the radiation effectively, for carrying out photosynthetic reaction[2]. From such respect, these molecules are expected as efficient photosensitizers for organic solar cell[3, 4].

Numerous theoretical efforts on the accurate description of the porphyrin analogs have been accumulated from chemical motivation stated above. The fact that reliable description on the electronic structure is a challenging subject due to the remarkable near degeneracy in the conjugated π states also promotes such theoretical study. In addition excited state calculations based on a hybrid of the density-functional theory and the mul-

tireference configuration interaction technique (DFT/MRCI)[5, 6] have been revealed the apparent immixture of doubly- and triply-excited configurations in the electronic spectra. The symmetry-adapted cluster and configuration interaction (SAC-CI)[7, 8] study has also been carried out on the excited states corresponding to Q- and B-bands of monomer and dimer of zinc-porphyrin, and the effect caused by addition of phenyl group has been discussed[9]. Another branch of the coupled cluster (CC) methodologies[10] for the excited state, the equation-of-motion coupled cluster with singles and doubles amplitudes (EOM-CCSD)[11, 12] and the completely renormalized variant with triples correction (CREOM-CCSD(T))[13, 14] have also been applied to ZnP and showed good agreement with the observed spectra[15]. Later, even larger π-conjugated systems are calculated also by the Kowalski's group as well as the performance of their massively parallelized program is benchmarked and analyzed in detail[16]. The intention of our modified polarization propagator is in common to their completely renormalization scheme which drastically reduces errors in the EOM-CCSD excitation energy under the existence of strong quasi-degeneracy. While the CREOM-CCSD(T) seems to be quite effective for porphyrin derivatives, the concomitant polynomial scaling by magnitude of seventh power of the system size still limits the routinely use of this theoretical framework to such the large molecules, without availability of the massively parallel machines. The structure, vibrational frequency and excitation energy for H_2P, ZnP and MgP have been calculated very recently by various methodologies composed of CC, DFT and multireference theories and carefully examined in Ref. [17].

Such the theoretical progress on porphyrin derivatives has been motivated by ad-

vances in powerful computational facilities equipped with many distributed memories and more than thousands of CPU cores because these highly correlated methods are scaled by magnitude of at least, sixth power of the system size. Therefore, we propose a modified second order polarization propagator approach[18], which is based on the algebraic-diagrammatic construction scheme (ADC(2))[19, 20] and seek the applicability of this approach. The polynomial scaling of the ADC(2) is merely fifth power of the system size. Hence, the practical applicability of this method is possibly outstanding. In addition, our modified propagator approach is expected to show significant resistance to the strong quasi-degeneracy due to the fact that the propagator framework is interpreted as based on the quasi-degenerated perturbation theory. To the best of our knowledge, the performance of the second order polarization propagator for such the chemically interesting species has never been assessed before. Relationship among the ADC(2), a series of quasi-degenerated variants of the configuration interaction singles (CIS)[21] with doubles correction (CIS(D))[22, 23] called CIS(D_n)[24, 25] and the second order approximated CC (CC2)[26, 27] has been already figured out by Hättig[28]. Our extension in the ADC(2) is based on Dykstra and Davidson's partial renormalization (PR) technique[29] in terms of the coupled-pair functional (CPF) scheme[30, 31].

In Ref. [32] the partially renormalized CIS(D) (PR-CIS(D)) is presented utilizing the spin-adapted formulation[33]. In this letter, the partially renormalized ADC(2) (PR-ADC(2)) is developed and implemented as a functionality of an efficient ADC program[34]. Initially, the performance for the formaldehyde and ethylene is examined and the PR effect is assessed by comparing to the CCSD and observed values. Then per-

formance for the porphyrin and its derivatives (ZnP, MgP) are assessed and compared with the higher order and observed values. As a consequence the encouraging agreement are obtained even though at the level of the second order of the fluctuation.

2. Theory

2.1. A summary of the ADC(2) model

Only a brief summary of the ADC(2) model is given in this section. For more detail and foundation of this theory, one ought to refer to the original papers[19, 20]. Moreover, the relationship to the other framework of response theory as discussed in Ref. [28] would also be helpful for further understanding. Originally, the ADC scheme is founded on the polarization propagator[18] defined as an expectation value in terms of the T-product[35],

$$P_{pq,rs}(t,t^{'}) = -i\langle\Psi_0|T[a_q^{\dagger}(t)a_p(t)a_r^{\dagger}(t^{'})a_s(t^{'})]|\Psi_0\rangle \tag{A.1}$$

where Ψ_0 represents the exact ground state wave function in Heisenberg notation. Hereafter, indices $ijklmn$ and $abcdef$ stand for the occupied and virtual orbitals, respecitvely while $pqrs$ denote the generic orbitals. Since the definition Eq. (A.1) depends only on the time difference $t-t^{'}$, the Fourier transformation gives the ω-dependent spectral form[35],

$$\begin{aligned} P_{pq,rs}(\omega) &= \int_{\infty}^{\infty} e^{i\omega(t-t^{'})}P_{pq,rs}(t,t^{'})d(t-t^{'}) \\ &= \lim_{\eta\to 0}\sum_{\alpha}\left\{\frac{\langle\Psi_0|a_q^{\dagger}a_p|\Psi_\alpha\rangle\langle\Psi_\alpha|a_r^{\dagger}a_s|\Psi_0\rangle}{\omega-E_\alpha+E_0+i\eta} - \frac{\langle\Psi_0|a_r^{\dagger}a_s|\Psi_\alpha\rangle\langle\Psi_\alpha|a_q^{\dagger}a_p|\Psi_0\rangle}{\omega+E_\alpha-E_0-i\eta}\right\} \end{aligned} \tag{A.2}$$

with respect to the α-th exact excited state designated by Ψ_α, which diverges if ω is equal to the exact excitation and de-excitation energies. There exists a relationship between the first and the second terms in Eq. (A.2), represented as $\mathbf{\Pi}_+$ and $\mathbf{\Pi}_-$, respectively,

$$\mathbf{\Pi}_+^{\dagger}(-\omega) = \mathbf{\Pi}_-(\omega). \tag{A.3}$$

Hence Eq. (A.3) argues that only one term in Eq. (A.2) is necessary and sufficient for seeking the pole structure of the polarization propagator.

In the ADC scheme, only the excitation term $\mathbf{\Pi}_+$ is expanded as

$$\begin{aligned}(\mathbf{\Pi}_+)_{pq,rs}(\omega) &= \langle\Psi_0|a_q^\dagger a_p(\omega - H + E_0 + i\eta)^{-1}a_r^\dagger a_s|\Psi_0\rangle \\ &= \sum_{\alpha,\beta}\langle\Psi_0|a_q^\dagger a_p|\tilde{\Psi}_\alpha\rangle\left\{(\omega\mathbf{1} - \mathbf{H}^{'})^{-1}\right\}_{\alpha,\beta}\langle\tilde{\Psi}_\beta|a_r^\dagger a_s|\Psi_0\rangle \qquad \text{(A.4)}\end{aligned}$$

where $\mathbf{H}'$ is referred to as the shifted-Hamiltonian, or the response matrix. Contrastingly, in the other propagator framework called the super operator algebra[18], both $\mathbf{\Pi}_+$ and $\mathbf{\Pi}_-$ terms are expanded in excitation and de-excitation manifolds. In Eq. (A.4), the intermediate state $\tilde{\Psi}_\alpha$ is generated as

$$|\tilde{\Psi}_\alpha\rangle = \tau_\alpha|\Phi\rangle \qquad \text{(A.5)}$$

where Φ is the reference wave function and α denotes the excitation level with respect to the replacement operator τ,

$$\{\tau_\alpha\} = \{\tau_i^a, \tau_{ij}^{ab}, \tau_{ijk}^{abc}, \cdots; a > b > c, i > j > k, \cdots\}. \qquad \text{(A.6)}$$

The orthonormality among each excited manifold is readily ensured by the successive Gram-Schmidt procedure. The matrix element of the response matrix is defined by the expectation value of the commutation relation,

$$(\mathbf{H}^{'})_{\alpha,\alpha'} = \langle\Phi|\tau_\alpha^\dagger[H, \tau_{\alpha'}]|\Phi\rangle \qquad \text{(A.7)}$$

where α and $\alpha^{'}$ label the excitation class presented in Eq. (A.6). The explicit formulae complete through the second order are expanded in the single and double replacement

manifolds, given as follows,

$$\mathbf{H}^{'} = \begin{pmatrix} \langle\Phi_0|\frac{1}{2}(1+P_{ij}P_{ab})\tau_i^{a\dagger}[H+[H,K],\tau_j^b]|\Phi_0\rangle & \langle\Phi_0|\tau_i^{a\dagger}[H,\tau_{mn}^{ef}]|\Phi_0\rangle \\ \langle\Phi_0|\tau_j^{b\dagger}[H,\tau_{kl}^{cd}]|\Phi_0\rangle^t & \langle\Phi_0|\tau_{kl}^{cd\dagger}[H^{(0)},\tau_{mn}^{ef}]|\Phi_0\rangle \end{pmatrix} \tag{A.8}$$

in which K and P stand for the Møller-Plesset first order (MP1) wave operator[36] and permutation operator which interchanges the subsequent indices, respectively and Φ_0 denotes the Hartree-Fock wave function. In Eq. (A.8), the non-relativistic electronic Hamiltonian is divided into the zeroth order part and the fluctuation, as $H = H^{(0)} + V$ in the Møller-Plesset manner[36]. Eventually, the secular equation of the ADC(2) is written as

$$\mathbf{H}^{'}\mathbf{X} = \mathbf{X}\mathbf{\Omega} \tag{A.9}$$

where $\mathbf{X}$ contains the transition amplitudes composed of the single and double excitation components in its column while $\mathbf{\Omega}$ is a diagonal matrix that possesses the excitation energies. The $\mathbf{X}$ and $\mathbf{\Omega}$ are equivalent to the second order poles and the associated residues of Eq. (A.4).

It is notable that the response matrix in the ADC(2) takes a symmetric form liberated from the imaginary part in the excitation energy, which is an advantage over the other response theories[28, 37]. In addition, the solution of the secular equation, Eq. (A.9), $\mathbf{X}$ and $\mathbf{\Omega}$ inherently satisfies the size-consistency[18]. The second order un-linked term that arises from the singles/singles block of Eq. (A.8) compensates the Møller-Plesset second order perturbation (MP2) correction for the ground state, and the construction of the σ-vector requires the tensorial contraction of only the fifth power of the system size. Therefore, the correlation level and the polynomial scaling of the ADC(2) are

completely consistent with the ground state MP2 theory. The second order terms, which survive eventually, in the singles/singles block of Eq. (A.8) are composed of the three Hugenholts diagrams[18] with 3 hole (h) - 3 particle (p) intermediate states, which give the subtracted correlation correction for the excited state from the ground state MP2 correction. Such the diagrams are recognized to represent the differential correlation (DC) effect in the CIS(D) sense[22, 23]. On the other hand, the remaining six diagrams of the second order originate from the coupling among the singles/doubles, doubles/singles and doubles/doubles blocks, corresponding to 2 h - 2 p intermediate states and are referred to as the orbital relaxation (OR) term. The OR terms are regarded to introduce the OR effect throughout the electronic excitation process.

2.2. The PR-ADC(2) scheme

In the MP2 energy and MP1 wave function expressions, the total electron correlation energy is calculated by summing up the pair-wise fractions for all the active electron pairs[36, 38]. So the correlation between electron pairs can not be accounted for at this level of the fluctuation although in the CC theory, such an effect can be counted even if truncating the cluster operator up to a given excitation level[10, 18]. By this fact, the correlation energy tends to be overrated at the MP2 level if the substantial quasi-degeneracy exists. By utilizing the partial renormalization scheme, such a situation can be somewhat remedied. The energy and wave function expressions for the PR-MP2[29] are written as

$$\tilde{K}|\Phi_0\rangle = \sum_P \frac{|\Psi_P\rangle}{1+\sum_Q T_{PQ}\langle\Psi_Q|\Psi_Q\rangle} \tag{A.10}$$

$$E_{PR-MP2} = \langle\Phi_0|V\tilde{K}|\Phi_0\rangle \tag{A.11}$$

where PQ stand for the indices of the electron pairs while $\Psi_{P,Q}$ represent the pair-correlation function[30, 38]. In Eq. (A.10), T_{PQ} denotes the so-called topological factor[30], which plays the central role on retaining the size-consistency of Eqs. (A.10) and (A.11) and $\tilde{K}$ denotes the partially renormalized wave operator. Setting $T_{PQ} = 0$, the usual MP2 expressions are recovered although in the case of unity, the size-consisitency is crucially violated. The optimal choice of T_{PQ} is given in Ref. [29] as

$$T_{PQ} = \frac{1}{4}(\delta_{ik} + \delta_{il} + \delta_{jk} + \delta_{jl}) \tag{A.12}$$

supposing $P = (i, j)$ and $Q = (k, l)$, which averages the contribution from the equivalent electron pairs appearing in denominator of Eq. (A.10). Also in Ref. [29], the potential energy curve calculated by using the PR-MP2 is shown to possess promising resistance to the quasi-degeneracy and behave properly even at a relatively long bond-length, without showing any singularity.

The explicit forms of PR-MP2 energy and PR-MP1 wave function are constructed as follows,

$$E_{PR-MP2} = \sum_{i>j} \sum_{a>b} V_{ab}^{ij} \tilde{K}_{ij}^{ab} \tag{A.13}$$

$$\tilde{K}|\Phi_0\rangle = \sum_{i>j} \sum_{a>b} \tilde{K}_{ij}^{ab} |\Phi_{ij}^{ab}\rangle \tag{A.14}$$

where V_{ab}^{ij} stands for the anti-symmetric electron repulsion integral in Dirac form with subscripts and superscripts representing the bra and ket MO indices, respectively. Then the partially renormalized MP1 amplitude $\tilde{K}_{ij}^{ab}$ is given as,

$$\tilde{K}_{ij}^{ab} \leftarrow \frac{K_{ij}^{ab}}{N_{ij}} \tag{A.15}$$

$$N_{ij} = 1 + \frac{1}{2}(1 + P_{ij})\rho_{ii}^{(2)} \tag{A.16}$$

in which K_{ij}^{ab} denotes the MP1 amplitudes. Moreover, the second order density matrix $\rho^{(\mathbf{2})}$ is given as

$$\rho_{ij}^{(2)} = \frac{1}{2} \sum_{a>b} \sum_{k} K_{ik}^{ab} K_{jk}^{ab} \tag{A.17}$$

in terms of the occupied/occupied space. It is notable that in second term of Eq. (A.16) the diagonal elements of the second order density matrix are averaged for the i and j occupied orbitals, which causes inclusion of the pair-wise correlation corrections after all.

Additional contraction to the strict ADC(2) fits in at most fourth power of system size as apparent from Eq. (A.16). Employing the partially renormalized amplitude defined by Eq. (A.15) in the actual construction of the contribution from singles/singles block of Eq.(A.8) to the σ-vectors, the pair-wise correction is accounted for in the excitation energy to be obtained as an eigenvalue in the secular equation, Eq. (A.9). This manner is completely consistent with the preceding PR-CIS(D) treatment offered in Ref. [32], even though PR-CIS(D) was derived on basis of the spin-adapted formulations. Finally, we name the newly developed partially renormalized scheme PR-ADC(2).

3. Computational consideration

Before examining the performance of the PR-ADC(2) for a series of the porphyrin derivatives, we had applied this method to formaldehyde and ethylene, which were common test cases for assessment of the excited state theory as seen in Refs. [22, 41]. As their structures, the geometries optimized at MP2/6-31G* level from Refs. [39, 40] were used. Only the strict and PR-ADC(2) computations were performed in this work. The CIS(D), PR-CIS(D) and CCSD values were taken from Ref. [32] and Ref. [22], respectively and 6-311G(2+,2+)G** basis set[39, 40] was employed for these two molecules. As pointed out by Hirata[41], the fourth and fifth lowest excited states 1^1A_1 and 2^1A_1 are known to possess very small values of the overlap between corresponding CIS and CCSD wave functions, up to 55 % and 57 %, respectively. On the other hand, the excited states in ethylene can be described rather nicely. By considering these speculations, we limited the range of discussions only to the lowest three excited states for formaldehyde.

To begin the evaluation of the theoretical model, the geometry optimizations were performed for H_2P, ZnP and MgP at B3LYP/6-31G*[42] level using the Gaussian09 program[42, 43]. In the succeeding excitation energy calculation, the CIS(D) and PR-CIS(D) computations were carried out with our ABINIT-MPX program[44]. In addition, all the strict and PR-ADC(2) calculations were executed using our local version of Psi3 quantum chemistry program suite[45] in which the ADC module[34] was implemented. This propagator module will be included in the upcoming Psi4 quantum chemistry program suite[46]. For the porphyrin derivatives, the 6-31G* basis set was employed for the

excited state calculation. In Table A.2, the calculated excitation energies are shown for the three types of the porphyrin derivatives. Moreover, the rotation angles (θ) defined by

$$\cos\theta = \frac{\tilde{\mathbf{X}}_{\mathbf{S}}^{t}\mathbf{b}^{CIS}}{|\tilde{\mathbf{X}}_{\mathbf{S}}| \cdot |\mathbf{b}^{CIS}|} \tag{A.18}$$

are also shown in parenthesis, in which $\mathbf{b}^{CIS}$ and $\tilde{\mathbf{X}}_{\mathbf{S}}$ represent the CIS wave function and the singles component of the PR-ADC(2) eigenvector. The definition, Eq. (A.18) is different from the theta diagnostic offered by M. Oumi et. al.[48], which gives the coupling between the CIS states near in energy but can be conceived as a generalization without any ambiguity on definition of the quasi-degenerated manifold.

Throughout a series of calculations, none of the occupied and virtual MOs had been frozen and the cartesian basis functions were employed. As also shown in the other preceding research as Ref. [9], the characteristic two peaks in the electronic spectra of porphyrin are associated with the (HOMO-1, HOMO)→(LUMO, LUMO+1) transitions and well described by these four orbitals as shown in Fig. A.1. The nature of the transitions are of typical valence excitation so that the diffused components were not added in the basis function for these cases.

4. Results and discussion

4.1. Benchmark computations for formaldehyde and ethylene

The several low-lying excited states of formaldehyde and ethylene have been chosen as test sets based on the assessment by Hirata[41]. As reported by M. Oumi[48], the CIS(D) has been diagnosed as valid for all the excited state summarized in Table A.1. In other words, the coupling among the CIS states has been found to be small so that the CIS eigenvector seems to be sufficiently similar to that of the ADC(2). By considering such the aspects, these excited states are good test cases for assessment of the effect caused by PR scheme into the ADC(2) theory. For formaldehyde, it is found that the PR-ADC(2) excitation energies are lower about 0.03 - 0.05 eV than those of the strict ADC(2). In addition, even for 1^1B_2 and 2^1B_2 states, which possess the Rydberg character, the PR-ADC(2) tends to fall short of the strict ADC(2). This lowering in the energy is also observed to the PR-CIS(D) values, in which the PR scheme improves only the DC effect as discussed in Ref. [29]. Such the similarity of the behaviors of the PR-CIS(D) and the PR-ADC(2) indicates that the PR scheme modifies solely the DC effect, even though through the diagonalization of the response matrix the DC and OR terms are mixed to give the excitation energy and transition amplitude as eigenvalue and eigenvector. The divergent behavior of the perturbative expansion of the energy of the 1^1A_2 lowest excited state has been figured out by Hirata[41], examining up to the third and partially fourth

order terms. In such the perturbative series, the first and second order terms correspond to the CIS and CIS(D) energies. Hence the perturbative series for the excited states have been shown to be more difficult to converge than that for the ground state, due to the fact that the effects other than the correlation, like the relaxation are also included in "the fluctuation" for the excited state. Even though the higher order effects are readily accounted for in such he PR based methods as the PR-CIS(D) and PR-ADC(2), the divergent behavior has not been observed in this work.

For ethylene, for which the CIS(D) has been diagnosed as more valid than the former case by M. Oumi[48] it is notable that the CIS(D) values are very similar to those of the ADC(2). As a consequence of the fact that the PR scheme corrects the PR-CIS(D) and PR-ADC(2) values mostly equally, the two partially renormalized approaches produce almost same energies except for the 1^1B_{1u} state. The PR-ADC(2) value for the 1^1B_{1u} state differ about 0.19 eV from that of the PR-CIS(D), which can be explained by the theta value in Ref.[48] that this state has a relatively large rotation angle up to 2.3° among the excited states of ethylene. Through this benchmark sets, it has been shown that the PR correction works to the PR-CIS(D) and PR-ADC(2) almost equally in order to improve mainly the DC effect.

4.2. The Performance of PR-ADC(2) scheme for H_2, ZnP and MgP

Table A.2 shows the calculated excitation energies for the three types of porphyrin molecules, H_2P, ZnP and MgP with the CIS(D), PR-CIS(D), ADC(2) and PR-ADC(2) as well as the CIS values and the reference and observed data from Refs. [6, 9]. Symmetry of the associated excited states and the spectral characters are also shown in Table A.2. In the spectra of H_2P, Q-band splits off into two Q_x and Q_y peaks due to its lower symmetry than that of the other two cases. It is found from Table A.2 that the elements in the singly excited eigenvector are obviously rotated by inclusion of the correlation and quasi-degeneracy up to about 20 degree. This fact indicates the diagonalization of the correlated response matrix is indispensable for these species so that the CIS(D) which treats the effects of the correlation and the relaxation in a pseudo-perturbative manner[49] is not appropriate. In other words, the validity of CIS(D) energy can be realized only if the the effect of quasi-degeneracy of the excited state is sufficiently small. On the other hand, the ADC(2) is considered as the quasi-degenerated perturbative theory so the ADC(2) should be more appropriate for this case. This speculation is also consistent with the odd behavior of the doubles correction in the CIS(D) energy for Q-bands, which raises the value of the CIS excitation energy and widen the discrepancy from the observed data up to 0.4 eV. By introducing the partial renormalization technique into MP1 amplitude in the CIS(D) energetic equation, such an erratic behavior is readily corrected and the moderately passable values are obtained for all the states except the Q_y-band of H_2P that is still a difficult case. The DC effect is tempered by inclusion of the correlation

between electron pairs and the overrated correction into the excitation energy seems to be properly modulated. This fact is coincident with the speculation that the odd behavior of the doubles correction of CIS(D) energy is caused by the overestimated MP2 correction for the ground state with the strong quasi-degenerated character. In the case of ADC(2), which is based on the quasi-degenerated perturbative treatment[28], such the values of the excitation energies fit in the observed data moderately good and are mostly comparable to those from the preceding SAC-CI study[9]. However for the Q_y-band of H_2P the correction is not yet sufficient and the gap between the calculated and observed excitation energies increases compared with the CIS level. At last PR-ADC(2) can reproduce the highly encouraging results even for the Q_y-band and the associated excitation energy is lowered from the CIS value.

By nature of the multiconfigurational character of the excited states, the DFT/MRCI values from Ref. [6] still show quite good agreement for all the states. Even utilizing the partial renormalization[29] into the DC term, the PR-ADC(2) is based on the single reference theory so that the deviations from observed data reach up to around 0.2 eV. However, it is notable that employing partially renormalized wave operator defined by Eq. (A.10) the contribution from the 3 h - 3 p terms is scaled with respect to the electron pairs, which results in lowering the excitation energy about 0.2 eV for both Q- and B-bands. Such an effect is caused by inclusion of the pair-pair correlation that appears as higher order effect beyond MP2 level description, as discussed by Dyktra and Davidson[29].

5. Summary

In this letter, we present a polarization propagator scheme[18, 19, 20] complete through the second order termed PR-ADC(2) in which the correlation between electron pairs is included for both the ground and the excited states. The newly developed propagator approach has been implemented in an efficient ADC program developed by MS. In addition, this approach preserves the size-consistency and unitary-invariance as well as is based on the CPF[30] typed modification[29] in terms of the MP2 energy and MP1 wave function. As a common test set, the PR-ADC(2) is applied to formaldehyde and ethylene. Then, it has been verified that the PR correction is negligible if the quasi-degeneracy is insignificant and the PR correction improves mostly the DC effect, but the OR effect still remains unmodified. To this point, development of the other modification scheme may be desired such as the self-energy shifting[50]. Eventually the PR-ADC(2) is applied for Q- and B-bands in three porphyrin molecules, H_2P, ZnP and MgP and shows encouraging results comparable to previous SAC-CI study[9] while the CIS(D) produces poor values especially for the Q-bands due to the fact that the simple doubles correction does not lower the CIS excitation energy. The ADC(2) can be regarded as one of the quasi-degenerated perturbative variants of the CIS(D) and the corresponding singly excited eigenvectors for such the bands are obviously rotated by effect of the strong quasi-degeneracy.

Bibliography

[1] C. Rimington, Biochem. J. 75 (1960) 620.

[2] D. Voet, J. G. Voet and C. W. Pratt, Fundamentals of Biochemistry: Life at the Molecular Level 3rd. ed. Wiley & Sons, Hoboken, 2008.

[3] J. Wienke, T. J. Schaafsma and A. Goossens, J. Phys. Chem. B 103 (1999) 2702.

[4] S. Cherinan and C. C. Wamser, J. Phys. Chem. B 104 (2000) 3624.

[5] S. Grimme and M. Waletzke, J. Chem. Phys. 111 (1999) 5645.

[6] A. B. J. Parusel and S. Grimme, J. Porph. Phthal. 5 (2001) 225.

[7] H. Nakatsuji, Chem. Phys. Lett. 67 (1979) 329.

[8] H. Nakatsuji, Chem. Phys. Lett. 67 (1979) 334.

[9] T. Miyahara, H. Nakatsuji, J. Hasegawa, A. Otsuka, N. aratani and A. Tsuda, J. Chem. Phys. 117 (2002) 11196.

[10] I. Shavitt, R. J. Bartlett, Many-Body Methods in Chemistry and Physics: MBPT and Coupled-Cluster Theory, Cambridge University Press, Cambridge, 2009.

[11] J. F. Stanton and R. J. Bartlett, J. Chem. Phys. 98 (1993) 7029.

[12] J. F. Stanton and R. J. Bartlett, J. Chem. Phys. 99 (1993) 5173.

[13] P. Piecuch, K. Kowalski, I. S. O. Pimienta and M. J. McGuire, Int. Rev. Phys. Chem. 21 (2002) 527.

[14] K. Kowalski and P. Piecuch, J. Chem. Phys. 120 (2004) 1715.

[15] P. -D. Fan, M. Valiev and K. Kowalski, Chem. Phys. Lett. 458 (2008) 205.

[16] K. Kowalski, R. M. Olson, S. Krishmoorthy, V. Tipparaju and E. Aprá, J. Chem. Theor. Chem. 7 (2011) 2200.

[17] R. K Chaudhari, K. F. Freed, S. Chattopadhyay and U. S. Mahapatra, J. Chem. Phys. 135 (2011) 084118.

[18] J. Simons, P. Jørgensen, Second Quantization-based Methods in Quantum Chemistry, Academic Press, Inc., New York, 1981.

[19] J. Schirmer, Phys. Rev. A 26 (1982) 2395.

[20] A. B. Trofimov, G. Stelter and J. Schimer, J. Chem. Phys. 117 (2002) 6402.

[21] J. B. Foresman, M. Head-Gordon, J. A. Pople and M. Frisch, J. Phys. Chem. 96 (1992) 135.

[22] M. Head-Gordon, R. J. Rico, M. Oumi and T. J. Lee. Chem. Phys. Lett. 219 (1994) 21.

[23] Y. M. Rhee and M. Head-Gordon, J. Phys. Chem. A 111 (2007) 5314.

[24] M. Head-Gordon, M. Oumi and D. Maurice, Mol. Phys. 96 (1999) 593.

[25] D. Casanova, Y. M. Rhee and M. Head-Gordon, J. Chem. Phys. 128 (2008) 164106.

[26] O. Christiensen, H. Koch and P. Jørgensen, Chem. Phys. Lett. 243 (1995) 409.

[27] O. Christiensen, H. Koch, P. Jørgensen and T. Helgaker, Chem. Phys. Lett. 263 (1996) 530.

[28] C. Hättig, in NIC Series, edited by J. Grotendorst, S. Blügel, and D. Marx (John von Neumann Institute for Computing, Jülich, Switzerland, 2006), Vol. 31, p. 245.

[29] C. E. Dykstra and E. R. Davidson, Int. J. Quantum Chem. 78 (2000) 226.

[30] R. Ahlrichs, P. Scharf and C. Ehrhardt, J. Chem. Phys. 82 (1985) 890.

[31] F. Neese, A. Hansen, G. Wennmohs and S. Grimme, Acc. Chem. Res. 42 (2008) 641.

[32] Y. Mochizuki and K. Tanaka, Chem. Phys. Lett. 443 (2007) 389.

[33] Y. Mochizuki, K. Tanaka, K. Yamashita, T. Ishikawa, T. Nakano, S. Amari, K. Segawa, T. Murase, H. Tokiwa and M. Sakurai, Theor. Chem. Acc. 117 (2007) 541.

[34] The program was developed by MS and detail on the implementation will be published elsewhere.

[35] A.L.Fetter, J.D.Walecka, Quantum Theory of Many Particle Systems, McGraw-Hill, New York, 1971.

[36] C. Møller and M. S. Plesset, Phys, Rev. 46 (1934) 618.

[37] C. Hättig, Adv. Quantum Chem. 50 (2005) 37.

[38] A. Szabo, N.S. Ostlund, Modern Quantum Chemistry, MacMillan, NewYork, 1982.
[8] D.G. Fedorov, K. Kitaura, J. Chem. Phys. 121 (2004) 2483.

[39] C. M. Hadad, J. B. Foresman and K. B. Wiberg, J. Chem. Phys. 97 (1993) 4293.

[40] K. B. Wiberg, C. M. Hadad, J. B. Foresman and W. A. Chupka, J. Phys. Chem. 97 (1993) 4293.

[41] S. Hirata, J. Chem. Phys. 122 (2005) 094105.

[42] J.B. Foresman, A. Frisch, Exploring Chemistry with Electronic Structure Methods, second ed., Gaussian Inc., Pittsburgh, 1996, references therein.

[43] Gaussian 09, Revision A.1, M. J. Frisch, G. W. Trucks, H. B. Schlegel, G. E. Scuseria, M. A. Robb, J. R. Cheeseman, G. Scalmani, V. Barone, B. Mennucci, G. A. Petersson, H. Nakatsuji, M. Caricato, X. Li, H. P. Hratchian, A. F. Izmaylov, J. Bloino, G. Zheng, J. L. Sonnenberg, M. Hada, M. Ehara, K. Toyota, R. Fukuda, J. Hasegawa, M. Ishida, T. Nakajima, Y. Honda, O. Kitao, H. Nakai, T. Vreven, J. A. Montgomery, Jr., J. E. Peralta, F. Ogliaro, M. Bearpark, J. J. Heyd, E. Brothers, K. N. Kudin, V. N. Staroverov, R. Kobayashi, J. Normand, K. Raghavachari, A. Rendell, J. C. Burant, S. S. Iyengar, J. Tomasi, M. Cossi, N. Rega, J. M. Millam, M. Klene, J. E. Knox, J. B. Cross, V. Bakken, C. Adamo, J. Jaramillo, R. Gomperts, R. E. Stratmann, O. Yazyev, A. J. Austin, R. Cammi, C. Pomelli, J. W. Ochterski, R. L. Martin, K. Morokuma, V.

G. Zakrzewski, G. A. Voth, P. Salvador, J. J. Dannenberg, S. Dapprich, A. D. Daniels, Ö. Farkas, J. B. Foresman, J. V. Ortiz, J. Cioslowski, and D. J. Fox, Gaussian, Inc., Wallingford CT, 2009.

[44] Y. Mochizuki, K. Yamashita, T. Murase, T. Nakano, K. Fukuzawa, K. Takematsu, H. Watanabe and S. Tanaka, Chem. Phys. Lett. 457 (2008) 396.

[45] T. D. Crowford, C. D. Sherrill, E. F. Valleev, J. T. Fermann, R. A. King, M. L. Leininger, S. T. Brown, C. L. Janssen, E. T. Seidl, J. P. Kenny and W. D. Allen, J. Comput. Chem. 28 (2007) 1610.

[46] J. M. Turney, A. C. Simmonett, R. M. Parrish, E. G. Hohenstein, F. Evangelista, J. T. Fermann, B. J. Mintz, L. A. Burns, J. J. Wilke, M. L. Abrams, N. J. Russ, M. L. Leininger, C. L. Janssen, E. T. Seidl, W. D. Allen, H. F. Schaefer, R. A. King, E. F. Valeev, C. D. Sherrill and T. D. Crawford, WIREs Comput. Mol. Sci., accepted(doi: 10.1002/wcms.93).

[47] U. Varetto, <MOLEKEL ver. 5.4.0.8>; Swiss National Supercomputing Centre: Manno (Switzerland).

[48] M. Oumi, D. Maurice, T. J. Lee and M. Head-Gordon, Chem. Phys. Lett. 279 (1997) 151.

[49] O. Christiansen, K. L. Bak, H. Koch and S. P. A. Sauer, Chem. Phys. Lett. 20 (1998) 47.

[50] Y. Mochizuki, Chem. Phys. Lett. 453 (2008) 109.

Table A.1: Calculations of the excitation energies (in eV) for several low-lying singlet excited states of formaldehyde and ethylene. The character of the excited states is shown in parenthesis as "V" and "R" denote the valence and Rydberg states, respectively.

	State	CIS	CIS(D)	PR-CIS(D)	ADC(2)	PR-ADC(2)	CCSD	Obs.
Formaldehyde	1^1A_2(V)	4.48	3.98	3.91	3.86	3.81	3.95	4.07
	1^1B_2(R)	8.63	6.44	6.41	6.28	6.25	7.06	7.11
	2^1B_2(R)	9.36	7.26	7.23	7.22	7.19	7.89	7.97
Ethylene	1^1B_{3u}(V)	7.13	7.21	7.16	7.19	7.15	7.31	7.11
	1^1B_{1g}(V)	7.71	7.84	7.80	7.82	7.78	7.96	7.80
	1^1B_{1u}(V)	7.74	8.04	7.99	8.00	7.80	8.14	7.60
	1^1B_{2g}(V)	7.86	7.86	7.81	7.85	7.80	7.99	8.01
	1^1A_g(R)	8.09	8.18	8.13	8.16	8.11	8.34	8.29

† Taken from Refs. [39, 40] and the references therein.

Table A.2: Singlet excitation energies (in eV) corresponding to Q- and B-bands for H_2P, ZnP and MgP systems calculated by various approaches along with the observed data. For the PR-ADC(2) singly excited eigenvalues, rotation angles from the CIS vectors are shown in parenthesis.

	CIS	CIS(D)	PR-CIS(D)	ADC(2)	PR-ADC(2)	DFT/MRCI[6]	SAC-CI[9]	Obs.†
H_2P								
$1^1B_{3u}/Q_x$	2.41	2.47	2.23	2.24	2.04 (15.75°)	1.97	1.70	1.98
$1^1B_{2u}/Q_y$	2.54	2.94	2.70	2.63	2.43 (16.67°)	2.38	2.19	2.42
$2^1B_{3u}/B$	4.52	3.47	3.29	3.52	3.35 (19.41°)	3.07	3.43	3.33
ZnP								
$1^1E_u/Q$	2.54	2.79	2.55	2.53	2.33 (15.24°)	2.21	1.84	2.28
$2^1E_u/B$	4.75	3.52	3.32	3.59	3.43 (14.98°)	3.28	3.50	3.04, 3.22, 3.05
MgP								
$1^1E_u/Q$	2.49	2.73	2.49	2.47	2.26 (15.57°)	2.16	2.01	2.07,2.14
$2^1E_u/B$	4.70	3.48	3.29	3.56	3.39 (15.78°)	3.25	3.63	3.05, 3.18

† Taken from Ref. [6] and the references therein.

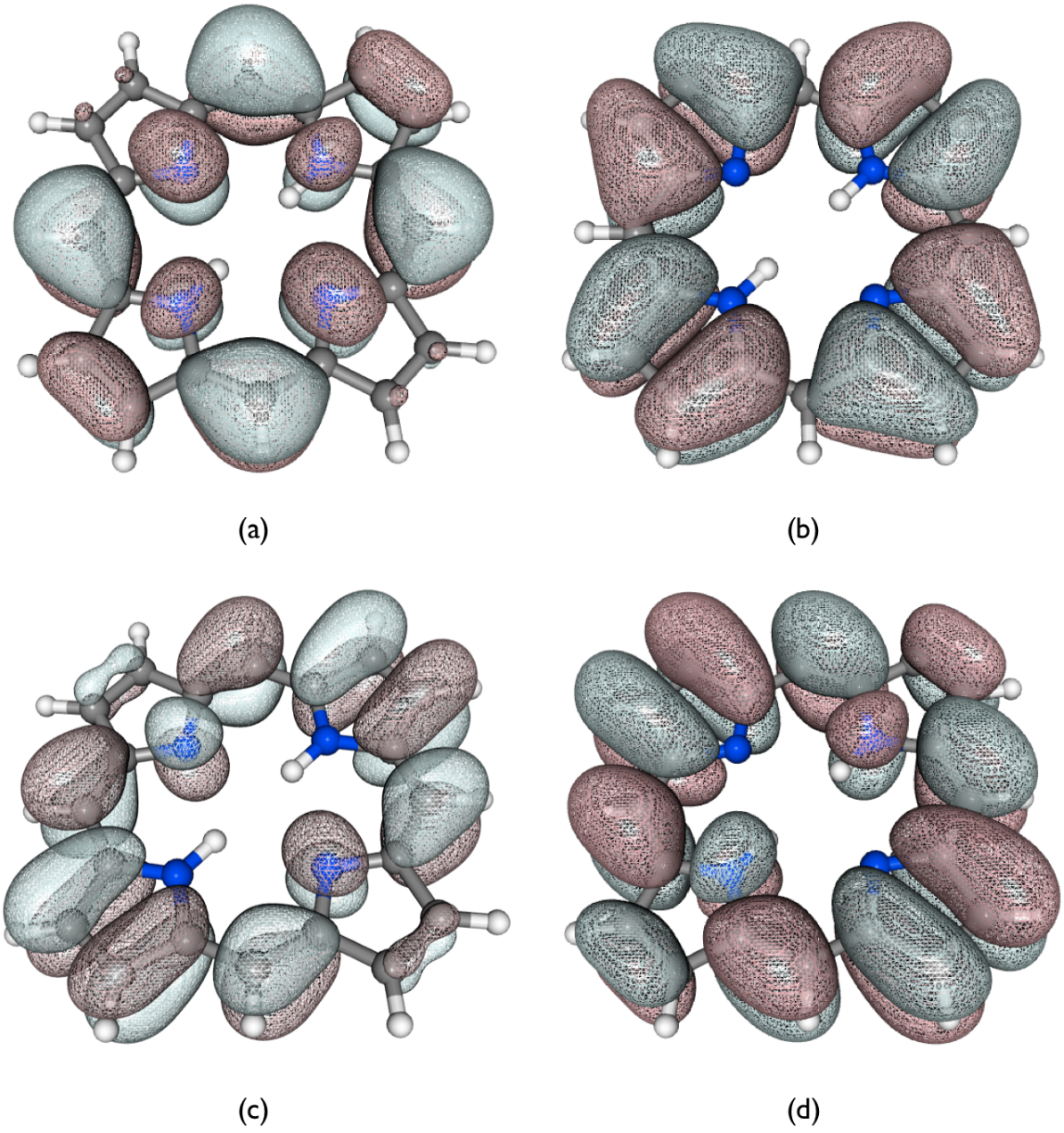

Figure A.1: The canonical (a) HOMO-1 (b) HOMO (c) LUMO (d) LUMO+1 in H_2P depicted by MOLKEL[47] program. In case of ZnP and MgP, increase in symmetry from D_{2h} to D_{4h} makes the LUMO and LUMO+1 degenerate.

Appendix B

Self-Energy Shifting in the Polarization Propagator

M. Saitow, T. Ida, and Y. Mochizuki, "Improved description of the orbital relaxation effect by practical use of the self-energy", *International Journal of Quantum Chemistry*, (in press).

B.1 Introduction

To determine the optical behavior of materials requires at least consideration of the excitation process, in terms of the ground state (GS) to an excited state (ES). In addition, if the optical phenomena under consideration range over the UV/vis region, then the electronic ESs must be assessed. From this perspective, reliable and accurate calculations of the excitation process are of central importance in the field of theoretical chemistry [1, 2, 3, 4, 5]. The ESs are categorized according to the characters of the associated initial and final states i.e., the core, valence and Rydberg states. In contrast to the two former types, the Rydberg ES is distinct, due to the transition of an electron to the highly diffused orbitals. Therefore accurate accounts for the orbital relaxation, which is an effect of the gross charge rearrangement through the excitation process, is merely at a qualitative level if uncorrelated methods such as the configuration interaction with singles excitation (CIS) [6] is utilized. The excutation energies (EEs) and properties obtained with the CIS frequently deviate from the observed values by approximately 1-2 eV or more.

Correlated treatment of the ES requires the second or higher order correction to the CIS energy. In the second order treatment, double and factorized triple excitation contributions with respect to the GS configuration are taken into account. This method is referred as CIS(D) [7, 8] and has been widely used due to its economic performance; therefore, moderately promising consequences is available for most of the typical singly excited states compared with the observed values at a cost of the fifth power of the

molecular size. Another branch of the correlated ES theory, which is referred to as the algebraic-diagrammatic construction (ADC), is available for the excitation propagator [9, 10, 11, 12], in which both the excitation energy and expectation value are treated at the arbitrary order of the fluctuation. The second order approximation, ADC(2) corresponds exactly to the second order Møller-Plesset expansion [13] for the ES and is strictly formulated in terms of the intermediate-state representation (ISR) [14, 12, 15]. The resemblance in formulas of the second order approximation for coupled-cluster with singles and doubles (CC2) [16, 17, 18] to ADC(2) is addressed and both theories are implemented with the resolution of the identity approximation [19].

The second order approaches for the ES are all capable of being implemented into a highly efficient programs because their tensor-contracted forms are simpler than the CCSD and the higher order methods. However, for the Rydberg excitations, the second order correction often overestimates the electron correlation and orbital relaxation (OR) effect and the error from the observed value appears to be enhanced. In the second order approach, the effect of the doubly excited configurations introduces the orbital relaxation corrections into the excitation energy. Since the diagonal block of the doubly excited configurations in the response matrix is expanded up to the zeroth order[7], the orbital relaxation effect tends to be overestimated for the Rydberg type excitations and this phenomena result in the values of the EE approximately 0.5 eV smaller than the CCSD values. To overcome this drawback, an optimal damping parameter is introduced into the OR term in combination with the scaled-opposite spin (SOS) parameterization for the CIS(D) model [20]. Another procedure to compensate this situation is Dyson-

shifting [21, 22], which is also known as the self-energy shifting [23, 24] in the OR term, in combination with the damping parameter. By shifting the denominator of the OR term with the correlated self-energy, the higher order effects are effectively introduced without a drastic increase in the computational effort. These approaches are known to retain size-consistency and is invariant under the rotation of the degenerate molecular orbitals (MOs)[25, 26]. Therefore they are reliably applicable to large, realistic molecular systems in a well balanced way between the Rydberg and valence states.

Because these methods are based on the CIS(D) theory which does not require the diagonalization of the response matrix, the correlated transition amplitude is unavailable. When the method based on the quasi-degenerated perturbation is utilized instead of the CIS(D), the correlated transition amplitude is made available as the eigenvector of the response matrix. Moreover, stronger resistance to the quasi-degeneracy of the electronic structure is also expected[27]. By utilizing the alternative methods such as the ADC(2), CIS(2X) [28, 5, 29] and a series of CIS(D_n) [30] theory a more well balanced and useful correction approach that is effective for both the valence and Rydberg states is thought to be achievable. We have already implemented CIS(D) and the corrected variant termed CIS$(D)_{SS}$ [31, 32] in the multilayer fragment molecular orbital (ML-FMO) framework by utilizing a massively parallel, integral direct algorithm [33] in our *ab initio* program entitled ABINIT-MPX [34]. The MLFMO-CIS$(D)_{SS}$ approach has been demonstrated as accurately and robustly applicable to various proteins including yellow- and blue-fluorescent [32] proteins.

From such a practical point of view, we present the self-energy shifting for the second

order response matrix in combination with the use of a damping parameter implemented in an efficient computer program. Results for several small to medium sized molecules are shown in this communication followed by the promising agreements that are confirmed for both the Rydberg and valence excitations.

B.2 Theory

B.2.1 Structure of the second order response matrix

For the perturbative treatment of the electron correlations, the second quantized electronic Hamiltonian is divided into a sum of the zeroth order part (H_0) and the fluctuation (U) in a way originally proposed by Møller and Plesset[13]:

$$H_0 = \sum_{pq} F_p^q a^p a_q \tag{B.1}$$

$$U = -\sum_{ipa} V_{ip}^{iq} a^p a_q + \frac{1}{4} \sum_{pqrs} V_{pq}^{rs} a^p a^q a_s a_r \tag{B.2}$$

where F and V represent the Fock matrix and the anti-symmetrized electron repulsion integral ($V_{pq}^{rs} = \langle pq|rs\rangle - \langle pq|sr\rangle$), respectively, in the spin-orbital notations while the a^p and a^q represent the usual electronic creation ($a_p^\dagger$) and annihilation (a_p) operators, respectively. Indices i, j, k, l and a, b, c, d represent occupied and virtual MOs, respectively, while the rests are used for the generic states. The reference Hartree-Fock (HF) function (Ψ_0) serves as the zeroth order wave function;

$$H_0|\Psi_0\rangle = E_0|\Psi_0\rangle \tag{B.3}$$

and the HF electronic energy is obtained as a sum of the zeroth and first order energies;

$$E_{HF} = \langle \Psi_0 | H_0 + U | \Psi_0 \rangle. \tag{B.4}$$

The electron correlation comes into play in the energy at the higher than or equal to the second order level of the fluctuation potential (Eq. (B.2)). The second order expression of the ground state energy (MP2 energy formula) is given as

$$\begin{aligned} E_2 &= \langle \Psi_0 | U | \Psi_1 \rangle & \text{(B.5)} \\ &= \sum_{ijab} V_{ab}^{ij} K_{ij}^{ab} & \text{(B.6)} \end{aligned}$$

where K is the first order amplitude;

$$K_{ij}^{ab} = \frac{V_{ij}^{ab}}{\epsilon_a + \epsilon_b + \epsilon_i - \epsilon_j} \tag{B.7}$$

assuming the canonicality of the MOs, i.e. $F_p^q = \epsilon_p \delta_p^q$. The first order wave function is constructed as

$$|\Psi_1\rangle = \frac{1}{4} \sum_{ijab} K_{ij}^{ab} a^a a^b a_j a_i |\Psi_{HF}\rangle. \tag{B.8}$$

In the ADC framework, the polarization propagator ($\mathbf{\Pi}_+$) in the ω-representation is given in the following form [9, 10, 11, 12];

$$\begin{aligned} (\mathbf{\Pi}_+)_{pq;rs}(\omega) &= \langle \Phi_0 | a^q a_p (\omega - H + E_0 + i\eta)^{-1} a^r a_s | \Phi_0 \rangle & \text{(B.9)} \\ &= \sum_{\alpha,\beta} \langle \Phi_0 | a^q a_p | \tilde{\Psi}_\alpha \rangle \left\{ (\omega \mathbf{1} - \mathbf{A})^{-1} \right\}_{\alpha,\beta} \langle \tilde{\Psi}_\beta | a^r a_s | \Phi_0 \rangle & \text{(B.10)} \end{aligned}$$

where Φ_0 represents the exact ground state wave function while the $\tilde{\Psi}$ is the intermediate state constructed by the action of the excitation operators to the HF reference function

$$\begin{aligned} |\tilde{\Psi}_\alpha\rangle &= \tau_\alpha |\Psi_0\rangle & \text{(B.11)} \\ \{\tau_\alpha\} &= \{a^a a_i, a^a a^b a_j a_i, a^a a^b a^c a_k a_j a_i, \cdots; a > b > c, i > j > k, \cdots\}. & \text{(B.12)} \end{aligned}$$

In Eq. (B.10), **A** refers to the response matrix whose elements are defined, by using the reference function Ψ_0, as

$$(\mathbf{A})_{\alpha;\beta} = \langle \Psi_0 | [\tau_\alpha^\dagger, [H, \tau_\beta]] | \Psi_0 \rangle. \tag{B.13}$$

Because the EEs are calculated as the poles of the polarization propagator (Eq. (B.10)), numerical problem to seek the pole structure of $\mathbf{\Pi}_+$ can be rewritten as the eigenvalue equation with respect to the response matrix;

$$\lim_{\omega \to \omega_{\text{pole}}} \mathbf{\Pi}_+(\omega) = \infty \Longleftrightarrow \lim_{\omega \to \omega_{\text{pole}}} (\omega \mathbf{1} - \mathbf{A}) = 0. \tag{B.14}$$

In the second order level of the fluctuation potential (U in Eq. (B.2)), the response matrix is to be expanded in terms of the singles (S), and doubles (D) excitation manifolds. The S/S block is treated up to the zeroth, first and second order while the D/D block is treated only up to the zeroth order [9, 16]. The coupling blocks (S/D and D/S elements) are expanded up to the first order. To our knowledge, the ADC(2) was originally derived using purely diagrammatic technique[9] by removing the de-excitation diagrams that appear in the random-phase approximation (RPA) equation[35, 36]. Later, an algebraic procedure for derivation of the arbitrary order ADC, i.e., ADC(n), known as intermediate-state representation (ISR), was developed [14] and the relationship to the quasi-degenerate variants of CIS(D) [30, 37] and CC2-LR was addressed[38]. In contrast to the RPA type approach such as the second order polarization propagator approach (SOPPA) [39, 40], this type of theory possesses a simpler structure in the response matrix due to the decoupling of the de-excitation manifolds. The numerical procedure for solving the ADC(2) equation appears to be more straightforward than that for the SOPPA

because the dimension of the ADC response matrix is a half of SOPPA one. Moreover, rather demanding four-virtual electron repulsion integral (ERI), which is necessary for SOPPA calculation, is no longer required.

The response matrix elements of ADC(2) in spin-orbital notation can be written explicitly as

$$(A_{SS})_{ia;jb} = F_{ab}\delta_{ij} - F_{ij}\delta_{ab} - V_{ja}^{ib} + \frac{1}{2}(1 + P_{ij}P_{ab}) \left[-\frac{1}{2} K_{mn}^{ae} V_{be}^{mn} \delta_{ij} - \frac{1}{2} K_{im}^{ef} V_{ef}^{jm} \delta_{ab} + K_{in}^{ae} V_{be}^{jn} \right] \tag{B.15}$$

$$(A_{SD})_{ia;ldkc} = V_{cd}^{al}\delta_{ik} + V_{di}^{kl}\delta_{ac} - V_{cd}^{ak}\delta_{il} - V_{ci}^{kl}\delta_{ad} \tag{B.16}$$

$$(A_{DD})_{iajb;ldkc} = F_{ad}\delta_{il}\delta_{jk}\delta_{bc} + F_{bc}\delta_{il}\delta_{jk}\delta_{ad} - F_{il}\delta_{jk}\delta_{ad}\delta_{bc} - F_{jk}\delta_{il}\delta_{ad}\delta_{bc} \tag{B.17}$$

where the Einstein summation convention and the Brillouin condition [41] are supposed. Eqs. (B.16) and (B.17) are in common with the corresponding super operator matrix elements for the SOPPA [39, 40, 41, 42]. In Eq. (B.15), the last term on the right-hand side arises from the decoupling of the de-excitation manifolds. In solving the eigenvalue equation in terms of the response matrix given by Eqs. (B.15) – (B.17), the D/D block, which appears as diagonal sub-matrix, is renormalized into the S/S block to give the energy dependent potential. As a consequence, a pseudo-eigenvalue equation with respect to the effective response matrix given in the S manifold,

$$\mathbf{A}_{SS}^{eff}(\omega) = \mathbf{A}_{SS} + \mathbf{A}_{SD}^{\dagger}(\omega\mathbf{E} - \mathbf{A}_{DD})^{-1}\mathbf{A}_{DS}. \tag{B.18}$$

In analogy with the CIS(D) theory [7], the second order terms in $\mathbf{A}_{SS}$ give the subtracted correlation correction between the ES and GS known as the differential correlation (DC) terms whereas the other second order terms, which arise from the second term in Eq.

(B.18), introduce the orbital relaxation (OR) effect throughout the electron transition. To calculate the EEs, one has to solve the state-specific eigenvalue equation

$$\mathbf{A}_{SS}^{eff}(\omega)\mathbf{X}_S = \omega\mathbf{X}_S \tag{B.19}$$

in self-consistent manner. In Eq. (B.19), $\mathbf{X}_S$ represents the effective singly excited amplitude. The diagonalization of the response matrix ($\mathbf{A}_{SS}^{eff}$) by using the block-Davidson algorithm[43, 44, 45] dominates the overall computational time. In the diagonalization, σ-vector (Matrix-Vector product) has to be constructed at each step;

$$\sigma_S(\omega) = \mathbf{A}_{SS}^{eff}(\omega)\mathbf{B}_S \tag{B.20}$$

where $\mathbf{B}_S$ refers to the Ritz vector for the effective singly excited amplitudes. The construction of Eq. (B.20) scales by $O(N^5)$ where N represents the magnitude of the size of the system unless the resolution-of-identity (RI) or the local correlation approach is employed. The explicit formulas of the energy-dependent σ-equation in spin-free form are given in Table B.1.

B.2.2 Self-energy shifting and use of the damping parameter for ADC(2)

For well balanced treatment of the valence and Rydberg type ESs, two requirements must be fulfilled; use of the sufficiently diffused basis set and inclusion of the higher than second order terms in the OR term of the effective response matrix. Since the exponents and contraction coefficient are optimized for the GS energy in most basis set, use of

relatively large basis set is desired for the EE calculations. Even in the calculations of the response properties, the situation is thought to be the same as the EE calculations. Even if a sufficiently large basis set is used, the EEs tend to deviate over approximately 0.5 eV from those obtained by the higher order methods such as CCSD [46, 47]. For the accurate calculation of the EE for the Rydberg excitation, one has to include the higher than the zeroth order terms in the OR term. In the response matrix at complete thorough the second order level, the D/D block is expanded up to the zeroth order and is given as diagonal matrix. For this specific simplicity, the efficient solution of the EE is available because there is no need to store the doubly excited amplitude in solving the quasi-eigenvalue equation in terms of the effective response matrix (Eq. (B.18)). The denominator shift can recover this dilemma by which the denominator in the OR term of the second order response matrix Eq. (B.18) is shifted by the correlated self-energy. The most strict way would possibly be to shift the denominator by the diagonal first order matrix elements of the D/D block. Let us note that such a diagonally-renormalized approach is not invariance under the unitary transformations of the degenerate MOs. On the other hand, the self-energy shifting retains the unitary-invariance when is applied to the theory that holds the unitary-invariance (e.g. ADC(2), CIS(D), ...) and is known to give the accurate EEs when used in the CIS(D) with use of the damping parameter.

When the self-energy shifting is used in the ADC(2), the D/D block of the response matrix (Eq. (B.17)) is modified as follows

$$(A_{DD})_{iajb;ldkc} = (\epsilon_a + \epsilon_b - e_i - e_j)\delta_{jk}\delta_{il}\delta_{ad}\delta_{bc} \tag{B.21}$$

where $\{e_i\}$ represents the single-ionization energies calculated as the poles of the second order electron propagator. The damping parameter (λ) is introduced in the ADC(2) framework as

$$\mathbf{A}_{SS}^{eff}(\omega) = \mathbf{A}_{SS} + \mathbf{A}_{SD}^{\dagger}(\lambda\omega\mathbf{E} - \mathbf{A}_{DD})^{-1}\mathbf{A}_{DS}. \tag{B.22}$$

In the *ab initio* electron propagator theory, the Dyson's equation gives the relationship of the zeroth order (Hartree-Fock) propagator ($\mathbf{G_0}$) with the correlated propagator ($\mathbf{G}$)

$$\mathbf{G}(e)^{-1} = \mathbf{G}_0(e)^{-1} - \mathbf{\Sigma}(e). \tag{B.23}$$

In Eq. (B.23), $\mathbf{\Sigma}$ represents the self-energy term which gives rise to the inclusion of the correlation effect. At the second order level of the fluctuation, the Dyson's equation (Eq. (B.23)) is written as

$$(G_2)_{p;q}(e)^{-1} = (e - \epsilon_p)\delta_{pq} - \left(\frac{1}{2}\sum_{iab}\frac{V_{ab}^{pi}V_{qi}^{ab}}{e + \epsilon_i - \epsilon_a - \epsilon_b} + \frac{1}{2}\sum_{ija}\frac{V_{ij}^{pa}V_{qa}^{ij}}{e + \epsilon_a - \epsilon_i - \epsilon_j}\right) \tag{B.24}$$

where the first and second terms on the right-hand side correspond to the $\mathbf{G}_0$ and $\mathbf{\Sigma}_2$, respectively. Furthermore, we use the quasi-particle approximation by which the non-diagonal elements of $\mathbf{G_2}$ are neglected ($(\Sigma_2)_{p;q} \rightarrow (\Sigma_2)_{p;q}\delta_{pq}$). With the quasi-particle approximation, the computational cost to solve Eq. (B.24) to obtain the second order ionization energies scales by $O(N^4)$ once the integral transformation from AO to MO basis is done. In this paper, we have used another type of the second order self-energy expression called parameterized GW2 (pGW2) model[48]. The pGW2 can be considered as a spin-component scaling type of modification[49] to the second order self-energy term.

In the case of ADC(2), adoption of the damping parameter as zero (setting $\lambda \rightarrow 0$ in Eq. (B.22)) eliminates the energy-dependence of the effective response matrix,

resulting in the working equations similar to the CIS(2X) model. Hereafter, we call such a second order method as ADC(2)$_{\lambda=0}$. Also, we name the modified ADC(2) that uses the self-energy shifted denominator (Eq. (B.21)) instead of Eq (B.17) as ADC(2)$_{SS}$. Our conventions for a series of the modified ADC(2) schemes are compiled in Table B.2.

B.2.3 Implementation

We have implemented the ADC(2) program in the `Psi3` open source quantum chemistry program package[50]. Our implementation is based on a completely file-based algorithm, so that the sorted tensorial quantities including ERIs and the Fock matrix elements were written to direct access files in symmetry blocked forms, which are the largest input files for the `ADC` module. The `ADC` module utilizes the direct-product decomposition technique [51]; the algorithms for molecular symmetry exploitation that largely reduces the floating-point operations and the memory requirement by a factor of $\approx h^2$, where h represents the order of the computational point-group. This algorithm enables tensorial quantities to be blocked out and stored according to their irreducible representation, such as the two-electron integrals, the σ-vectors and the intermediates encountered through the computation. As a result, the tensor contraction requires only the matrix-matrix manipulation of the symmetry-allowed, non-zero blocks. The main routine of our program performs the diagonalization of the effective response matrix (Eq. (B.18)) in a self-consistent manner; due to the energy dependence, the quasi-eigenvalue equation has to be solved for each ES. The outer iteration to obtain the self-consistent eigenvalue is accelerated by using the Newton-Raphson algorithm[52] and because of this, the total

computational time becomes approximately half.

The `ADC` program is ported to `Psi4`, the latest version of the package[53], and is now available under the open source license as a part of the release. Moreover, our program is capable of performing the partially-renormalized ADC(2) calculation[54].

We also have implemented the electron propagator program to calculate the correlated ionization energy according to the second order and pGW2 self-energy approximations[55]. The algorithm used to seek the pole structure is based on Ref. [42].

B.3 Computational details

All of the geometries were optimized via the MP2 / aug-cc-pVDZ [56, 57] level computation using the MPQC program [58], and used as input data for calculation of the vertical EEs using CIS(D), CC2, ADC(2), ADC(2)$_{SS}$ and EOM-CCSD as references. . The calculated EE values were compared to the experimental data [59, 60] for benzaldehyde and styrene. For the water molecule, the basis set dependence of the EEs obtained with ADC(2) and the modified variants were tested by varying the basis sets from aug-cc-pVDZ to aug-cc-pV7Z [56, 57, 61, 62, 63, 64]. All the calculations were performed with our local version of the `PsI3` quantum chemistry program package, in which we implemented the ADC module, named `ADC`. Our `Psi3` is capable of performing the strict and modified ADC(2) computations for the EEs in combination with the our electron propagator program.

B.4 Test cases and results

B.4.1 Adoption of λ into accounting of the orbital relaxation effect

Firstly, we examine the corrections purely from inclusion of the damping parameter λ [20] in the OR term. Medium-sized molecules such as glycine, naphthalene and styrene, benzaldehyde were selected. For the former two species, the calculated values are compared to those at the CCSD level, while the latter two with the experimental data because of convenient availability. For all the calculations, aug-cc-pVDZ basis set was used. These results are shown in Tables B.3 and B.4, where the characteristics of the associated ES are represented in parenthesis as "R" for Rydberg and "V" for valence states. In addition, the deviations from those values of the references are summarized graphically in Figs. B.1 - B.3 for ease of visualizing the tendencies. In Table B.3, it is notable that the glycine molecule, for which by nature of the Rydberg excitations, CIS(D), ADC(2) and CC2 tend to fall short from the CCSD values by up to 0.5 eV. On the other hand, in case of CIS, without any consideration of the correlation and the relaxation, it is easily recognizable that all of the states are largely overshot by 0.5-1.5 eV, even though the second order correction works and reduces the errors. This tendency is a typical error in these cases because of the weakness of the second order approach. When the first order description is not merely at the qualitative level, such as in case of Rydberg excitation, the second order correction tends to be overestimated. The introduction of λ as zero results in recovery from such a drawback, as in the case of CIS(D), which approaches close

to those of CCSD, as shown in Fig. B.1. However, for π^* excitations, which are frequently encountered in naphthalene, the situation is somewhat different. For such cases, all of the values are overshot, especially for the B_{3u} and B_{2g} states with significant deviations recognizable from the values at the CCSD level, while the strict ADC(2) fits moderately well for both states. From Table B.4, it is readily conceived that the typical second order methods are all clearly overrated from the experimental values. By inserting λ into the OR term as zero, the separation is largely widened and λ acts to correct such a situation with respect to the substantially quasi-degenerated states. Expansion of the OR term in Eq. (B.18) as an infinite series shows that the adoption of λ as zero is equivalent to the lowest order treatment on quasi-degeneracy. Although in Ref. [30], the zeroth order model with respect to the quasi-degeneracy, CIS(D_0) is superior to CIS(D) in accuracy, which is the same situation presented in Table B.4. This would be ascribed to the geometries optimized via non-correlated calculations, while in this work MP2 geometries were employed.

By adopting the λ parameter, the encouraging remediation is thus recognized for the Rydberg state, as already reported for CIS(D), although for the other type of ES, the calculated values are largely overrated to widen the absolute values of discrepancy from the reference values. Thus, the inclusion of λ as zero seems to be insufficient for both types of excitation.

B.4.2 Correction ascribable to self-energy shifting in the OR term

Here we examine the correction by the self-energy shifting [21, 22], by considering several molecules, formaldehyde, water, and 2,3,5,6-tetrafluorobenzene, for which the results are shown in Table B.5. For formaldehyde, a typical test case for comparison of the Rydberg and valence excitations, as presented in Ref. [21], all of the second order methods including ADC(2) almost give the values at the CCSD level for a $1A_2$ state of valence character. However, for the other two ESs, $1B_1$ and $2B_1$, which possess Rydberg character, accordance falls far short. Behavior such as the latter case can be retrieved by employing λ, but in this case, the valence state $1A_2$ tends to become too high compared with the reference value. This dilemma is also observed in the previous section. For the water molecule, which possesses countless numbers of Rydberg states, as with the previous example, for strong $3p$-type character that gives rise to the oxygen atom, all of the lowest ESs shown in Table B.5 are of the Rydberg type for which λ improves the original OR term by significantly lifting up the excess accounting such that almost identical outcomes to the reference are obtained. The use of self-energy, abbreviated as SS and the adopted self-energy term therein is represented by subscript in parenthesis, slightly diminishes the correction introduced solely by λ, which results in broadening of the deviation at this level of basis set.For this case, considerations of the basis set dependence and the behavior toward the limit will be given in **3. C**.

As the last case described here, 2,3,5,6-tetrafluorobenzene is considered, for which the

deviations by each method are depicted in Fig. B.4. This molecule has both types of excitation and is thus an ideal example for this type of benchmark. If λ only is adopted to dampen the OR term, then the EEs are lifted up to over 1 eV from those of the strict ADC(2) that deviate up to approximately 0.8 eV. Such an overestimation over 0.5 eV is recognized regardless of the character of the state, even for Rydberg states such as the A_g state and for the B3u valence state. When the self-energy is also used to shift the denominator of the OR term, the overrated correction is buffered to give good agreement. Especially when the second order self-energy expression is used in shifting the denominator, the calculated EEs are found to be in good accordance for all the states. When both the damping parameter and the self-energy shifting are used, the deviations from the reference values are fairly within approximately 0.3 eV, regardless of the type of the ESs.

B.4.3 Basis set dependence in EEs for cases where self-energies are adopted

As mentioned in **3. B**, the water molecule was chosen as the benchmark for the aug-cc-pVNZ basis, where N varies D to 7, to observe the behavior of the EEs calculated using both the strict and the shifted ADC(2) methods compared with the CCSD values. In Table B.6 and Fig. B.5, the relationship between the four lowest EEs and the basis set is given. We have found that as the number of the basis function increases, the differences between the values of the ADC(2) and the CC2 is reduced. Therefore, in Fig. B.5, only the ADC(2) values are shown. As the number of the basis set increases, the EEs

calculated by the ADC(2)$_{\lambda=0}$ tends to overshoot the EEs and discrepancy between EEs calculated by the ADC(2)$_{\lambda=0}$ and the CCSD values keeps being larger even though all the states given in Fig. B.5 are of Rydberg excitations. At the aug-cc-pV5Z level, all the curves tend to increase reasonably parallel and mostly reach their limit. The ADC(2) curves are found to be almost parallel to the CCSD curve. In the case of ADC(2)$_{SS}$ also, similar behavior is readily recognized, and as the basis set grows the energy curves follow those of CCSD in a highly promising manner, although with aug-cc-pVDZ, ADC(2)$_{\lambda=0}$ is preferable for these types of excitation. The shifted ADC(2) methods tend to give the EEs between those of the strict ADC(2) and ADC(2)$_{\lambda=0}$ and the good agreement with the reference CCSD values is observed.

B.5 Concluding remarks

The typical second order methods for ESs, including ADC(2) [9], tend to fall short of the higher order methods or the observed values upon calculation with respect to the Rydberg excitations. Even though for the valence excitations moderately relatively good agreement is available by using these approaches, for Rydberg state the deviations over approximately 0.5 eV from the CCSD level, are frequently observed. In order to overcome these ill behavior of the ADC(2), we introduced the self-energy shifting into the OR term. When the damping parameter is also employed, the accuracy of the EEs becomes almost comparable to the CCSD value at a cost of merely O(N^5) operations. We term these methods as the ADC(2)$_{SS(2);\lambda=0}$ and ADC(2)$_{SS(pGW2);\lambda=0}$ where in the subscripts,

$SS(2)$ and $SS(pGW2)$ represents the second order and pGW2 self-energy expressions, respectively, which are used to shift the denominator of the OR term of the ADC(2) response matrix. This type of modification scheme has already been developed in the framework of the CIS(D) and proved to give uniformly improved EEs for both the valence and Rydberg states. Since the ADC(2) is a variant of the CIS(D) in the sense that it is based on the quasi-degenerate perturbation theory, for systems that possess the quasi-degeneracy in the electronic state, the shifted ADC(2) model is expected to work more effectively than the shifted CIS(D) method.

As a consequence the damping parameter alone does not generally suffice because while it remedies the defect for Rydberg states, it also gives too much redundant correction that causes extra deviation for the other types of excitation. Employing the self-energy shifting in the OR term provides a balanced treatment for both valence and Rydberg states. On the other hand, we have observed that the ADC(2)$_{SS;\lambda=0}$ shows quite similar behavior to the CCSD for both the valence and the Rydberg states. Throughout this work, CCSD was chosen as a reference for which the accuracy of the ADC(2)$_{SS;\lambda=0}$ was assessed. It has been reported that CCSD tends to overshoot the EEs for the valence states by approximately 0.2 eV from the more accurate *ab initio* models in which the triply excited correction is taken into account[65, 66]. Because ADC(2)$_{SS;\lambda=0}$ tends to give somewhat higher EEs for the valence states by up to approximately 0.2 eV than the CCSD values, the specific care might be required for seeking the ESs other than the Rydberg states. Again we stress that the our modification requires the floating-point operations of only $O(N^4)$, which arises from the construction of the second order self-

energy term with the quasi-particle approximations. Moreover, the self-energy shifted ADC(2) methods retain the size-consistency and unitary-invariance, and give the EEs of the CCSD quality by the floating-point operations of totally $O(N^5)$. The correction scheme developed and its performance is examined in this work and we have found that our modified scheme is regarded as reliable and reasonable for the calculation of large molecules.

By the nature of the file-based algorithm, our `ADC` module is not specialized for truly large, realistic molecules without spatial symmetry. However, it is applicable to moderately large-sized molecules if they possess high symmetry by utilization of both point-group and spin symmetries. Although the largest tested case in this communication is naphthalene, our module is readily applicable for even larger molecules, including porphyrin derivatives. We are presently developing a more efficient algorithm and code that will be readily applicable for even larger systems by utilizing a massively parallelized programming model.

Bibliography

[1] A. Strachan, E. M. Kober, A. C. T. van Duin, J. Oxgaard, and W. A. G. III, J. Chem. Phys. **122**, 054502 (2005).

[2] I. B. Jr., A. J. A. Aquino, M. Barbatti, and H. Lischka, Int. J. Quant. Chem. **109**, 2348 (2009).

[3] A. G. Taube and R. J. Bartlett, J. Chem. Phys. **130**, 133112 (2009).

[4] T. Fleig, S. Knecht, and C. Hättig, J. Phys. Chem. A **111**, 5482 (2007).

[5] C. R. Kozak, K. A. Kistler, Z. Lu, and S. Matsika, J. Phys. Chem. B **114**, 1674 (2010).

[6] J. B. Foresman, M. Head-Gordon, J. A. Pople, and M. Frisch, J. Phys. Chem. **96**, 135 (1992).

[7] M. Head-Gordon, R. J. Rico, M. Oumi, and T. J. Lee, Chem. Phys. Lett. **219**, 21 (1994).

[8] Y. M. Rhee and M. Head-Gordon, J. Phys. Chem. A **111**, 5314 (2007).

[9] J. Schirmer, Phys. Rev. A **26**, 2395 (1982).

[10] A. B. Trofimov, G. Stelter, and J. Schirmer, J. Chem. Phys. **111**, 9982 (1999).

[11] A. B. Trofimov, G. Stelter, and J. Schirmer, J. Chem. Phys. **117**, 6402 (2002).

[12] J. Schirmer and A. B. Trofimov, J. Chem. Phys. **120**, 11449 (2004).

[13] C. Møller and M. S. Plesset, Phys. Rev. **46**, 618 (1934).

[14] J. Schirmer, Phys. Rev. A **43**, 4647 (1991).

[15] A. B. Trofimov, I. L. Kridina, J. Weller, and J. Schirmer, Chem. Phys. **329**, 1 (2006).

[16] O. Christiansen, H. Koch, and P. Jørgensen, Chem. Phys. Lett. **243**, 409 (1995).

[17] O. Christiansen, H. Koch, P. Jørgensen, and T. Helgaker, Chem. Phys. Lett. **263**, 530 (1996).

[18] K. Hald, C. Hättig, D. L. Yeager, and P. Jørgensen, Chem. Phys. Lett. **328**, 291 (2000).

[19] C. Hättig and K. Hald, Chem. Phys. Chem. Phys. **4**, 2111 (2002).

[20] Y. M. Rhee and M. H. Gordon, J. Phys. Chem. A **111**, 5314 (2007).

[21] P. Surján and Á. Szabados, Int. J. Quant. Chem. **69**, 713 (1997).

[22] P. Surján, Á. Szabados, and Z. Szekeres, Int. J. Quant. Chem. **90**, 1309 (2002).

[23] Y. Mochizuki, Chem. Phys. Lett. **453**, 109 (2008).

[24] Y. Mochizuki, Chem. Phys. Lett. **472**, 143 (2009).

[25] M. Nooijen and J. Snijders, J. Chem. Phys. , 1681 (1995).

[26] M. Deleuze, J. Delhalle, B. T. Pickup, and J.-L. Calais, Adv. Quantum Chem. **26**, 35 (1995).

[27] L. Meissner, Mol. Phys. **104**, 2073 (2006).

[28] D. Laikov and S. Matsika, Chem. Phys. Lett. **448**, 132 (2007).

[29] J. X. Liang and S. Matsika, J. Am. Chem. Soc. **133**, 6799 (2011).

[30] M. Head-Gordon, M. Oumi, and D. Maurice, Mol. Phys. **96**, 593 (1999).

[31] Y. Mochizuki et al., Chem. Phys. Lett. **433**, 360 (2007).

[32] N. Taguchi, Y. Mochizuki, and T. Nakano, Chem. Phys. Lett. **504**, 76 (2010).

[33] Y. Mochizuki et al., Theor. Chem. Acc. **117**, 541 (2007).

[34] Y. Mochizuki et al., Chem. Phys. Lett. **457**, 396 (2008).

[35] T. H. Dunning and V. M. McKoy, J. Chem. Phys. **47**, 1735 (1967).

[36] P. Jørgensen and J. Linderberg, Int. J. Quantum Chem. **4**, 587 (1970).

[37] D. Casanova, Y. M. Rhee, and M. Head-Gordon, J. Chem. Phys. **128**, 164106 (2008).

[38] C. Hättig, NIC Series **31**, 245 (2006).

[39] J. Oddershede and P. Jørgensen, J. Chem. Phys. **66**, 1541 (1977).

[40] J. Oddershede, P. Jørgensen, and D. L. Yeager, Comput. Phys. Rep. **2**, 33 (1984).

[41] J. Simons and P. Jørgensen, *Second Quantization-Based Methods In Quamtum Chemistry*, Academic Press, New York, 1981.

[42] J. Linderberg and Y. Öhrn, *Propagators In Quamtum Chemistry 2nd Ed*, Wiley-InterScience, New Jersey, 2004.

[43] E. R. Davidson, Chem. Phys. **17**, 87 (1975).

[44] B. Liu, *Report on the Workshop: Numerical Algorithms in Chemistry: Algebraic Methods*, Lawrence Brekeley Lab., Univ. of California, California, 1978.

[45] N. Kosugi, J. Comput. Phys. **55**, 426 (1984).

[46] H. Koch and P. Jørgensen, J. Chem. Phys. **93**, 3333 (1990).

[47] H. Koch, H. J. A. Jansen, T. Helgaker, and P. Jørgensen, J. Chem. Phys. **93**, 3345 (1990).

[48] C.-H. Hu, D. P. Chong, , and M. E. Casida, J. Elec. Spec. Rel. Phen. **85**, 39 (1997).

[49] S. Grimme, J. Chem. Phys. **118**, 9095 (2004).

[50] T. D. Crowford et al., J. Comput. Chem. **28**, 1610 (2007).

[51] J. F. Stanton, J. Gauss, J. D. Watts, , and R. J. Bartlett, J. Chem. Phys. **94**, 4334 (1991).

[52] W. von Niessen, J. Schirmer, and L. S. Cederbaum, Comput. Phys. Rep. **1**, 57 (1984).

[53] J. M. Turney et al., WIREs Comput. Mol. Sci. **2**, 556 (2012).

[54] M. Saitow and Y. Mochizuki, Comput. Phys. Lett. **525**, 144 (2012).

[55] M. Saitow, T. Ida, and M. Mizuno, Chem. Phys. Lett. **486**, 171 (2010).

[56] R. Kendall, T. Dunning, Jr., and R. Harrison, J. Chem. Phys. **96**, 6796 (1992).

[57] R. Kendall, D. Woon, and J. T.H. Dunning, J. Chem. Phys. **98**, 1358 (1993).

[58] The Massively Parallel Quantum Chemistry Program (MPQC), Version 2.4.0, Prerelease, Curtis L. Janssen, Ida B. Nielsen, Matt L. Leininger, Edward, F. Valeev, Edward T. Seidl, Joseph P. Kenny, http://www.mpqc.org.

[59] K. Kimura and S. Nagakura, Theor. Chim. Acta. **3**, 164 (1965).

[60] K. Kesper, N. Munzel, W. Pietzuch, H. Specht, and A. Schweig, J. Mol. Struct. (THEOCHEM) **200**, 375 (1989).

[61] D. E. Woon, K. A. Peterson, and J. T. H. Dunning, *(unpublished)* .

[62] K. A. Peterson and D. E. Woon, *(unpublished)* .

[63] A. K. Wilson, T. van Mourik, and J. T. H. Dunning, J. Mol. Struct. (THEOCHEM) **388**, 339 (1997).

[64] This aug-cc-pV7Z basis is an unofficial version, already implemented in `Psi3` program package and is based on the Feller and co-worker's aug-pV7Z basis sets.

[65] S. P. A. Sauer, M. Schreiber, M. R. Silva-Junior, and W. Thiel, J. Chem. Theory Comput. **5**, 555 (2009).

[66] M. R. Silva-Junior, S. P. Sauer, M. Schreiber, and W. Thiel, Mol. Phys. **108**, 453 (2010).

Table B.1: Intermediate tensors and σ-equations for the ADC(2) singlet excitations where the singly excited amplitude and orbital energy are represented by b and ϵ. The electron repulsion integral is given in the Dirac notation.

formula
$K_{ijab} \leftarrow \frac{\langle ij\|ab\rangle}{\epsilon_i+\epsilon_j-\epsilon_a-\epsilon_b}$
$X_{ij} \leftarrow \sum_{kab} K_{ikab}\langle jk\|ab\rangle$
$X_{ab} \leftarrow \sum_{ijc} K_{ijac}\langle ij\|bc\rangle$
$A_{aibj} \leftarrow \delta_{ij}\left[\delta_{ab}\epsilon_a - \frac{1}{2}(X^t_{ab}+X_{ab})\right] - \delta_{ab}\left[\delta_{ij}\epsilon_i + \frac{1}{2}(X^t_{ij}+X_{ij})\right]$ $+2\langle ij\|ab\rangle - \langle ia\|jb\rangle$
$D_{ia} \leftarrow \sum_{jb}(2\langle ji\|ba\rangle - \langle ji\|ab\rangle)b_{jb}$
$\sigma_{ia} \leftarrow \frac{1}{2}\sum_{jb}(2K_{ijab} - K_{ijba})D_{jb}$
$E_{ia} \leftarrow \sum_{jb}(2K_{jiba} - K_{jiab})b_{jb}$
$\sigma_{ia} \leftarrow \frac{1}{2}\sum_{jb}(2\langle ij\|ab\rangle - \langle ij\|ba\rangle)E_{jb}$
$X_{jiab} \leftarrow \sum_c \langle jc\|ab\rangle b_{ic}$
$Y_{ijab} \leftarrow \sum_k \langle ak\|ij\rangle b_{kb}$
$Z_{ijab} \leftarrow X_{jiab} - Y_{ijab}$
$B_{ijab} \leftarrow \frac{2Z_{ijab}-Z_{ijba}+2Z_{jiba}-Z_{jiab}}{\omega+\epsilon_i+\epsilon_j-\epsilon_a-\epsilon_b}$
$\sigma_{ia} \leftarrow \sum_{jbc} B_{ijbc}\langle aj\|bc\rangle$
$\sigma_{ia} \leftarrow -\sum_{jkb}\langle jk\|ib\rangle B_{jkab}$
$\sigma_{ia} \leftarrow \sum_{jb} A_{aibj}b_{jb}$

Table B.2: Our naming conventions for the modified ADC(2) schemes are summerized. λ represents the damping parameter used to scale the energy dependence of the effective response matrix (see Eq. (B.22)) while $\mathbf{\Sigma}$ represents the self-energy employed in Eq. (B.21). The self-energy formulae are given in the spin-free representation assuming the closed-shell system.

Models	Value of λ	Formula of self-energy $(\mathbf{\Sigma})_{p;q}$
ADC(2)	1	–
$\mathrm{ADC(2)}_{\lambda=0}$	0	–
$\mathrm{ADC(2)}_{SS(2);\lambda=0}$	0	$\sum_{iab} \frac{\langle pi\|ab\rangle(2\langle ab\|qi\rangle - \langle ab\|iq\rangle)}{e+\epsilon_i-\epsilon_a-\epsilon_b} + \sum_{ija} \frac{\langle pa\|ij\rangle(2\langle ij\|qa\rangle - \langle ij\|aq\rangle)}{e+\epsilon_a-\epsilon_i-\epsilon_j}$
$\mathrm{ADC(2)}_{SS(pGW2);\lambda=0}$	0	$\sum_{iab} \frac{0.96\langle pi\|ab\rangle\langle ab\|qi\rangle}{e+\epsilon_i-\epsilon_a-\epsilon_b} + \sum_{ija} \frac{0.96\langle pa\|ij\rangle\langle ij\|qa\rangle}{e+\epsilon_a-\epsilon_i-\epsilon_j}$

Table B.3: Lowest vertical EEs (eV) for glycine and naphthalene calcllated by using the CIS, CIS(D), ADC(2) and CC2 with the aug-cc-pVDZ are shown. Also, the CCSD values calculated with the same basis set are given.

Symmetry	CIS	CIS(D)	ADC(2)	CC2	ADC(2)$_{\lambda=0}$	CCSD
glycine						
1A"(R)	6.70	5.70	5.47	5.71	5.89	5.74
1A$'$(R)	7.40	5.79	5.71	5.74	6.15	6.08
2A"(R)	8.42	6.75	6.71	6.74	7.22	7.13
2A$'$(R)	8.57	6.45	6.50	6.55	7.03	6.99
naphthalene						
B_{2u}(V)	5.01	5.14	4.80	4.80	5.24	5.05
B_{3u}(V)	5.15	4.44	4.42	4.41	4.88	4.38
A_u(V)	5.67	5.49	5.46	5.44	5.87	5.61
B_{2g}(V)	6.02	5.86	5.84	5.82	6.27	6.01
B_{1g}(V)	6.33	6.16	5.86	5.85	6.42	6.09
A_u(V)	6.65	6.42	6.40	6.39	6.88	6.59
B_{2g}(V)	6.86	6.55	6.53	6.51	7.03	6.68

Table B.4: Lowest vertical EEs (eV) for styrene and benzaldehyde calculated by using the CIS, CIs(D), ADC(2), CC2, and ADC(2)$_{\lambda=0}$ with aug-ccpVDZ basis set are shown. The accuracy of the calculated EEs are compared with the experimental ones.

Symmetry	CIS	CIS(D)	ADC(2)	CC2	ADC(2)$_{\lambda=0}$	Exp.
styrene						
$1A^{'}$	5.30	5.38	5.28	5.30	5.67	5.21
$2A^{'}$	5.67	4.92	4.83	4.82	5.29	4.42
benzaldehyde						
$1A^{"}$	4.75	3.88	3.65	3.86	3.96	3.34
$1A^{'}$	5.67	5.01	4.86	4.85	5.34	4.51
$2A^{'}$	5.72	5.79	5.54	5.57	5.99	5.34

Table B.5: Lowest few EEs (eV) for formaldehyde, water and 2,3,5,6-tetrafluorobenzene calculated by using the CIS, CIs(D), CC2, strict and shifted ADC(2) with aug-ccpVDZ basis set are shown. As a reference, the CCSD values are also given.

					ADC(2)$_{\lambda=0}$			
Symmetry	CIS	CIS(D)	ADC(2)	CC2	-	$SS(2)$	SS(pGW2)	CCSD
formaldehyde								
$1A_2$(V)	4.56	4.06	3.93	4.10	4.24	4.00	4.12	4.03
$1B_1$(R)	8.53	6.34	6.26	6.39	6.82	6.50	6.65	7.03
$2B_1$(R)	9.40	7.45	7.37	7.47	7.94	7.66	7.79	7.98
water								
$1B_1$(R)	8.67	6.97	6.97	7.10	7.44	7.18	7.28	7.46
$1A_2$(R)	10.36	8.73	8.63	8.75	9.22	8.95	9.06	9.22
$1A_1$(R)	11.00	9.41	9.36	9.48	9.96	9.73	9.82	9.86
$2B_1$(R)	12.14	10.55	10.59	10.72	11.23	11.01	11.09	11.09
2,3,5,6-tetrafluorobenzene								
B_{3u}(V)	6.06	5.05	4.94	4.98	5.57	5.21	5.37	5.04
B_{2g}(R)	6.96	6.33	6.18	6.14	6.62	6.31	6.45	6.37
B_{2u}(V)	6.47	6.74	6.43	6.50	7.07	6.80	6.92	6.62
B_{3g}(R)	7.64	7.19	7.02	6.99	7.50	7.26	7.37	7.12
B_{1u}(R)	7.87	7.09	7.00	6.94	7.50	7.20	7.34	7.18
A_u(R)	8.02	7.19	7.10	7.07	7.63	7.31	7.45	7.36
A_g(R)	9.80	9.28	8.25	8.32	9.47	8.88	9.07	8.72
B_{1g}(R)	9.43	8.73	8.54	8.52	9.20	8.91	9.04	8.78

Table B.6: Lowest four EEs (eV) for water calculated by using the CIS, CIs(D), CC2, strict and shifted ADC(2) with aug-ccpVNZ basis set are shown where N = D-7. As a reference, the CCSD values are also given. Because of the limitation of the computational resource, ADC(2)$_{SS;\lambda=0}$ calculations could not be performed.

					ADC(2)$_{\lambda=0}$			
Symmetry	CIS	CIS(D)	ADC(2)	CC2	-	SS(2)	SS(pGW2)	CCSD
aug-cc-pVDZ								
$1B_1$(R)	8.67	6.97	6.97	7.10	7.44	7.18	7.28	7.46
$1A_2$(R)	10.36	8.73	8.63	8.75	9.22	8.95	9.06	9.22
$1A_1$(R)	11.00	9.41	9.36	9.48	9.96	9.73	9.82	9.86
$2B_1$(R)	12.14	10.55	10.59	10.72	11.23	11.01	11.09	11.09
aug-cc-pVTZ								
$1B_1$(R)	8.69	7.19	7.20	7.25	7.70	7.46	7.55	7.61
$1A_2$(R)	10.39	8.94	8.86	8.90	9.48	9.24	9.33	9.37
$1A_1$(R)	10.97	9.53	9.53	9.58	10.15	9.94	10.03	9.96
$2B_1$(R)	11.80	10.28	10.33	10.38	11.00	10.79	10.87	10.82
aug-cc-pVQZ								
$1B_1$(R)	8.69	7.24	7.30	7.32	7.79	7.56	7.65	7.68
$1A_2$(R)	10.36	9.04	8.96	8.97	9.59	9.36	9.46	9.44
$1A_1$(R)	10.95	9.61	9.62	9.63	10.21	10.02	10.01	10.01
$2B_1$(R)	11.60	10.11	10.18	10.19	10.84	10.63	10.72	10.65

Table B.6: (continued)

					ADC(2)$_{\lambda=0}$			
Symmetry	CIS	CIS(D)	ADC(2)	CC2	-	SS(2)	SS(pGW2)	CCSD
aug-cc-pV5Z								
$1B_1$(R)	8.69	7.31	7.35	7.35	7.84	-	-	7.71
$1A_2$(R)	10.36	9.07	9.00	9.00	9.62	-	-	9.47
$1A_1$(R)	10.94	9.61	9.64	9.65	10.25	-	-	10.01
$2B_1$(R)	11.40	9.89	9.95	9.94	10.62	-	-	10.44
aug-cc-pV6Z								
$1B_1$(R)	8.69	7.31	7.35	7.36	7.86	-	-	7.72
$1A_2$(R)	10.36	9.10	9.02	9.01	9.64	-	-	9.48
$1A_1$(R)	10.92	9.59	9.63	9.63	10.24	-	-	10.03
$2B_1$(R)	11.26	9.69	9.76	9.74	10.44	-	-	10.27
aug-cc-pV7Z								
$1B_1$(R)	8.69	7.37	7.38	7.37	7.88	-	-	7.73
$1A_2$(R)	10.36	9.10	9.04	9.02	9.66	-	-	9.49
$1A_1$(R)	10.91	9.56	9.61	9.61	10.24	-	-	10.01
$2B_1$(R)	11.24	9.67	9.73	9.71	10.42	-	-	10.25

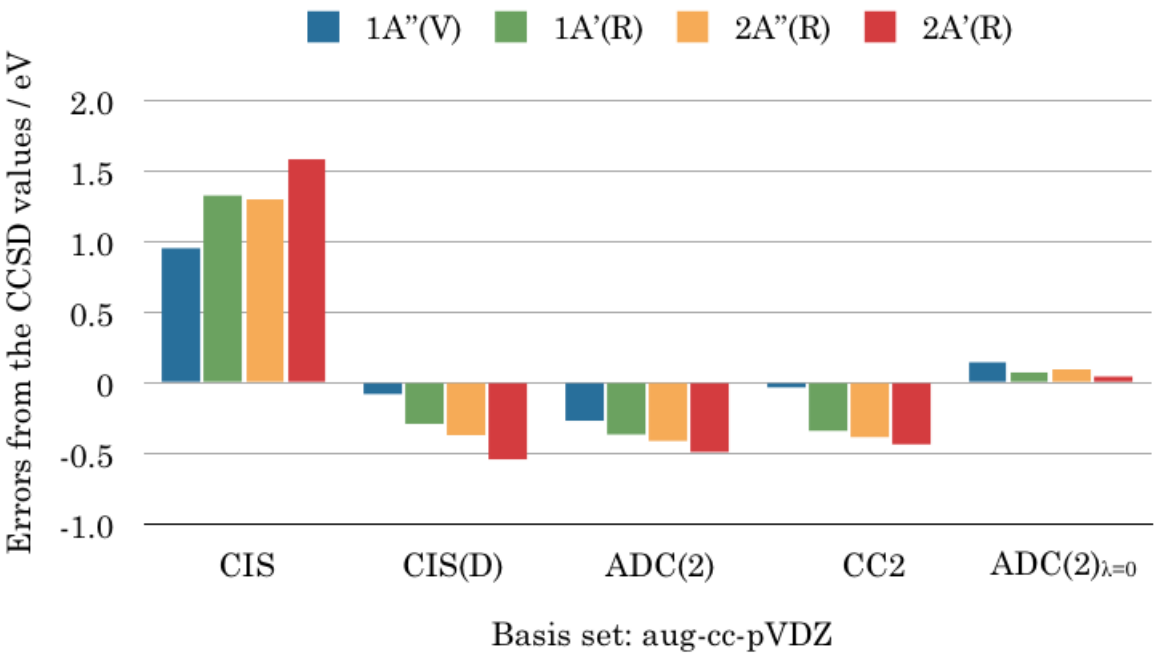

Figure B.1: Errors of the CIS and the second order methods (CIS(D), ADCC(2), CC2, $ADC(2)_{\lambda=0}$) from the CCSD values for glycine are shown. As a basis set, aug-cc-pVDZ was used.

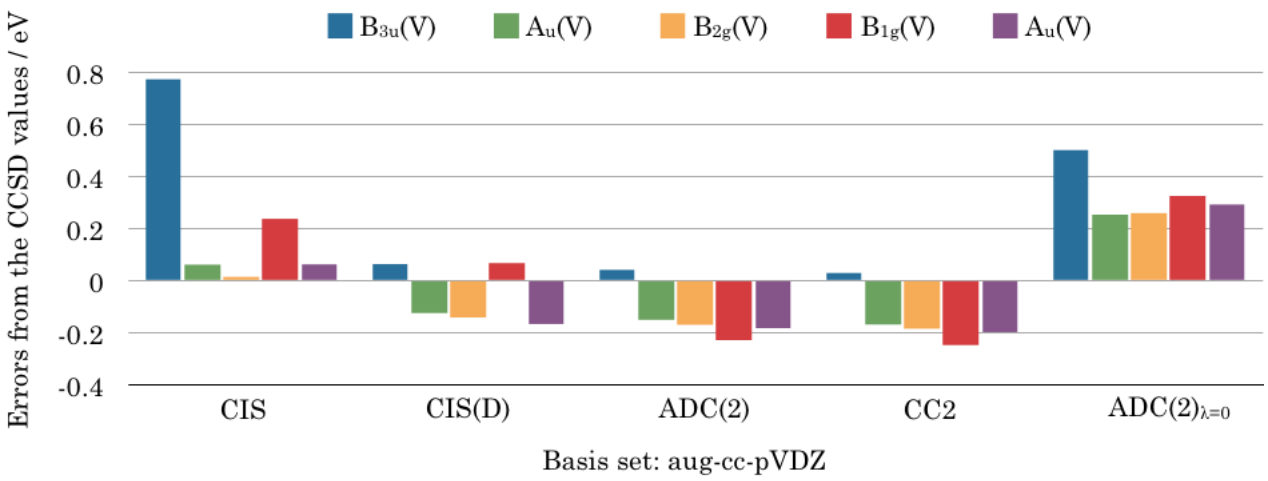

Figure B.2: Errors of the CIS and the second order methods (CIS(D), ADCC(2), CC2, $ADC(2)_{\lambda=0}$) from the CCSD values for naphtalene are shown. As a basis set, aug-cc-pVDZ was used.

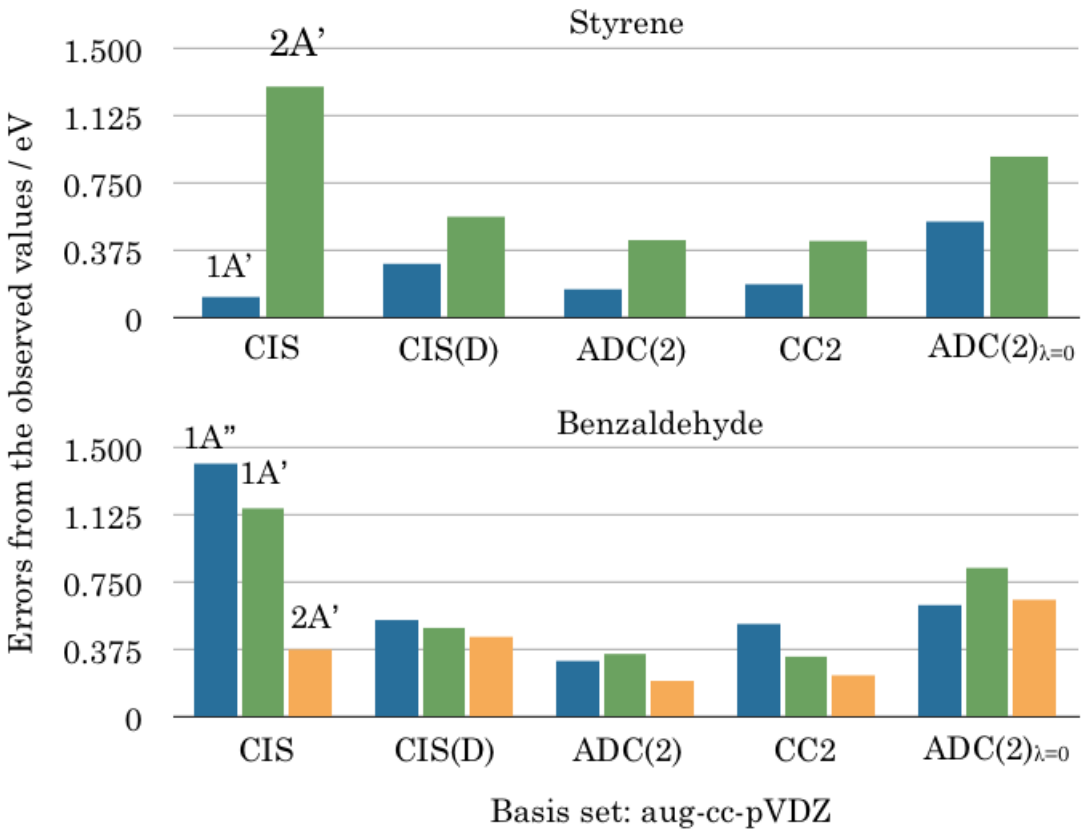

Figure B.3: Errors of the CIS and the second order methods (CIS(D), ADCC(2), CC2, ADC(2)$_{\lambda=0}$) from the CCSD values for styrene and benzaldehyde are shown. As a basis set, aug-cc-pVDZ was used.

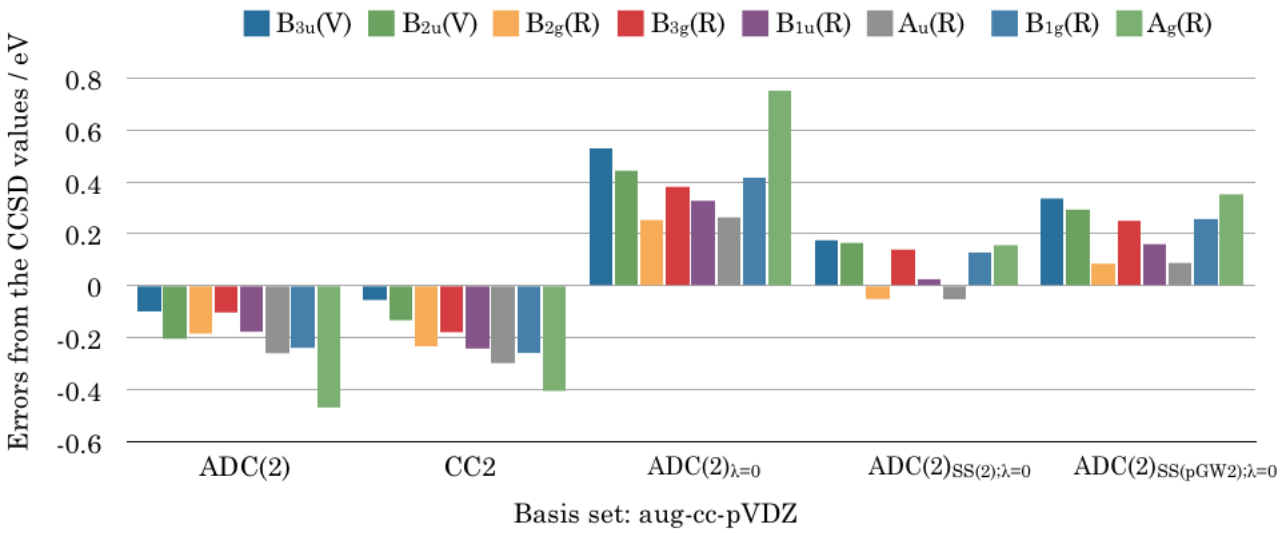

Figure B.4: Errors of the CIS and the second order methods (CIS(D), ADCC(2), CC2, ADC(2)$_{\lambda=0}$) from the CCSD values for 2,3,5,6-tetrafluorobenzene are shown. As a basis set, aug-cc-pVDZ was used.

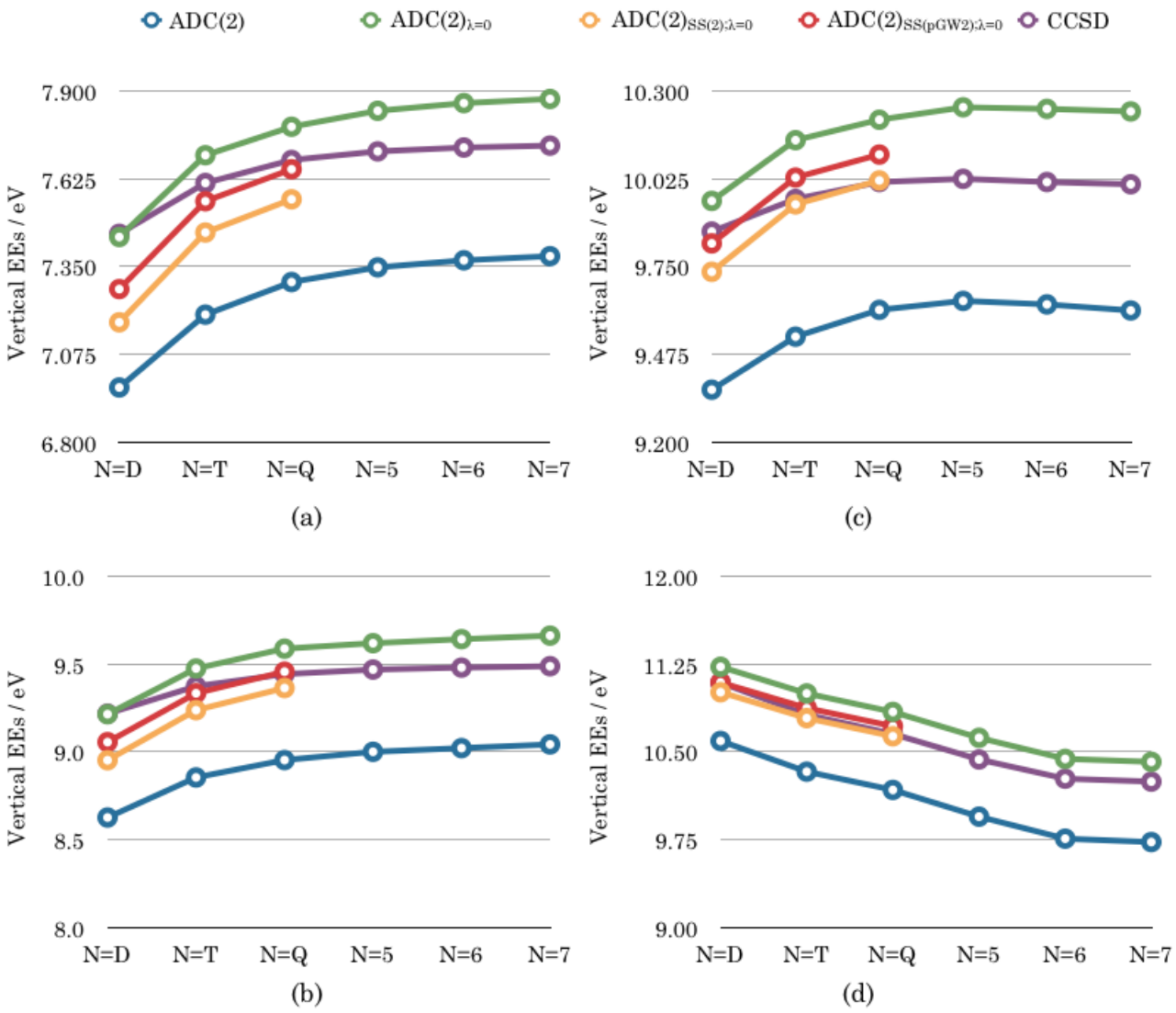

Figure B.5: Calculated EEs for (a) $1B_1$(R), (b) $1A_2$(R) and (c) $1A_1$(R), (d) $2B_1$(R) states by using the strict and shidted-ADC(2) methods by using the six types of basis set; aug-cc-pVNZ (N = D-7). Also, the CCSD values are shown as a reference.